MECHANICS OF BENDING OF FIBER ASSEMBLIES

by

PETER POPPER

B.S., Lowell Technological Institute
(1957)

S.M., Massachusetts Institute of Technology
(1959)

Mech.E., Massachusetts Institute of Technology
(1964)

Submitted in partial fulfillment
of the requirements for the degree of

Doctor of Science

at the
Massachusetts Institute of Technology

February, 1966

Signature of Author.....
Fibers and Polymers Division, March 11, 1966

Certified by.....
Thesis Supervisor

Accepted by.....
Chairman, Departmental Committee on Graduate Students
Department of Mechanical Engineering

MECHANICS OF BENDING OF FIBER ASSEMBLIES

by

Peter Popper

Submitted to the Department of Mechanical Engineering on March 11, 1966 in partial fulfillment of the requirement for the Degree of Doctor of Science in Mechanical Engineering.

This investigation is directed towards a determination of how fiber-to-fiber friction and fiber mobility in a fibrous structure affect bending and unbending behavior. The classical theories for predicting this behavior involve the assumption of either a negligible or infinite interfiber frictional interaction, and the results based on these limiting assumptions cover a wide range of possible behavior. Experimental and analytical investigations of the intermediate cases of frictional interaction have shown that the way in which fibers move relative to each other during bending can have a strong effect on the manner in which the properties of the individual fibers develop the properties of the fibrous structure. Moreover, it was shown that the actual bending behavior and bending recovery obtained for the cases of intermediate frictional interaction differ both quantitatively and qualitatively from that of the limiting cases.

In order to evaluate the bending behavior of textile materials, a special instrument was designed and constructed to measure bending moment as a function of imposed curvature. Data obtained on this equipment were used to establish the bending parameters of the various materials under investigation.

As a complement to the fundamental considerations of textile structures, a study was undertaken on the mechanics of multi-layer beams with interlayer friction. This was done analytically and the results were verified experimentally.

Thesis Supervisor: Professor Stanley Backer

Title: Professor, Mechanical Engineering
Head, Fibers and Polymers Division

ACKNOWLEDGEMENTS

I would like to acknowledge the valuable assistance and advice that I have received during the course of this investigation. Most of all, I am deeply grateful for the many stimulating suggestions, technical advice, and constant encouragement given to me by Professor Stanley Backer, the Chairman of my Thesis Committee.

I would also like to thank three organizations for their financial support during my studies and research: the Chemstrand Research Center for their research grant covering the initial stages of this investigation; the Camille Dreyfus Foundation for their fellowship during my graduate studies; and the U. S. Department of Agriculture for their research grant under which the major portion of this work was done.

Thanks also go to the staff and students of the Fibers and Polymers Division and to the members of my Thesis Committee for the advice and assistance given. In particular, I acknowledge the advice of Dr. Aly El-Shiekh and Mr. Pierfranco Marzoli given in connection with the design of the test equipment; the assistance of Mr. Abdel Sid-Ahmed in the experimental work and the preparation of fabric cross sections; and the untiring labors of Miss Dorothy Eastman in the typing of this thesis.

I also thank my wife, Rosalie, for her encouragement and for the personal sacrifices which she has made during the period of my doctoral studies. Finally, I thank my three beautiful daughters, Lisa, Linda, and Laura (who was born during the early stages of the thesis) for just being around, and brightening the sometimes gloomy days. The thesis is dedicated to them--Rosalie, Lisa, Linda, and Laura.

TABLE OF CONTENTS

INTRODUCTION

One of the fundamental differences between textile materials and other types of sheet structures is that textiles generally exhibit unusually high flexibility. Because of this, they can be used satisfactorily in a wide variety of applications requiring extremely low bending rigidity, the most significant, of course, being clothing. Textile fabrics are made of large numbers of fine fibers that may have considerable freedom of motion relative to each other. When this mobility exists, the fiber strains which develop during bending or creasing of the fabric are considerably lower than those which develop in bending of corresponding solid sheet materials. With this mobility the potential flexibility of the fibers can be realized and the fabric structure will, in turn, have a low bending rigidity. If, on the other hand, fiber mobility is restricted, the strains which develop during bending will be of considerable magnitude and the fabric will be correspondingly more rigid.

Another important attribute of textile materials is their ability to recover from imposed bending deformations. This recoverability, like flexibility, also depends on the fineness of the fibers and their ability to move relative to each other. When the fiber diameters are much less than the fabric thickness, and when interfiber mobility exists, the strains which develop during bending or creasing will be moderate. The permanent fiber deformation will be small and the recovery of the structure will be good. If the fibers do not have mobility in the structure, the strains which develop during bending will be considerably greater and cause more permanent fiber deformation and poorer recovery of the structure.

Since both the bending and bending recovery behavior of textiles are of prime importance in their end use, it is important to understand the factors which determine this behavior. The most important factor is, of course, the indivual fiber properties. Fabrics made of flexible fibers are generally flexible and fabrics made of fibers with a high degree of tensile recovery generally have a high bending recovery. However, this holds true only if the fibers have mobility in the structure. If relative fiber motion is restricted, then a structural interaction develops which can have a strong affect on the translation of fiber to fabric properties. This interaction generally increases the fabric rigidity and decreases bending recoverability. In the limiting case of an interfiber interaction that prevents all relative fiber motion, the fabric will behave almost as a solid sheet structure. For this reason, it is of fundamental significance to develop an understanding of the factors which govern the motion of fibers in textile structures. These motions depend on the geometric arrangement of fibers, the fiber properties, and the interfiber frictional interactions. Determination of this dependence and of the effect of fiber mobility on fabric behavior is the fundamental objective of this investigation.

In the most general sense, what is required for a full understanding of the mechanics of bending of textile structures is a relation between bending behavior, fiber properties, and structural geometry. This involves an understanding of how the properties of the individual fibers develop the properties of the structure for any given geometric configuration. The complete answer to this question is not available at present, nor will it be for some time. Nevertheless, it is hoped that the information reported here will contribute

significantly to our understanding of this phenomena and that it will stimulate continuing research in this area.

There are a number of important reasons for understanding the bending mechanics of textiles that should be of importance to both fiber and textile manufacturers. For the fiber manufacturer it is important to know the relative importance of the various fiber properties on bending behavior. This facilitates the modification of existing fibers or the development of new ones to meet specific needs. The textile manufacturer, on the other hand, would be interested in selecting the proper fiber for a particular use and determining how to best convert it into a fabric. He would also like to be able to predict the effect of any particular finishing treatment and then be able to characterize accurately the bending and recovery of the materials produced.

The problem of pre dicting bending behavior in textiles is classically dealt with in the literature by means of one of two limiting assumptions . The fibers are either assumed to have complete freedom of motion, or no freedom of motion. In the first case, the frictional effects are neglected; and in the second, they are assumed to be of sufficient magnitude to prevent any relative fiber motion. The differences in the predictions for the two cases are considerable as would be expected. A loosely made fabric with complete freedom of motion is much more flexible than one that has been treated with starch, for example, and has no freedom of fiber motion.

Since the difference between the predictions for these limiting conditions is very large, it is important to have a means of understanding the mechanics of the intermediate cases of frictional interaction. That is the specific problem dealt with in this research. It will be shown that the

behavior for these cases need not be the same qualitatively as that found in the limiting cases. In particular, the energy losses that occur when fibers slide against a frictional restraint produce a non-linear behavior that is qualitatively different. This affects both bending and recovery as will be discussed in detail in the text.

A number of previous investigations have dealt with the intermediate effects of friction. Platt et al[8] assumed that one way friction can act is to cause the fibers to form clusters in the structure. On this basis they developed certain predictions of bending behavior. Abbott et al[9] proposed that the intermediate effect was to cause lengthwise segments of yarn in a fabric to bend alternatingly with complete and no freedom of motion. Later, Zorowski and Chen[10] found that a ply yarn could be considered to bend with a core of non-moving fibers surrounded by fibers acting under complete freedom of motion. In the mathematical treatments to be presented it will be shown that some of these proposed mechanisms can be explained in terms of the mechanics of slip propagation during bending.

Non-linear effects of bending were also found by some investigators. Isshi[11], Eeg-Olofsson[12], and Livesey and Owens[7] found them in constant moment tests; and Zorowski[10], and Grosberg[13] found them in cantilever and buckling tests. These will also be considered in the treatments to be presented.

Frictional effects on bending recovery were considered in a number of investigations. Bostwick et al[14] demonstrated that low amplitude mechanical vibrations during recovery could improve the ability of fabrics to straighten; and Daniels[15] showed that friction can have a strong effect on recovery, especially for low curvature bends. In addition,

others[16] have shown that fiber surface treatments often have strong effects on bending recovery.

During the course of this work it was found that some means for carefully measuring the bending behavior of fabrics was needed. Since there was no commercial instrument available and since previous designs of instruments of this kind were not considered optimal, a special test instrument was designed and constructed. On this piece of equipment it is possible to measure continuously the moment-curvature relation of textile materials. From this measurement, two parameters were found to be capable of describing bending behavior for low curvature bends.

The thesis is divided into four chapters. In the first, the mechanical behavior of multi-layer beams with friction between the layers will be examined. This type of structure has many aspects of mechanical behavior analagous to that of textiles, and the results obtained are applied to textile structures whenever possible. In the second and third chapters, the bending and bending recovery respectively are discussed for various types of textile structures. These investigations were performed by both experimental and analytical means. Then, in the last chapter the test instrument developed will be described in detail, together with all of the experimental procedures used.

There are a number of applications to which the results of this research may be applied. The proposed theory of multi-layer beams may be used to solve a number of problems for layered structures in which frictional effects are significant. In addition, the unusual effect of "reverse curvature" which was noted from the mathematics and demonstrated experimentally may have some practical implications. This effect involves unusual deflections in this type of structure

under certain types of loading.

The primary significance of the work done on the bending of textile structures is to add to the information already available and to clarify some of the mechanisms by which friction acts. The specific applications of this information relate to such factors as fabric stiffness, hand, aesthetics, comfort, drape, buckling behavior, non-linear behavior, energy absorption; and others. In addition, the approaches taken can in some cases be applied to pressurized fabric structures where rigidity and recovery are often of prime concern. For example, in the design of a full pressure suit[27] the requirements are for low rigidity, and contrary to the case of textiles in general, poor recovery from bending.

The results of the investigation on bending recovery can be used to aid in the improvement of this extremely important property for clothing fabrics. From the results obtained, it is possible to estimate the effects which can be expected by a given frictional treatment, fiber modification, or structural rearrangement.

The experimental techniques used in this investigation may have applications in continuing research on this general problem. In particular, the instrument designed for measuring the moment-curvature relation may be useful for other research investigations or for routine measurements.

While the analyses and experimental results presented in this thesis certainly do not answer more than a fraction of the overall problems in this field, it is hoped that they represent a useful contribution to the existing technology and that they can be used to help others in continuing this work.

CHAPTER I THE BENDING OF MULTI-LAYER BEAMS WITH FRICTION BETWEEN THE LAYERS

In order to establish the fundamentals of mechanical behavior of a complex structure, it is often useful to consider the mechanics of a highly idealized model. If the essential features of both are the same, then an analysis of the model will provide an understanding of the behavior of the structure.

If the complex structure of interest is a textile material subjected to bending, then a useful idealization can be found in a multi-layer beam having friction between the layers. In both the textile and the multi-layer beam the individual elements--the fibers or the layers--slide by one another as the system bends. This sliding may be resisted by frictional interactions in both cases and this results in an alteration of the mechanical behavior as compared to the case where no friction exists between the layers. First, the friction system is stiffer than the zero friction system; second, there may be energy lost in bending; and third, imposed deformations are not generally completely recoverable. These three effects can occur in a friction system even if the individual elements are completely elastic. They are observed in both textile materials and layered beams which display frictional interactions.

This chapter will deal exclusively with multi-layer beams and the results applicable to textile structures will be utilized in the following chapters of this thesis. The general problem under consideration here is the determination of how interlayer friction affects the mechanics of multi-layer beams. More specifically, such things as load-geometry relation, strain distribution, slip distribution, recovery from loading, and propagation of slip are to be analyzed.

As a first approach to the problem the limiting cases of frictional interaction can be considered--namely, zero and

infinite friction. When there is no friction between the layers, the beam will deform as a classical beam having a rigidity equal to the sum of the individual layer rigidities. There will be no energy loss due to frictional interaction and the beam will recover completely from an imposed load. When the frictional interaction is infinite (or large enough to prevent any relative motion between the layers) the beam will clearly act as though it were a solid rather than a multi-layer beam. In this case the rigidity will be considerably higher than that of the previously described beam and again there will be no energy loss due to bending and the beam will recover completely if the material is elastic. The mechanics of both limiting cases of frictional effect have been considered in classic textbooks on strength of materials and a number of special investigations[1,2,3].

When friction acts between the layers of a beam, there will be an energy loss at each layer interface when the layers move relative to each other. This will have a significant effect on the mechanical behavior of the beam. The relation between load and deflection will be non-linear, it will depend on the direction of loading, and the recovery will not be complete. The case of a two-layer beam with friction and constant normal pressure has been investigated by Goodman[4] for an end loaded cantilever. He found this type of behavior to hold true in his investigation. In bending measurements of textile materials, Livesey and Owens[7] found similar results for fabric samples.

From fundamental engineering considerations, a general analysis of a multi-layered beam will be developed. From this, a number of special cases will be solved and experimental results presented. The information useful for the analysis of textile structures will be extracted and used in the following chapters of the thesis.

GENERAL ANALYSIS OF MULTI-LAYERED BEAMS WITH FRICTION

Load-Geometry Relation. The general problem to be solved is the deflected shape of a multi-layered beam subjected to arbitrary transverse loading. More specifically, consider the beam shown in figure 1-1. There are N layers indexed with the subscript "i" starting at a value of one for the bottom layer. Furthermore, let:

E = tensile modulus (lb/in^2)

w = layer width (in)

h = layer height (in)

I_ℓ = layer moment of inertia (in^4)

N = number of layers

V_i = shear force on i-th layer (lb)

M_i = bending moment on i-th layer (in/lb)

T_i = tension on i-th layer (lb)

f_i = shear stress per unit width on bottom of i-th layer (lb/in)

f_k = shear stress per unit width corresponding to sliding friction force (lb/in)

f_s = shear stress per unit width corresponding to static friction force (lb/in)

V = shear force on beam (lb)

M = bending moment on beam (in/lb)

T = tension on beam (lb)

k = curvature of centerline of beam (in^{-1})

e_i = tensile strain in x-direction in i-th layer

y = coordinate measured from center of beam to arbitrary point (in)

y_i = coordinate measured from center of beam to center of i-th layer (in)

x,z = space coordinates of centerline of beam (in)

C_i = average tensile strain on i-th layer

b_i = strain discontinuity term for i-th layer

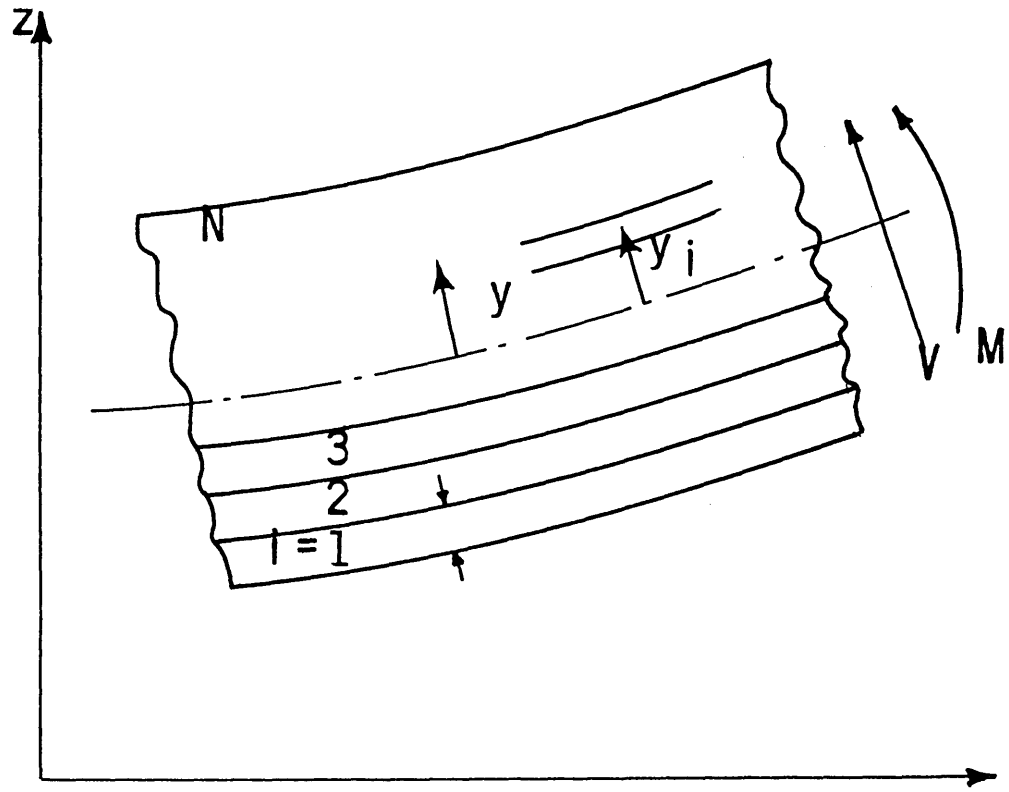

Fig. 1-1 MULTI-LAYER BEAM

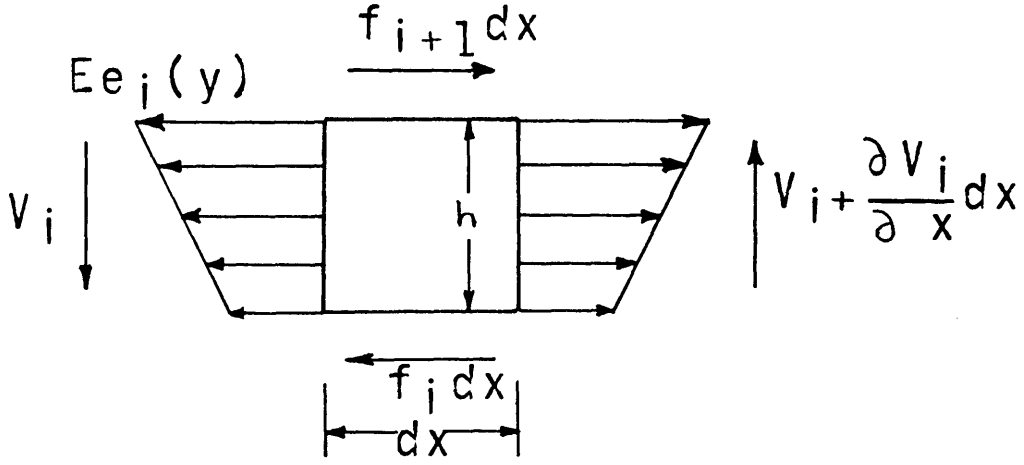

Fig. 1-2 ELEMENT OF MULTI-LAYER BEAM

C_i, D_i = integration constants

$u_{i+1,i}$ = relative motion between layers i, i+1 (in)

s = length coordinate along beam (in)

k_o = initial curvature (in^{-1})

φ = tangent angle

φ_o = initial tangent angle

It will be assumed that:

1. The radius of curvature of the beam is small compared to the beam thickness.

2. The material is linearly elastic.

3. The loading consists only of transverse loads.

4. The displacements are small.

The procedure used in formulating this analysis will first be to establish the types of strain distributions which are possible for a multi-layer beam and then to insure that each element of the beam is in equilibrium with the imposed loads.

The strain distribution in each layer consists of two parts, one related to the curvature of the layer in question and the other to the average tensile strain C_i. Expressed mathematically, this is,

$$e_i = y\left(\frac{k}{1 + y_i k}\right) - y_i\left(\frac{k}{1 + y_i k}\right) + C_i \qquad (1\text{-}1)$$

Under assumption 1, i.e. $y_i k$ is small, this becomes,

$$e_i = yk + b_i \qquad (1\text{-}2)$$

where b_i is $C_i - y_i k$. Note that the result of the strain analysis indicates that the strain on any layer consists of two terms, only one of which (b_i) depends on the layer index.

Since the value of b_i may be different for each layer the resulting strain distribution may be discontinuous. Although this is not possible for a conventional beam, it is certainly the case for multi-layered beams. The difference between the values of b_i for two adjacent layers is, of course, a measure of this strain discontinuity; and, as will be demonstrated later, a measure of the relative layer motion.

In the extreme case of no relative motion between the layers, all the b_i's are zero and the strain distribution is the same as the classical case. ($e_i = yk$). When there is no frictional interaction and the layers act independently, the equation reduces to $e_i = k\,(y - y_i)$. The intermediate cases of friction, which are of interest here, follow the form of equation 2 and the particular values of b_i will depend on the loading and the frictional interaction.

It should be noted that the values of k and b_i vary with position along the beam and k is a function of x only, and b varies with both x and i.

The equilibrium conditions will be established by assuring that each element of each layer and the beam as a whole is in equilibrium with the imposed forces and moments. Taking first the force equilibrium in the x-direction of an element h dx of one layer and referring to figure 1-2 gives,

$$T_i = Ew \int_{y=y_i-\frac{h}{2}}^{y_i+\frac{h}{2}} (ky + b_i)\,dy = Ewky_ih + Ewb_ih \qquad (1\text{-}3)$$

$$\frac{dT_i}{dx} = f_i - f_{i+1} \qquad (1\text{-}4)$$

$$Ewh\,\frac{dk}{dx}\,y_i + Ewh\,\frac{db_i}{dx} + f_{i+1} - f_k = 0 \qquad (1\text{-}5)$$

The force balance on the beam as a whole under the assumption of small deflections and transverse loads results in the requirement that the total beam tension be zero. In terms of the variables of interest, this becomes,

$$T = \sum_{i=1}^{N} T_i = 0 \qquad (1\text{-}6)$$

$$\sum_{i=1}^{N} (ky_i + b_i) = 0 \qquad (1\text{-}7)$$

The moment equilibrium requirement of an element of one layer can be found by again referring to figure 1-2. Summing moments about the centerline of an arbitrary layer gives,

$$\frac{dM_i}{dx} - V_i + \left(f_{i+1} + f_i\right)\frac{h}{2} = 0 \qquad (1\text{-}8)$$

$$V_i = EI_{\ell}\frac{dk}{dx} + \frac{h}{2}\left(f_{i+1} + f_i\right) \qquad (1\text{-}9)$$

Note that the sign convention established for the f_i terms is shown on figure 1-2. Summing the individual shear forces gives the overall shear force.

$$V = NEI_{\ell}\frac{dk}{dx} + \frac{h}{2}\sum_{i=1}^{N}\left(f_{i+1} + f_i\right) \qquad (1\text{-}10)$$

This equation may be written in terms of the moment on the beam. For this purpose, the classical relation between shear force and bending moment may be used. This relation is independent of the frictional effects within the beam.

$$\frac{dM}{dx} = V \qquad (1\text{-}11)$$

Alternatively, an equation for bending moment on the beam may be obtained by integrating the individual components of stress across the beam. The result of this operation gives the same effective result as equation 10, but in different form.

$$M = N^3 EI_{\ell}\, k + Ewh\sum_{i=1}^{N} b_i\, y_i \qquad (1\text{-}12)$$

One other relation required is the equation for determining the location of the center of the i-th layer. This can be shown to be,

$$y_i = \frac{h}{2}\left[2i - (N+1)\right] \qquad (1\text{-}13)$$

Algebraic manipulation of the above equations gives the relation between loading and geometry for a fixed frictional interaction. In this relation, load is expressed by the shear force and the geometry is given in terms of the curvature.

$$V = NEI_{\ell} \frac{dk}{dx} + h \sum_{i=2}^{N} f_i \qquad (1\text{-}14)$$

The shear stress terms, f_i, in equation 14 must be evaluated in order to solve the equation. This can be done immediately for two special cases: one in which there is no strain discontinuity; and one in which the shear stress is constant from layer to layer.

When there is no motion between the layers of the beam, the strain discontinuity (hence b_i) is zero and the load geometry relation can be obtained from equations 11 and 12.

$$V = N^3 EI_i \frac{dk}{dx} \qquad \text{(no slip)} \qquad (1\text{-}15)$$

When all the layers move relative to each other (the condition of complete slip), and when the normal force (between layers) and the coefficient of friction at any location along the beam are constant, the frictional forces, f_i, will also be constant at any location. This type of behavior corresponds to a complete slippage between the layers against frictional restraint. For a region of the beam where the direction of slip is such that the friction forces are positive according to the established sign convention, the result is,

$$V = NEI_i \frac{dk}{dx} + h\,(N-1)\,f_k \qquad \text{(complete slip)} \qquad (1\text{-}16)$$

This equation gives the load-geometry relation for loads sufficiently high to produce complete slip. The applicable range of equation 15 and of equation 16 will depend on the nature of the propagation of slip through the beam. This will be considered in greater detail later.

An interesting consequence of equation 16 can be found by examining the effect of the friction term. If the equation is integrated, it shows that the curvature of the multilayer beam may be different from zero even in a region having zero moment. Furthermore, this equation shows that in the region of non-zero moment it is possible to have a point of zero curvature. Both of these effects are not found in conventional beams. They will be explored in greater detail in the applications section of

this chapter.

For the case of no frictional interaction, the behavior of the multilayer beam is governed by equation 16 without the second term. This is the same as an equivalent beam having a rigidity equal to the sum of the individual rigidities of the layers. The difference in rigidity between this case and the case of infinite frictional effect is obtained by comparing this result with that of equation 15. The solid beam will be stiffer than the zero friction multilayer beam by a factor of N^2.

Strain Distribution. The strain distribution in the beam can be written from the equations already derived. The general form is,

$$e_i = yk + b_i \tag{1-2}$$

For the case of no relative motion this becomes,

$$e_i = yk \qquad \text{(no slip)} \tag{1-17}$$

For the case of complete slippage against a constant frictional restraint the strain may be computed by establishing the values of k and b_i from equations 5 and 16 in integrated form. The results are,

$$e_i = \begin{cases} \left(\frac{V-h(N-1)f_k}{NEI_i}\right)x\ (y-y_i) + \mathcal{C}_y + \mathcal{D}_i, & i \neq 1,\ N \\ \left(\frac{V-h(N-1)f_k}{NEI_i}\right)x\ (y-y_i) + \mathcal{C}_y + \mathcal{D}_i - \frac{f_k x}{Ewh}, & i=1 \\ \left(\frac{V-h(N-1)f_k}{NEI_i}\right)x\ (y-y_i) + \mathcal{C}_y + \mathcal{D}_i + \frac{f_k x}{Ewh}, & i=N \end{cases} \qquad \text{(complete slip)} \tag{1-18}$$

The quantities $\mathcal{C}$ and $\mathcal{D}$ are integration constants determined from the nature of the loading. The subscript on $\mathcal{D}$ indicates that the value of this constant depends on the layer in question. Note that during the case of complete slip, the interior layers have identical strain distributions differing only in the integration constant; and this constant is zero for many situations.

Slip Distribution. The relative motion between two layers can be found by taking the difference between the absolute motion of points at the interface of two adjacent layers. The displacement of a point at the top of layer i can be shown to be,

$$\frac{du}{dx}_{top,i} = e_{top,i} \tag{1-19}$$

Similarly, the displacement of a point at the bottom of layer i + 1 is,

$$\frac{du}{dx}_{bot.,i+1} = e_{bot.,i+1} \tag{1-20}$$

Combining these two equations and substituting for the strain discontinuity between the two layers gives the relative motion. The direction of positive relative motion has been chosen to correspond to a positive frictional force and the result is,

$$\frac{du}{dx}_{i+1,i} = b_{i+1} - b_i \tag{1-21}$$

The slip distribution may be formulated in an alternate way to provide a result that is useful for certain calculations. Consider a multilayer beam having an initial curved shape that is deformed to a new geometry. Assume that the layers remain in contact and that the relative slip may be approximated by that of a beam having no friction. Let s be a coordinate running along the interface between the i + 1 and i-th layers. The relative motion of the layers can be found in terms of the strain distributions as before.

$$\frac{du}{ds}_{i+1,i} = e_{bot.,i+1} - e_{top,i} \tag{1-22}$$

In this case, however, the strains may be evaluated in terms of the changes of curvature to give the relative slip.

$$e_{bot.,i+1} = -\frac{h}{2}(k - k_o) \tag{1-23}$$

$$e_{top,i} = \frac{h}{2}(k - k_o) \tag{1-24}$$

$$\frac{du}{ds}_{i+1,i} = -h(k - k_o) \tag{1-25}$$

This analysis is not restricted to small deflections and the most useful result is obtained by replacing the curvature with the derivative of tangent angle with respect to arc length.

$$k = \frac{d\varphi}{ds} \tag{1-26}$$

$$\frac{du_{i+1,i}}{ds} = -h\left(\frac{d\varphi}{ds} - \frac{d\varphi_o}{ds}\right) \tag{1-27}$$

Integrating gives,

$$u_{i+1,i}(s) = -h\left[\varphi(s) - \varphi_o(s)\right] + u_{i+1,i}(o) \tag{1-28}$$

This equation shows the interesting result that the displacement at any point depends only on the change of tangent angle at a given location and an additive constant. It means that the relative motion an element feels is not dependent on the change in shape of the beam, but only dependent on that particular element's change of tangent angle. For the case of an initially straight beam with the coordinate s measured from a point having no relative slip, the relative motion will be,

$$u_{i+1,i} = -h\varphi \tag{1-29}$$

Longitudinal Shear Stress. In the previous analysis, the general equations were reduced to the special cases of no relative motion and complete relative motion against a frictional restraint. The question still remaining is to find how slip propagates through the beam as the load is increased.

The approach taken is to compute to local shear stresses tending to separate the layers of the beam before slip occurs and compare this value to the shear stress that can be resisted by static friction between the layers. Clearly, if the imposed shear stress is below that which can be resisted, there will be no slip and if it is greater, there will be slip.

In order to make the comparison between the imposed and allowable shear stresses, it is necessary to know the nature of the loading. However, the values of imposed shear stress can be

calculated in a fairly general sense. That will be done in this section; and, the results obtained will be used to compute the propagation of slip in two of the examples given in the applications section of this chapter.

The longitudinal shear stress of a solid beam has been solved by classical beam theory methods[6]. In this case, the shear stress results from an imposed transverse shear force on the beam. In multilayer beams a shear force will also produce a longitudinal shear stress, but surprisingly enough it is possible to have a longitudinal shear stress even if there is no transverse shear force. This is because discontinuous stress distributions can occur in multilayer beams, and they can cause longitudinal shear stresses. For this reason the computation will be broken into two parts and the two contributing factors to longitudinal shear stress will be analyzed separately.

Longitudinal Shear Stress due to Transverse Shear Force. To have a measure of the shear stress tending to separate the layers, the shear stress distribution must be computed for an arbitrary number of layers sticking together. In addition, it is necessary to allow any combination of surface shear forces to act on top and bottom of these layers. There are three such combinations of interest: in the first, all the layers stick together and there is zero surface shear stress; in the second, a group of interior layers sticks together and there is a constant shear stress corresponding to sliding friction on both sides of the group; and in the third, a group of layers has one side on the interior of the beam where the sliding frictional stress acts and one side at the surface of the beam where there is no shear stress.

In order to solve for the three cases mentioned above for any number of layers sticking together in a group, consider an element h^*dx of the beam shown in figure 1-3, also a subelement $(h^*/2 - y^*)dx$. Now let:

f_t = shear stress per unit width on top of element (lb/in)

f_b = shear stress per unit width on bottom of element (lb/in)

f_{y^*} = shear stress per unit width at position y^* (lb/in)

y^* = coordinate measured from center of the group (in) to the bottom of the subelement.

T_s = tensile force on subelement of figure 1-3 (lbs)

h^* = height of element (in)

e = strain at any point

e_t = average strain on element, $h^* dx$

ζ = dimensionless coordinate.

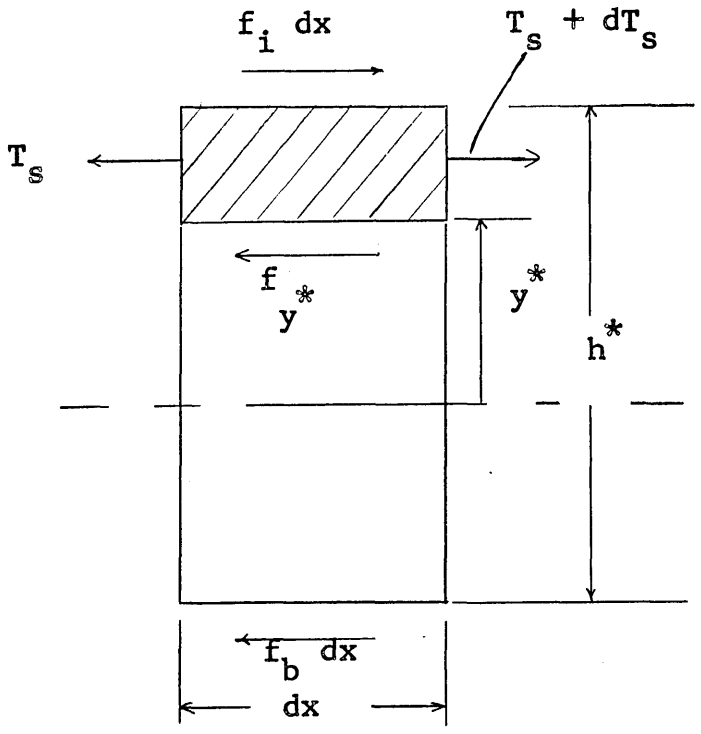

Fig. 1-3 Force Balance on a Volume Element in a Group of Non-Sliding Layers

An equation for the shear stress at any position within the group of layers may be obtained from the condition of force equilibrium in the x-direction. For the subelement shown in figure 1-3 this is,

$$\frac{dT_s}{dx} = f_{y^*} - f_t \tag{1-30}$$

A similar force balance for the h^*dx element of figure 1-3 yields,

$$\frac{de_T}{dx} = \frac{f_b - f_t}{Ewh^*} \tag{1-31}$$

The tension on the subelement may be found by integrating the stress distribution.

$$T_s = \int_{y^*}^{h^*/2} Ewedy^* = \frac{Ew}{2}\left[k\frac{h^*}{2} + ky^* + 2e_T\right]\left[\frac{h^*}{2} - y^*\right] \tag{1-32}$$

Substituting this result into equations 30 and 31 and using a dimensionless coordinate in place of y^* gives the result,

$$f_{y^*} = \frac{Ewh^{*2}}{8}\frac{dk}{dx}(1 - \zeta^2) + \frac{(f_b - f_t)}{z}(1 - \zeta) + f_t \tag{1-33}$$

$$\zeta \equiv \frac{2y^*}{h^*} \tag{1-34}$$

The three special cases mentioned before can be solved by taking the appropriate values for the shear stress on top and bottom of the group of layers. The results are:

Case 1 $f_b = f_t = 0$ (group of layers corresponds to total beam)

$$f_{y^*} = \frac{Ewh^{*2}}{8}\frac{dk}{dx}(1 - \zeta^2) \tag{1-35}$$

Case 2 $f_b = f_t = f_k$ (group of layers is on interior of beam)

$$f_{y^*} = \frac{Ewh^{*2}}{8}\frac{dk}{dx}(1 - \zeta^2) + f_k \tag{1-36}$$

Case 3 f_b 0, $f_t = f_k$ (bottom of group of layers lies on surface of beam and top of group lies in interior)

$$f_{y^*} = \frac{Ewh^{*2}}{8} \frac{dk}{dx} (1 - \zeta^2) + \frac{f_k}{2} (1 + \zeta) \qquad (1\text{-}37)$$

Note that the distribution of shear stress is parabolic in all cases and has the appropriate values on the boundaries. It is expressed in terms of rate of change on curvature instead of shear force. This is because the relation between shear force and rate of change of curvature depends on the particular problem in question and the mode of slip propagation.

In the applications section of this chapter the imposed shear stress will be computed and compared to the allowable shear stress. This will permit calculation of the development of slip throughout one type of loaded beam.

Longitudinal Shear Stress due to Discontinuous Strain Distribution. The shear stress developed by a discontinuous strain distribution exists even if there is no net shear force on the beam. To demonstrate this point, consider a multilayer beam subjected to a symmetrical four-point loading. In the central region of the beam there will be a constant moment and no shear force. However, if the friction between the layers is moderate, they will slide by one another even in the region where the shear force vanishes. The explanation for this phenomenon lies in the fact that if slip occurs in the region just outside of the constant moment zone, the stress distribution at the boundary of the zone will be discontinuous. This discontinuity will produce a shear stress along the interface of two layers as shown on figure 1-4.

The shear stress will be greatest at the beginning of a region of no slip and it will decrease to zero in a relatively short distance. If it exceeds the shear stress that can be resisted by static friction, slip will start propagating into the material. As the slip propagates, the strain discontinuity will diminish

due to a reduction of curvature, and thereby reduce the imposed shear stress. The propagation will then continue until the imposed shear stress is no longer great enough to overcome friction.

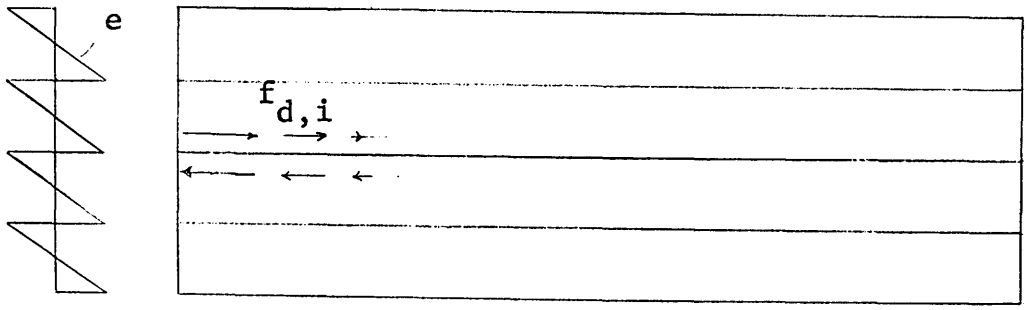

Fig. 1-4 Longitudinal Shear Stress in Non-Slipping Region Developed by Discontinuous Strain Distribution

In order to estimate the shear stress for the case of strain discontinuity a two-dimensional stress analysis was used. The shear stress distribution was assumed to be the same as that in a large solid block of material subjected to a sawtooth stress distribution on each side. This assumption makes it possible to use the available solutions for the stress distribution in a material loaded by sinusoidally varying loads on both sides. This solution can be summed by a Fourier series to obtain the results for the discontinuous loads actually applied. The details of the calculation are given in the Appendix A and the resulting shear stress function is,

$$f_{d,i} = \frac{Ew}{\pi}\left[\frac{2\pi x}{h}\right]\frac{e^{\frac{-2\pi x}{h}}}{1 - e^{\frac{-2\pi x}{h}}}\,(b_{i-1} - b_i) \qquad (1\text{-}38)$$

Where:

$f_{d,i}$ = shear stress per unit width on bottom of i-th layer due to discontinuous strain distribution.(lbs/in)

x = distance along the beam measured from beginning of no slip region. (in).

The shear stress decays rapidly and at a distance equal to about one layer height its magnitude is about 1% of the original value. The maximum shear stress occurs at the beginning of the no-slip region and its value is,

$$f_{\substack{d,i \\ max}} = \frac{Ew}{\pi} (b_{i-1} - b_i) \qquad (1\text{-}39)$$

This imposed stress will determine whether or not slip will propagate into a multilayer beam when it is compared to the static friction force per length that can be generated between the layers.

APPLICATIONS OF THE THEORY OF BENDING OF MULTILAYERED BEAMS WITH FRICTION

Simply Supported Beam with Constant Normal Force--Theoretical. As a first example of the proposed theory, consider a beam that is simply supported as shown on figure 1-5. From symmetry the beam can be replaced by a cantilever of one-half the length as shown.

The problem is to establish the deflected shape of the beam for a given loading. To do this, the following assumptions will be made:

1. The assumptions of the general analysis hold
2. The normal force between layers is constant and unaffected by the imposed bending loads
3. The slip has propagated throughout the beam. (This last assumption will be dropped later when the transition region is examined in detail.)

Let:

a = position of load application

L = length of cantilever

x,z = coordinate system for describing centerline deflection.

with other variables as before.

The equation for relating load to geometry can be obtained from equation 16 by substituting the appropriate values of shear force in each of the two regions of the beam. The result is,

$$\frac{dk}{dx} = \begin{cases} \dfrac{-h(N-1)f_k}{NEI_e} & 0<x<a \\ \dfrac{V-h(N-1)f_k}{NEI_e} & a<x<L \end{cases} \qquad (1\text{-}40)$$

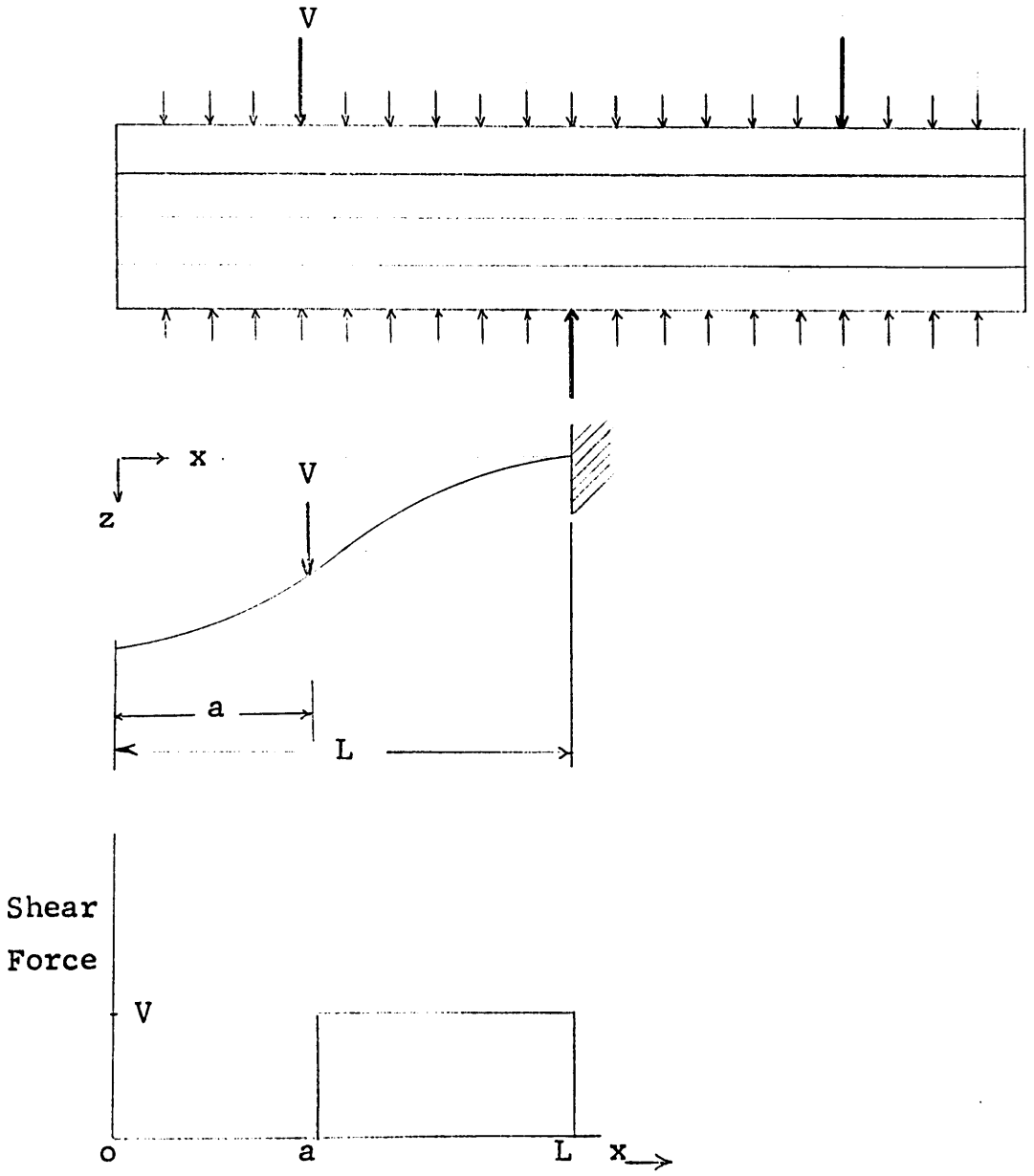

Fig. 1-5 Simply Supported Multi-Layer Beam under Constant Transverse Pressure

Equation 40 can be integrated and the constants evaluated by setting the curvature equal to zero at the free end and by assuring its continuity between the two regions. Then, the resulting curvature function can be set equal to the second derivative of the displacement since the deflections are assumed small.

$$k(x) = \frac{d^2z}{dx^2} = \begin{cases} \dfrac{-h(N-1)f_k x}{NEI_\ell} & o < x < a \\ \dfrac{(V-h[N-1]f_k)x}{NEI_\ell} - \dfrac{Va}{NEI_e} & a < x < L \end{cases} \qquad (1\text{-}41)$$

An interesting observation can be made from this equation. In the region of the beam outside the point of load application there is neither a shear force nor a bending moment. However, there <u>is</u> a curvature in this region, and its direction is opposite to that in the region near the wall. This effect will be referred to as "reverse curvature". It has been observed experimentally (see figure 1-8) and constitutes perhaps one of the most interesting effects of friction in a multilayered beam. When the frictional forces are sufficiently great so that the beam behaves as a solid, there is no reverse curvature; and, when the interlayer friction is zero, there is also no reverse curvature. Clearly then, this effect is limited to those intermediate cases of friction where there is relative motion against a frictional restraint.

Another interesting effect which is predicted by equation 41 and was observed experimentally is that the curvature is zero between the load and the wall . This occurs at a point at which the bending moment exists. In classical beams that are originally straight, inflection points occur only at points of zero moment.

The differential equation for the beam deflection can most easily be solved by first converting it to dimensionless form. For this purpose let,

$v = z/L$ = dimensionless deflection

$u = x/L$ = dimensionless coordinate along beam

$\gamma = a/L$ = dimensionless load location

$$R = \frac{(N-1)f_k h L^2}{NEI_\ell} = \text{dimensionless measure of relative effect of friction to elasticity}$$

$$S = \frac{L^2 V}{NEI_\ell} = \text{dimensionless deflection of end loaded cantilever with no friction.}$$

Substituting these variables into equation 41 gives the dimensionless differential equation and the boundary conditions.

$$\frac{d^2 v}{du^2} = \begin{cases} -Ru & o<u<\gamma \\ (S-R)u - S\gamma & \gamma<u<1 \end{cases} \qquad (1\text{-}42)$$

$$\frac{dv}{du}(1) = v'(1) = 0$$

This equation can be solved with the additional requirement that the displacement and slope be continuous at the point of load application. The resulting solution is,

$$v = \begin{cases} S\left[\frac{1}{3}(1-\gamma)^3 + \frac{1}{2}(1-\gamma)^2(\gamma-u)\right] - R\left[\frac{1}{2}(1-u)^2 - \frac{1}{6}(1-u)^3\right] & o<u<\gamma \\ S\left[\frac{1}{2}(1-\gamma)(1-u)^2 - \frac{1}{6}(1-u)^3\right] - R\left[\frac{1}{2}(1-u)^2 - \frac{1}{6}(1-u)^3\right] & \gamma<u<1 \end{cases} \qquad (1\text{-}43)$$

This equation is plotted on figure 1-6 for $\gamma = \frac{1}{2}$ and for several values of R/S which is a measure of the relative effect of friction versus the imposed load.

As a check on the solution it is necessary to determine whether the direction of relative slip at each point corresponds to the direction of friction force. Since the friction force was taken as being positive for the loading cycle, the relative slip must also be positive (based on the sign convention established previously). The slip distribution can be determined by first establishing the strain distribution from equation 18 and then integrating this result in accordance with equation 21. The result is that the directions do not correspond for all points along the beam and it becomes necessary to make a slight modification of the solution. This can most easily be done by using the method of equation 29 to determine slip direction. Applied

Fig. 1-6 Deflected Shape of Multi-Layer Cantilever with Point Loading

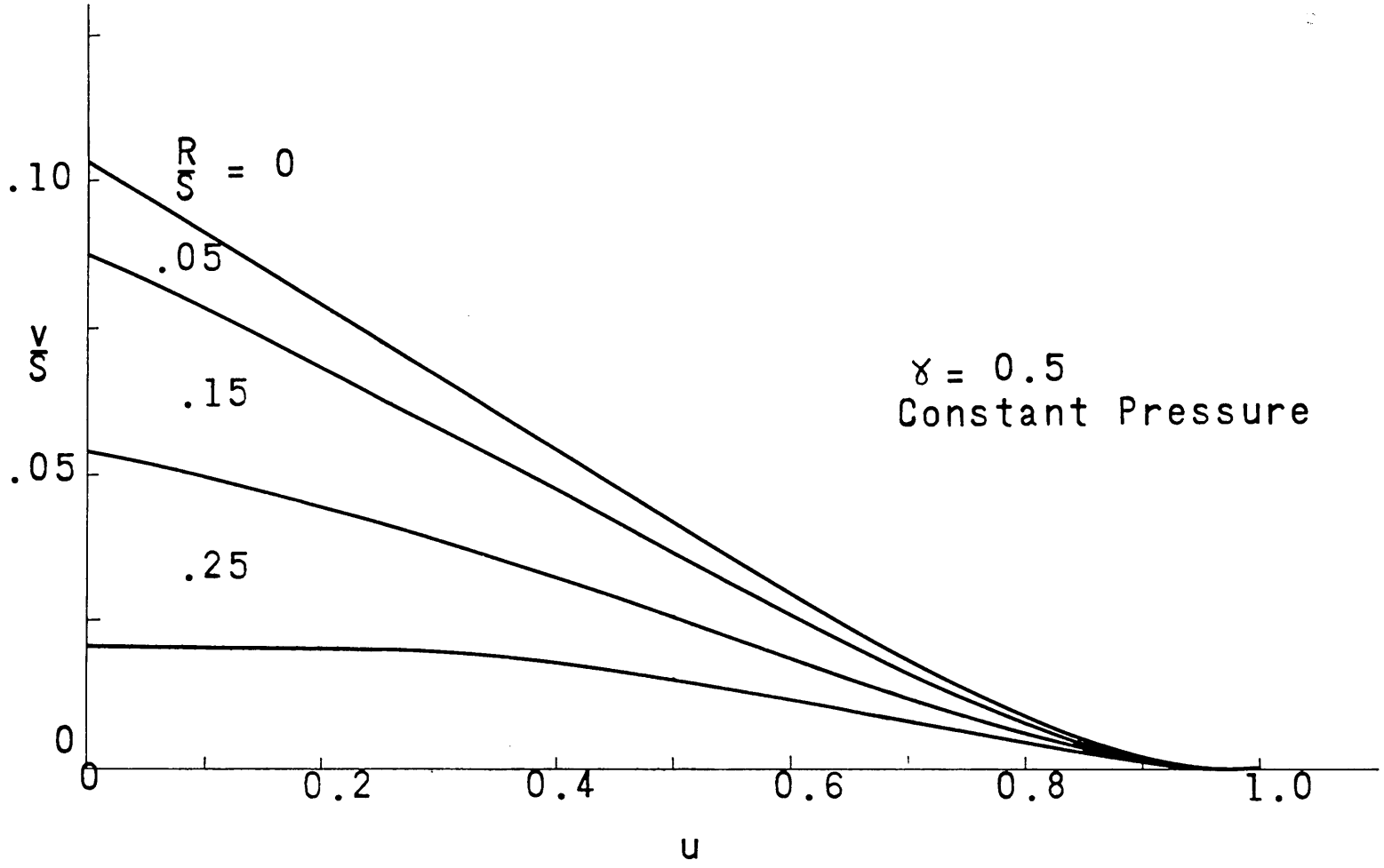

to this case the equation states that the slip will be positive when the slope of the deflection curve is negative. This means that the solution holds when all points on the beam, except at the wall, have negative slopes. This will be the case when the applied load exceeds a certain level which depends on the frictional interaction and geometry of the beam. This level of load can be calculated by finding the conditions under which the slope of the deflection equation goes to zero in the interior of the beam. From equation 43 it can be shown that this slope goes to zero when,

$$\frac{1}{2}(1-\gamma)^2 - \frac{R}{S}\left[\frac{1}{2}(1-u)^2 - (1-u)\right] = 0 \qquad (1\text{-}44)$$

The point of zero slope calculated from this equation must lie outside of the beam itself for the deflection solution to hold. From equation 44 it can be shown that this is the case when,

$$\frac{S}{R} = \frac{V}{(N-1)f_k h} > \frac{1}{(1-\gamma)^2} \qquad (1\text{-}45)$$

At loads below the value indicated by this equation, the original deflection equation does not hold and the deflection shape must be computed by a different procedure. For positions u, which do not reach the point of zero slope, the beam acts as a solid beam and the deflection curve for these positions is horizontal. For values of u greater than this, the original equation can be used with revised boundary conditions. Nevertheless, the original equation still holds when the condition of equation 45 is satisfied.

A useful relation for experimental investigations of the proposed theory can be obtained by finding how the load varies with the displacement at the point of load. This can be found directly from equation 43 by setting $u = \gamma$.

$$V(\gamma) = S\left[\frac{1}{3}(1-\gamma)^3\right] - R\left[\frac{(1-\gamma)^2(2+\gamma)}{6}\right] \qquad (1\text{-}46)$$

In terms of force versus displacement this equation becomes,

$$V = \left[\frac{NEI_\ell}{L^3}\ \frac{3}{(1-\gamma)^3}\right]\delta + \left[(N-1)f_k h\ \frac{(2+\gamma)}{2(1-\gamma)}\right] \qquad (1\text{-}47)$$

Where,

δ = displacement under the load.

This predicted force-displacement equation consists of two terms. The first represents the linear relation between force and displacement which is obtained for a multilayer beam without friction. The second represents the additional amount of force which has to be added to overcome the frictional restraint. During unloading, the direction of slip reverses and the sign of the second term changes.

In accordance with the assumptions made in the analysis, equation 47 is valid only after the slip has propagated throughout the beam. The behavior preceding this condition consists of an initial region in which the beam acts as a solid unit and a transition region in which the slip develops. This will be considered in greater detail later.

Simply Supported Beam with Constant Normal Force--Experimental. An experiment was performed to determine the validity of the theoretical relations developed for the simply supported multilayer beam. This was done by taking a number of strips of polyvinyl-chloride and subjecting them to a normal force created by an arrangement of rods and elastic strips as shown on figure 1-7.

Prior to the bending tests, measurements were made to determine the quantities required for the theoretical expressions. The results were:

EI_{ℓ} = 0.37 lb-in^2

N = 15

L = 6 in.

h = 0.028 in.

w = 0.50 in.

The one remaining value which was required--the friction force per length--was measured separately for each normal force which was applied. The procedure used in making all the measurements is described in detail in Chapter IV. This includes the preliminary

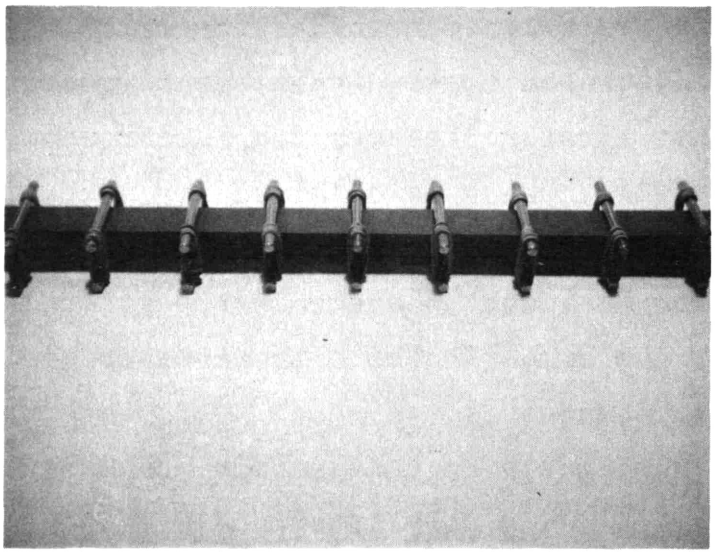

Fig.1-7 EXPERIMENTAL MULTI-LAYER BEAM UNDER CONSTANT PRESSURE

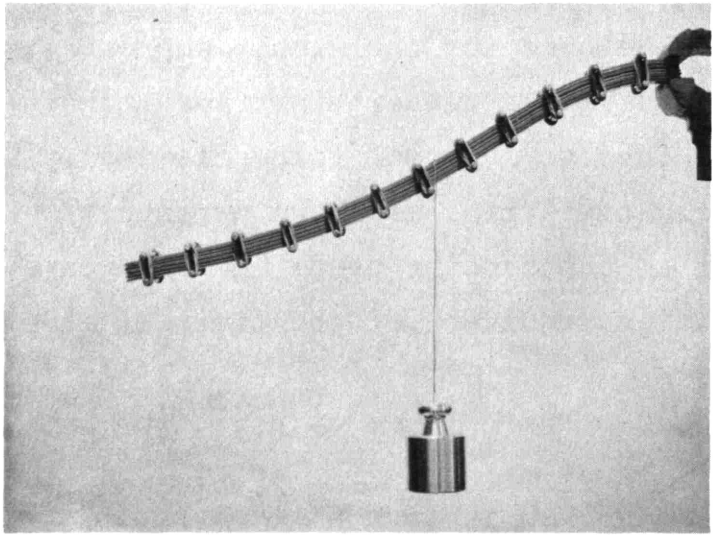

Fig.1-8 REVERSE CURVATURE RESULTING FROM INTERLAYER FRICTION

measurements and the bending tests.

Measurements were made of the force-displacement curve at the point of loading. This was done for three different pressures and for loads applied at varying positions along the beam. A three-point loading as shown on figure 4-8 was used. The effective cantilever length was half the total length, and the force-displacement curve was measured for the outside loads. The loads were applied by means of an Instron Tensile Testing Machine which imposed a constant rate of displacement.

The results showed that the relation between force and displacement was as shown on figure 9.

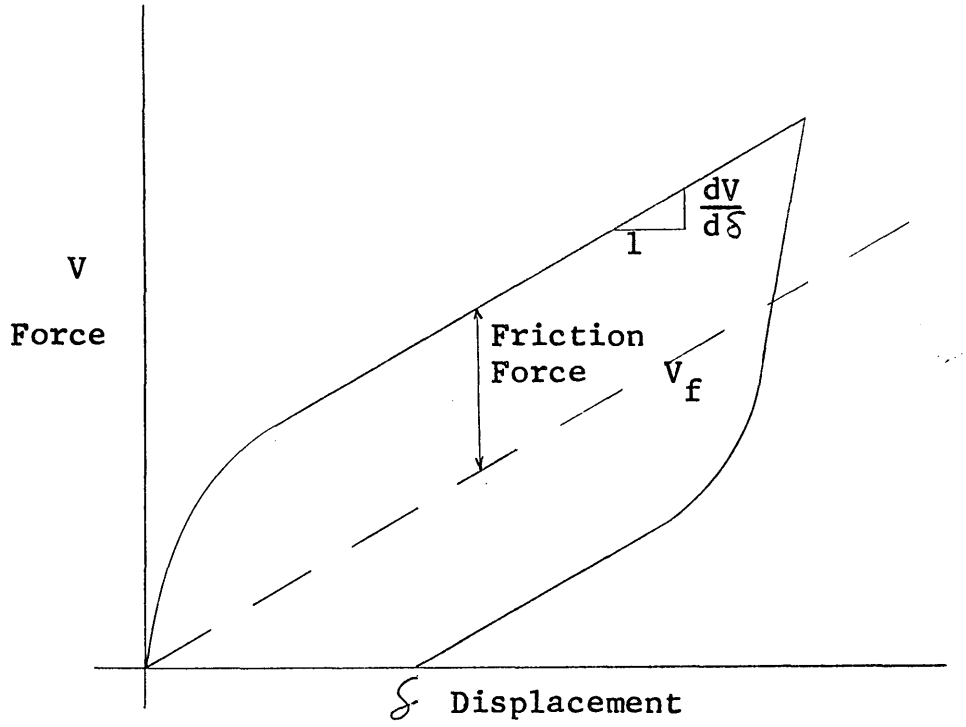

Fig. 1-9 Typical Force-Displacement Curve Measured for Simple Supported Multi-Layer Beam

The slope and friction force of each curve was measured for comparison with the values predicted by equation 47. This equation can be rewritten in the following form.

Fig. 1-10 Multi-Layer Beam Stiffness vs Position of Load

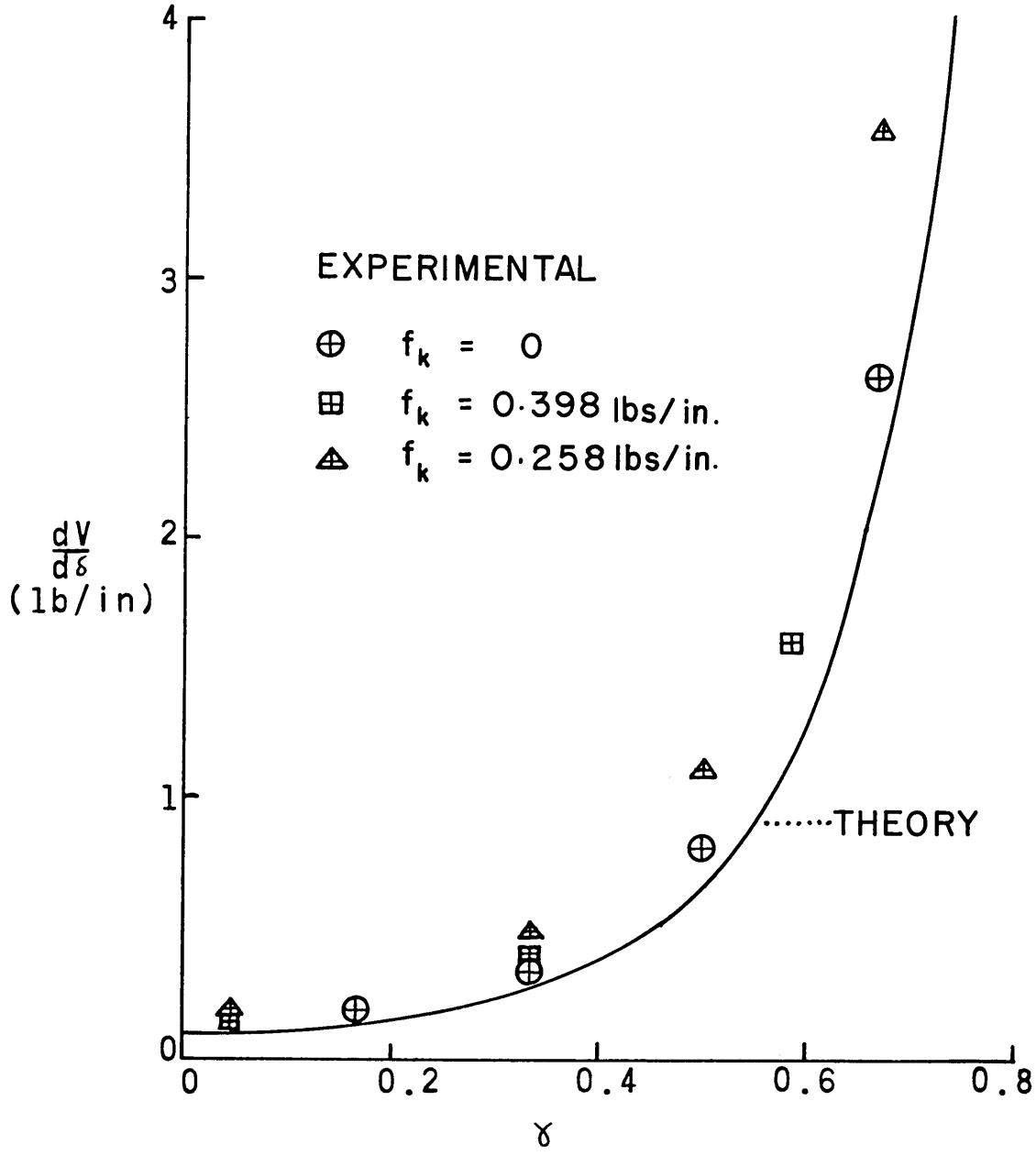

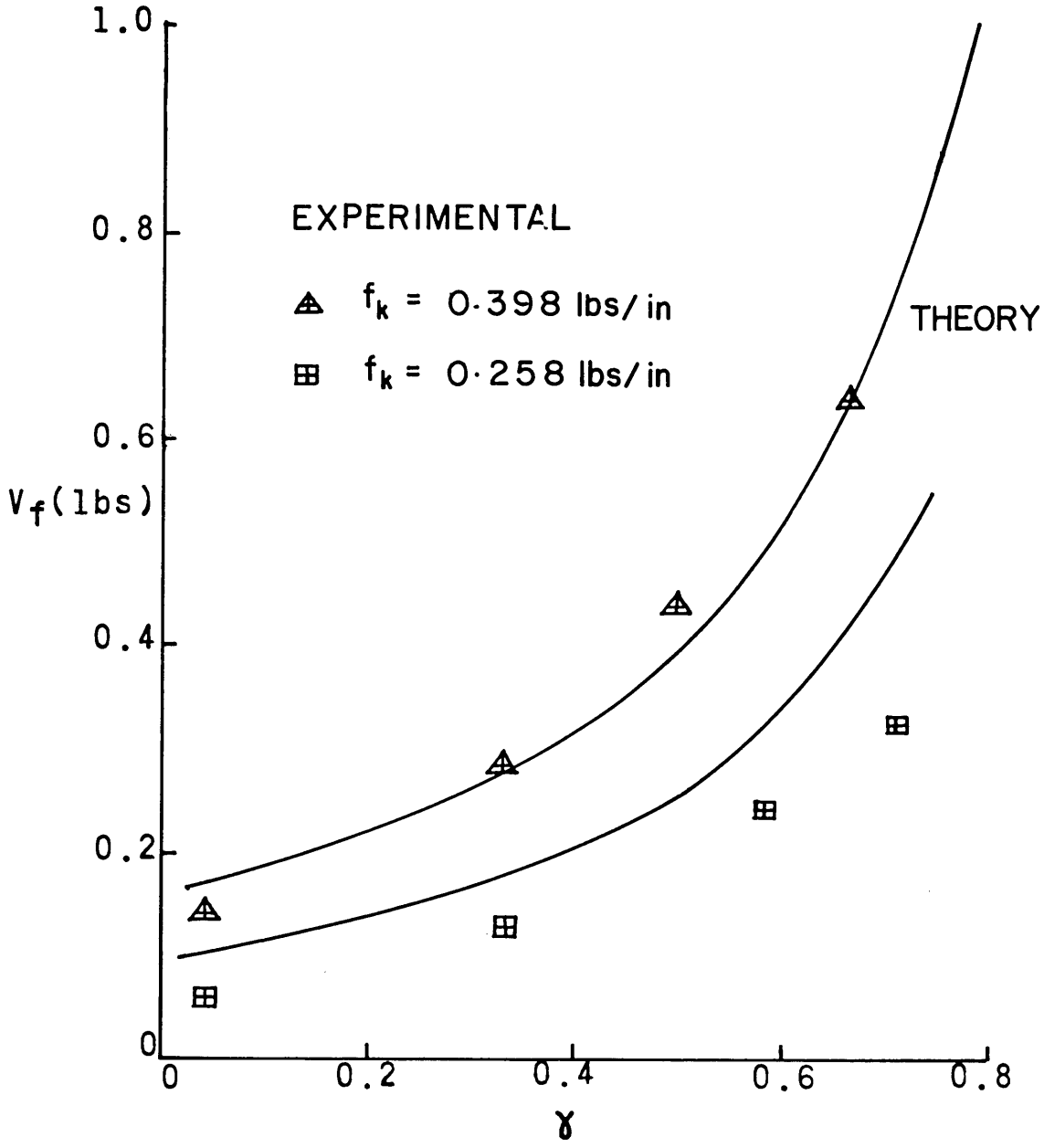

Fig. 1-11 FRICTION FORCE VS POSITION OF LOAD

$$\text{Slope} = \frac{dV}{d\delta} = \frac{3}{(1-\gamma)^3} \frac{NEI_\ell}{L^3} \tag{1-48}$$

$$\text{Friction Force} = V_F = \frac{2+\gamma}{2(1-\gamma)} f_k(N-1)h \tag{1-49}$$

These quantities are plotted on figures 10 and 11 as functions of γ using the measured values of N, EI_ℓ, L, f_k, and h. The measured values are plotted on the same graphs.

Agreement between theory and experiment appears to be good. On the basis of the properties of the individual layers of the beam, the interaction between layers, and the geometry of system it was possible to predict the bending behavior. Note, however, that the predicted slope was independent of the amount of frictional interaction, whereas there was a difference between the measured values. This indicates that the assumption that slip has propagated through the beam and continues to do so as loading proceeds is not entirely justified. For this reason the propagation of slip was investigated in greater detail and will be discussed later.

During the bending tests, some of the loaded beams were photographed to measure the deflection curves. These measured shapes were compared to the predicted shapes and the results are shown on figure 1-12. Here the parameters input to the deflection theory were the measured slope and friction force. Again, the results indicate agreement between measurement and prediction. Note, however, that the measured reverse curvature was greater than that predicted. This may be due to the approximation made in setting the curvature equal to the second derivative of displacement. It may also be due to a lengthwise variation in friction force caused by the applied loads.

Propagation of Slip in Simply Supported Beam. The previous analysis of the simply supported beam was limited to beams in which slip had propagated throughout the structure. In this analysis the nature of the slip propagation phenomenon will be

Fig. 1-12 Theoretical and Measured Deflection Curves

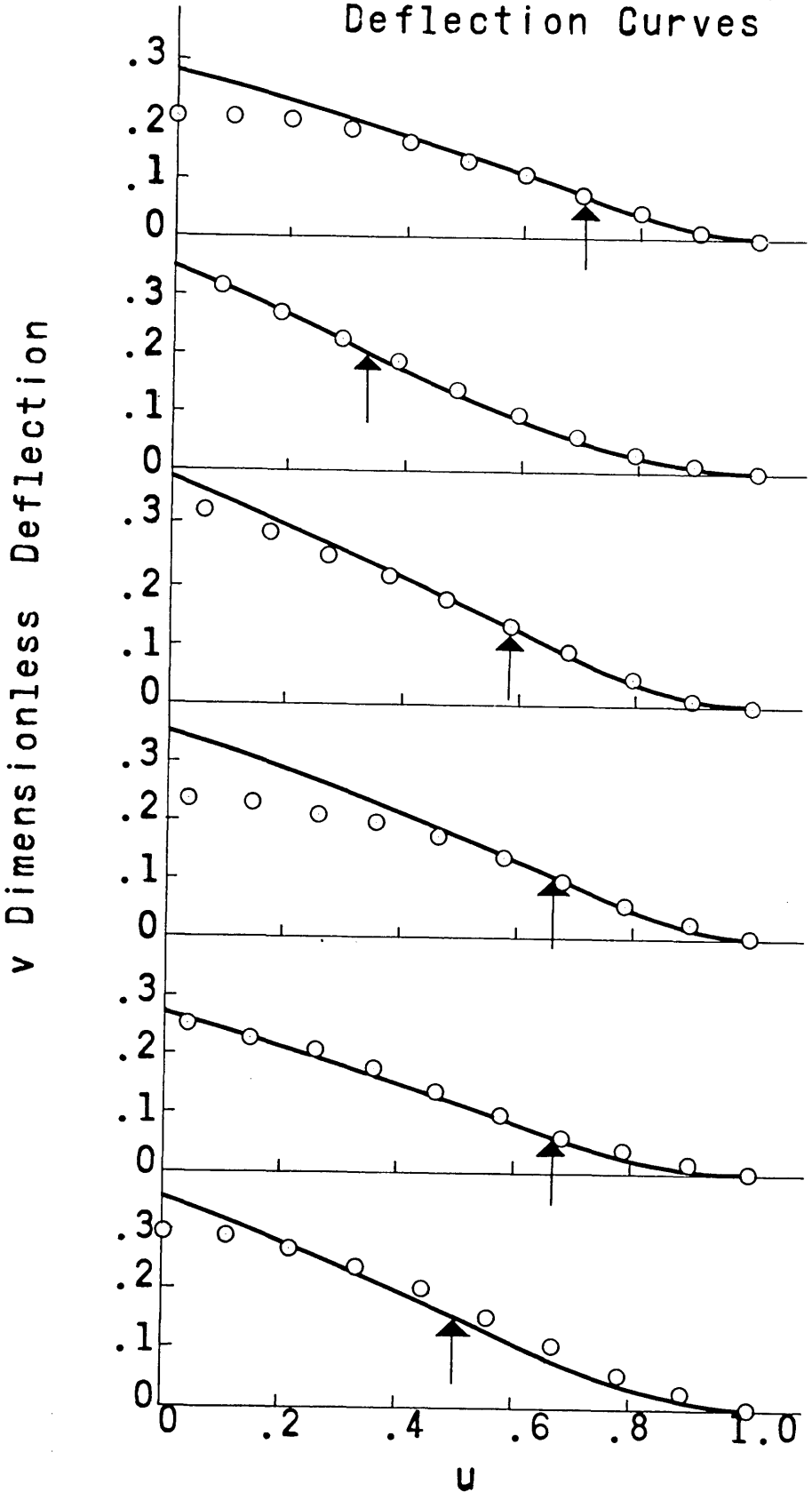

considered in detail in an attempt to determine the shape of the force-displacement curve in the initial region. The basic principle to be used is that two layers will slide relative to each other when the shear stress tending to cause this movement exceeds the shear stress which can be resisted by static friction.

The analysis will be limited to the simply supported beam which has no overhang. ($\gamma = 0$). This is, of course, the same problem as a cantilever with a point load at the end. The assumptions which will be used are the same as those of the previous analysis with the additional assumption that the static and kinetic coefficients are equal. The results for this assumption will be analyzed qualitatively to determine the effect of differences between the coefficients. It will also be assumed that slip will continue once it has occurred at an interface.

When the beam of figure 1-5 with $\gamma = 0$ is loaded, the initial shear stress distribution can be obtained from equation 35 by letting $h^* = Nh$. The maximum value occurs at the center. For an even number of layers there will be an interface at this point and slippage will occur when the imposed stress equals the amount which can be resisted.

$$\left(\frac{dk}{dx}\right)_{\substack{1st \\ slip}} = \frac{8f}{Ewh^2N^2} \tag{1-50}$$

The subscript has been dropped from the friction force term because of the assumptions of equal coefficients of friction. As the load exceeds the point of first slip, the beam will behave as two halves slipping at the center. Because of the slippage, the surface force on each of these two halves will remain fixed at a level corresponding to the friction force. The shear stress distribution in each half will follow the form of equation 36 with $h^* = Nh/2$. This distribution increases in magnitude as the load increases and will continue to do so until a second interface attains a shear stress great enough to produce slip. This second slip will be at the layers above and below the center of the beam

since the shear stress will reach the critical value first at those locations. At this second point of slip,

$$\left.\frac{dk}{dx}\right|_{\substack{2nd\\slip}} = \frac{8f}{Ewh^2N(N-2)} \tag{1-51}$$

Following this second slip the beam will consist of two sliding layers in the center surrounded by two groups of layers that have not yet slipped. As the load increases further, the slip propagation will proceed outward from the center until each layer slips. A general formulation can be made to define the point of each slip, using the same procedure as above. The result is,

$$\left.\frac{dk}{dx}\right|_{\substack{j\text{-th}\\slip}} = \begin{cases} \dfrac{8f}{Ewh^2}\dfrac{1}{N^2} & j=1 \\ \dfrac{8f}{Ewh^2}\dfrac{1}{[N-2(j-2)]\,[N-2(j-2)-2]} & j=2,3,4,\ldots\dfrac{N}{2} \end{cases} \tag{1-52}$$

Alternatively, this equation can be written in terms of the number of layers sliding in the interior of the beam. Letting

S = number of layers sliding in center of beam,

$$\left.\frac{dk}{dx}\right|_{\substack{end\ of\ S\\layers\\sliding}} = \begin{cases} \dfrac{8f}{Ewh^2}\dfrac{1}{N^2} & 1st\ Slip \\ \dfrac{8f}{Ewh^2}\dfrac{1}{(N-S)(N-S-2)} & S=0,2,4,\ldots N-4 \end{cases} \tag{1-53}$$

As the load increases and the slip propagates, the shear stress distribution changes from the parabolic shape which exists at the point of first slip to one which levels out to a distribution of small parabolic sections for each of the sliding layers. This is illustrated in figure 1-12.

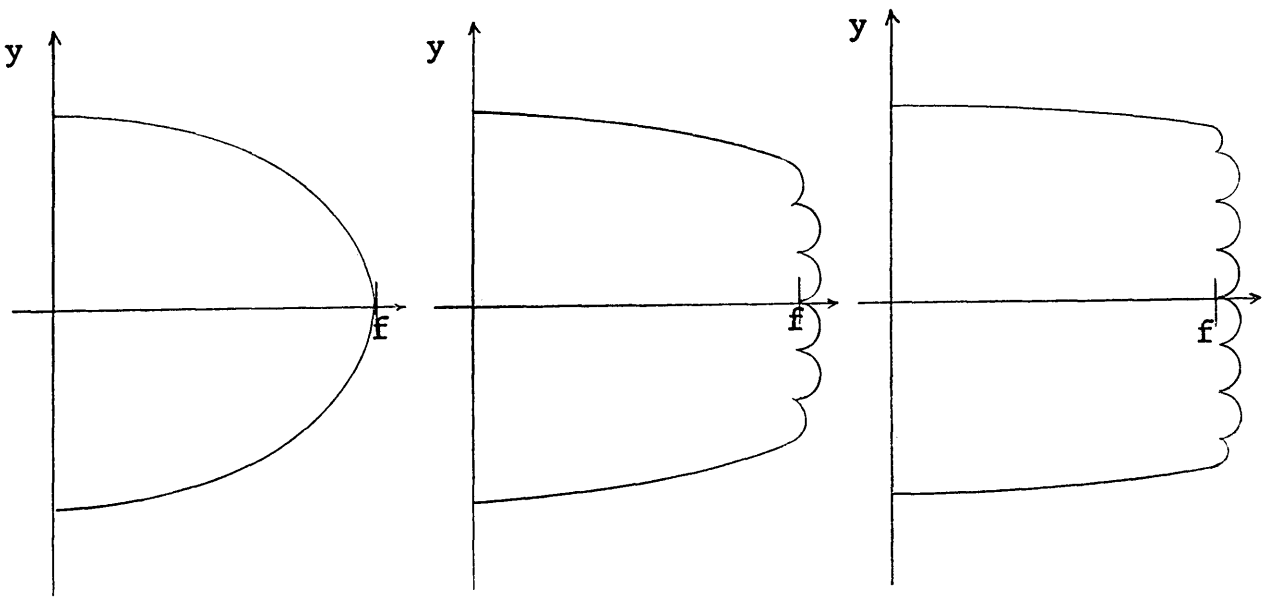

a. At 1st Slip b. At Intermediate Stage c. After Complete Slip

Fig. 1-13 Shear Stress Distribution Transition in Beam with Constant Shear Force

For the assumptions made here, it was possible to determine the mode of slip propagation. Now it is necessary to compute the load-deflection behavior that the beam undergoes during each of the intermediate modes. This can be done by applying the equations derived in the general analysis to the case of layers of varying thickness sliding against a frictional restraint. The result is,

$$V = \begin{cases} EI_e \frac{dk}{dx} N^3 & \text{before 1st slip} \\ EI_e \frac{dk}{dx}\left[S+\frac{1}{4}(N-S)^3\right] + fh\left[\frac{N+S}{2}\right] & S=0,2,4,6,\ldots N-4 \\ EI_e \frac{dk}{dx} N + fh\left[N-1\right] & \text{after last slip} \end{cases} \qquad (1\text{-}54)$$

Each mode has a behavior indicated by the above equation. The relation between V and dk/dx is linear for each stage of deformation; and the slope gets progressively smaller while the V-intercept increases. This is shown qualitatively on figure 1-13.

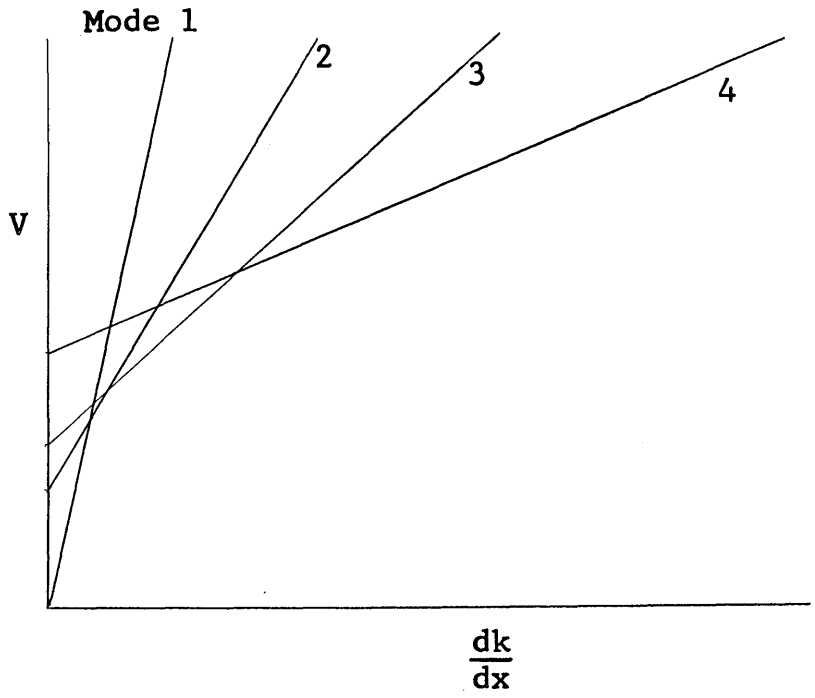

Fig. 1-14 Relation Between Load and Geometry for Each Mode of Slip

In order to obtain the final behavior, the force-geometry relation at each mode (equation 54) must be combined with the relation which gives the points of slip (equation 53). The result of this computation shows that for the assumption of equal static and kinetic coefficients of friction the points of slip correspond to the intersection of the load-geometry curves of equation 54 and figure 1-13. This fact considerably simplifies the calculations since the entire transition behavior can be defined by equation 54. Each individual equation holds until it intersects with the next equation.

The transition can be written in terms of force versus deflection by converting the derivative of curvature to the displacement under the load.

$$\frac{d^3z}{dx^3} = \frac{dk}{dx} = \text{constant}$$

$$\frac{dz}{dx}(L) = 0 = z(L)$$

$$z(0) \equiv \delta$$

$$\therefore \quad \delta = \frac{L^3}{3}\frac{dk}{dx} \qquad (1\text{-}55)$$

Before writing the final equation it is convenient to define two variables: the spring constant of a solid cantilever (c); and the total thickness of the beam (H).

$$c = \frac{3N^3 EI_\ell}{L^3} \tag{1-56}$$

$$H = Nh \tag{1-57}$$

Combining equations 54 and 55 and putting the variables in dimensionless form gives the solution for the transition region and the final behavior

$$\frac{V}{Hf} = \begin{cases} \frac{c}{fH}\,\delta & \text{before 1st slip} \\ \frac{c}{fH}\left[\frac{S + \frac{1}{4}(N-S)^3}{N^3}\right]\delta + \frac{N+S}{2N} & S=0,2,4,\ldots,N-4 \\ \frac{c}{fH}\left[\frac{1}{N^2}\right]\delta + \frac{N-1}{N} & \text{after last slip} \end{cases} \tag{1-58}$$

Each line segment holds until its intersection with the next segment, to give a single valued function $V(\delta)$.

Equation 58 is plotted on figure 1-15 for various values of N. This plot represents the force deflection behavior of a beam of constant total thickness and constant pressure that has been divided into various numbers of layers. The intersection of each line segment on this plot indicates a change from one slip mode to another. When the slip is complete, the beam follows the basic equation used in the preceding analysis.

As the deflection of the end of the beam is increased, the propagation of slip proceeds rapidly at first and then gets progressively slower. This may be seen on figure 1-15 by observing that the distance between intersection points increases with deflection. At large deflections the slip propagation may not be complete and yet the relation between load and deflection still retains the same general form as found for complete slip. In this case, the friction force would be close to the final result, but the slope of the force deflection curve could be considerably

Fig.1-15 FORCE-DISPLACEMENT RELATION FOR END LOADED MULTI-LAYER CANTILEVER

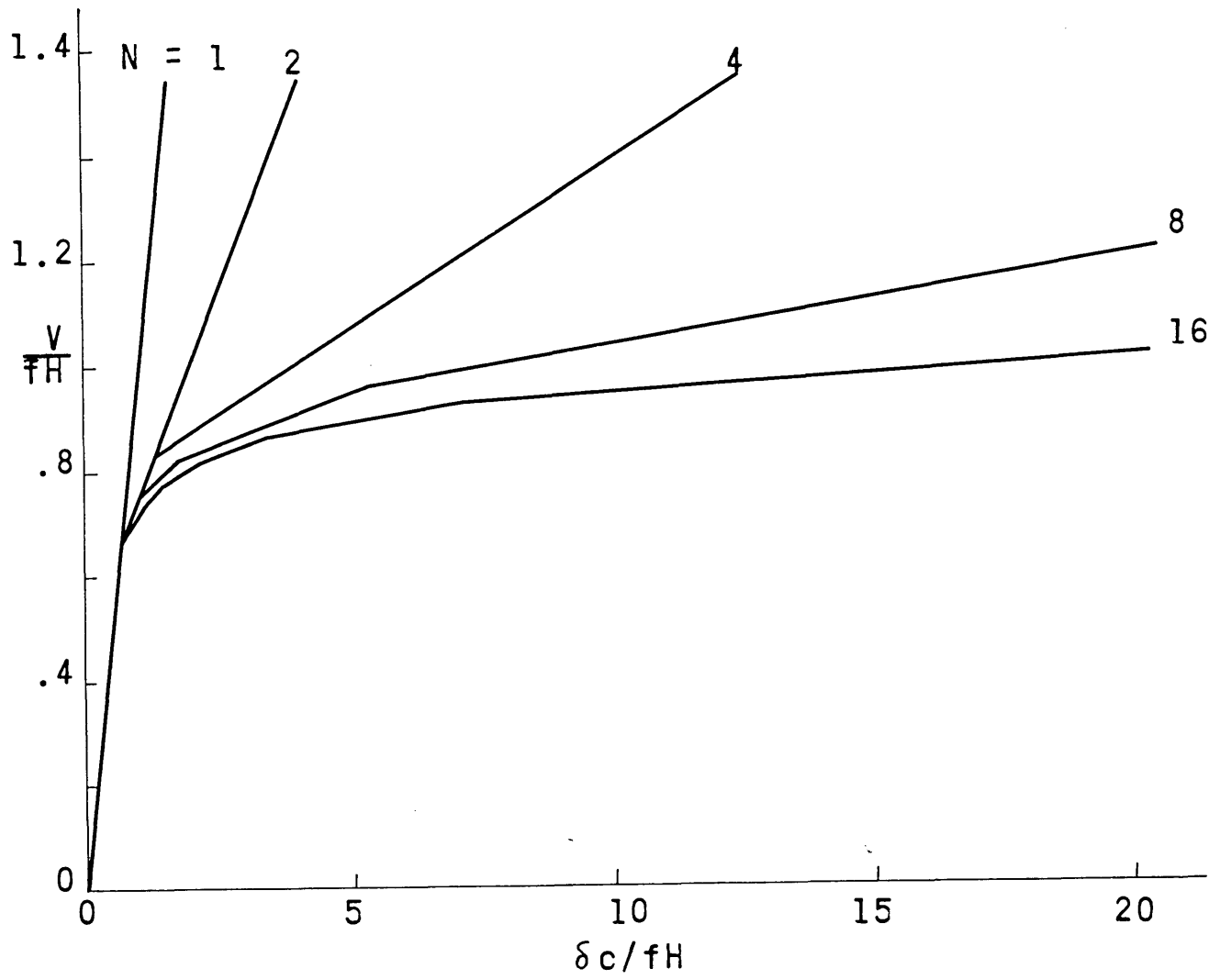

different. This may explain the deviations between measured and theoretical results of figure 1-10.

In materials having differences between the static and kinetic coefficients of friction the mode of slippage may be different from that computed here. Each time the maximum allowable shear stress is reached, and slippage starts between two layers, the shear stress on the surface of the layers will drop below the level required to initiate slip. Then the mode of slip propagation may not be exactly the same as for the case which was considered. The second slip, for example, may be more than one layer distant from the center of the beam, depending on the current shear stress distribution relative to the locations of the interfaces. Then the modes of slip propagation will be considerably more complicated than for the case considered here.

Another effect of differences in the coefficients of friction is that the points of slip will not correspond to the intersections of the load deflection curves of each mode. The beam will follow the curve for a particular mode and change to the next mode beyond the intersection of the line segments. This will cause a rapid drop in load at the points of mode change and will give the load deflection behavior a sawtooth appearance. In addition, the beam will remain in one deformation mode for greater changes of end deflection.

The analysis presented here defines the transition region for a constant shear force in the beam and slip was found to propagate through the thickness of the beam. In a later case, the question of lengthwise propagation will be discussed in detail.

Beam Loaded with Constant Bending Moment. Another example of the application of the proposed theory is the case of a beam subjected to a constant bending moment. This type of loading can be produced in the center of a beam by four points of loading as shown on figure 1-15. For the purpose of this analysis the central region will be taken as being under a constant pressure and the regions

in which the point loads are applied will be taken as being under zero pressure.

Using the same symmetry condition as before the beam will be replaced by a cantilever having a two-point couple at the end. This is shown on figure 1-16 together with the definition of the variables to be used in the analysis.

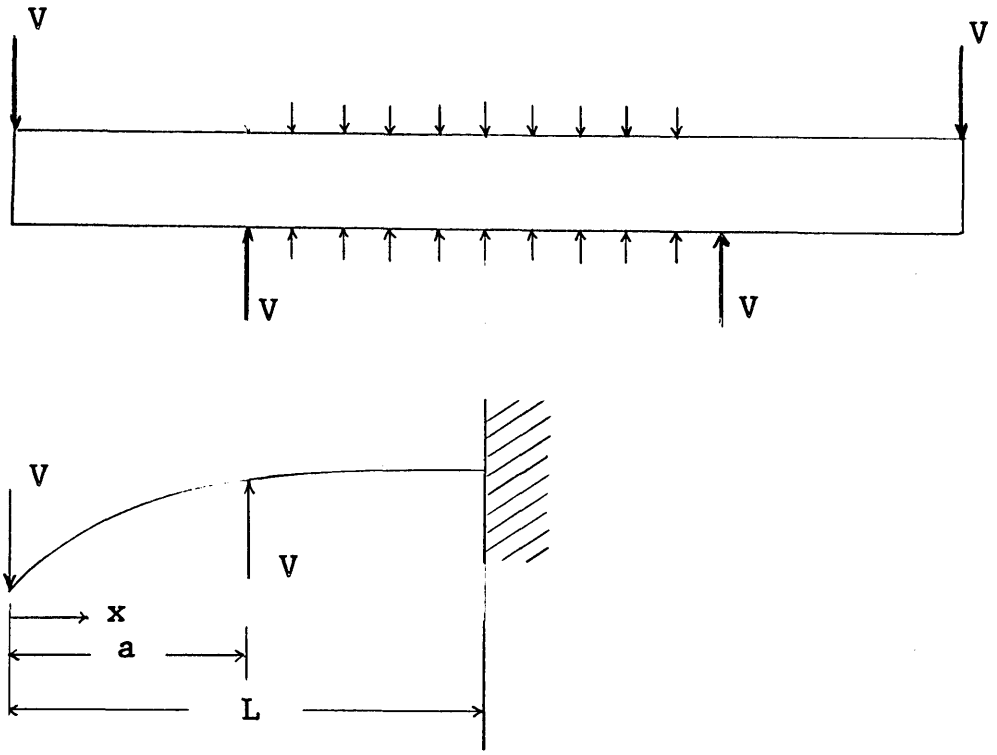

Fig. 1-16 Four Point Loaded Multi-Layer Beam Under Constant Pressure in Central Region

The assumptions made in this analysis will be the same as those made for the simply supported beam. In this case the shear force maintains a constant value in the initial region of the beam and falls to zero in the central region. The friction force, on the other hand, is zero in the initial region and constant for values of x between a and L. Substituting this information into equation 16 gives the differential equation for the curvature

distribution.

$$\frac{dk}{dx} = \begin{cases} \dfrac{V}{NEI_\ell} & 0<x<a \\ \dfrac{-h(N-1)f_k}{NEI_\ell} & a<x<L \end{cases} \tag{1-59}$$

Solving this equation gives,

$$k = \begin{cases} \dfrac{V}{NEI_\ell}\, x & 0<x<a \\ \dfrac{-h(N-1)f_k x}{NEI_\ell} + \dfrac{h(N-1)fa}{NEI_\ell} + \dfrac{Va}{NEI_\ell} & a<x<L \end{cases} \tag{1-60}$$

Note that the curvature varies in the region of constant moment. This is in sharp contrast to a classic beam where the curvature would be constant.

The average curvature ($\bar{k}$) in the constant moment region can be determined from equation 60. The result is,

$$\bar{k} = \frac{Va}{NEI_\ell} - \frac{h(N-1)f_k(L-a)}{2NEI_\ell} \tag{1-61}$$

Solving the equation for the imposed bending moment (Va) and writing the result in terms of the length of the central region gives,

$$M = NEI_\ell\, \bar{k} + \frac{1}{4}\, h(N-1)f_k L_b \tag{1-62}$$

This equation expresses the moment-curvature relation for the multilayer beam under consideration. It reduces to the classical result of a zero friction beam when the second term vanishes. However, when the second term exists, the behavior follows the same pattern as in the simply supported beam. Elasticity produces a linear relation between load and deformation to which is added or subtracted a constant term that depends on the frictional effect. This term is added during the loading cycle and subtracted during unloading.

In both types of loading situations considered, the frictional

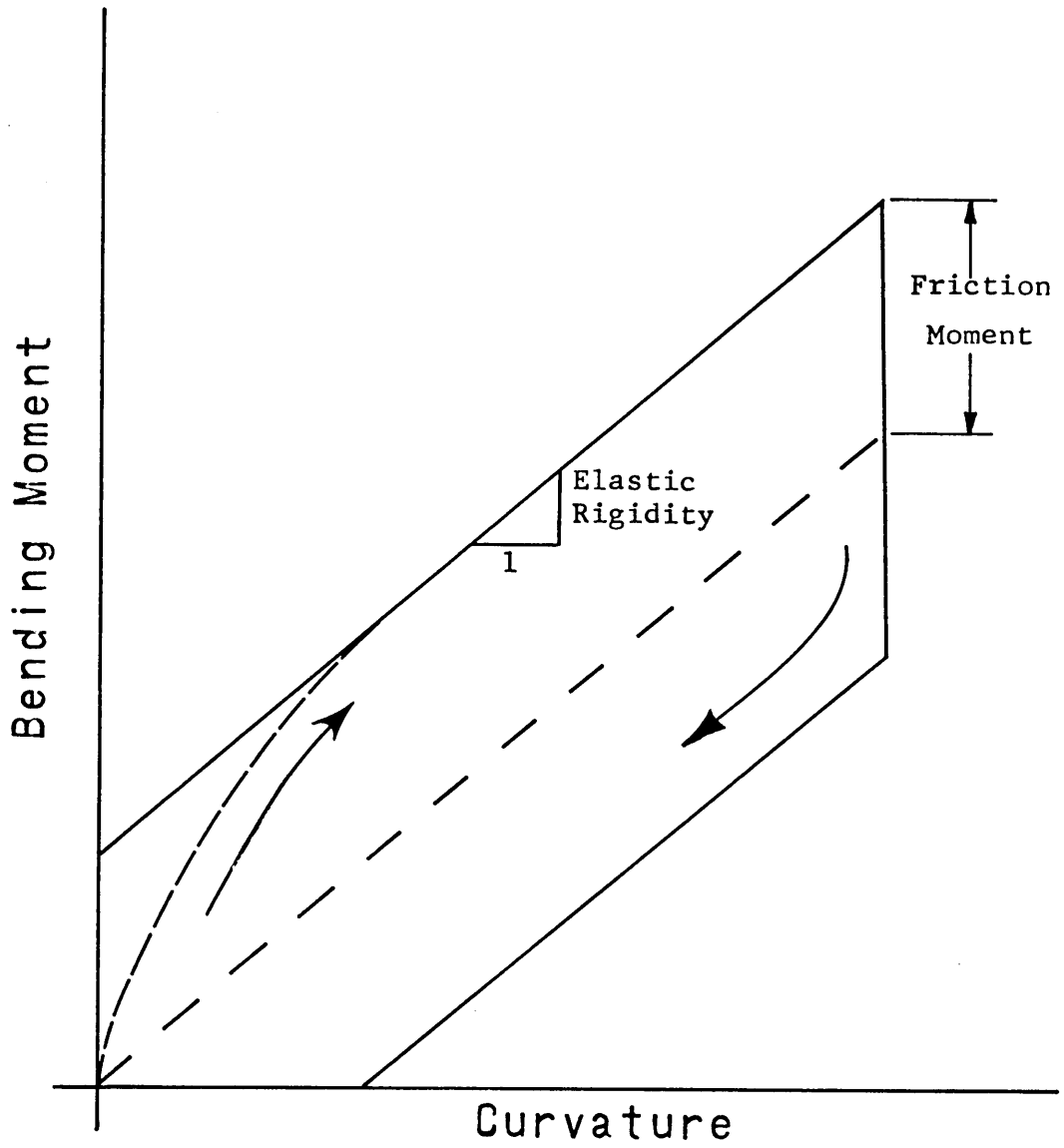

Fig. 1-17 Effect of Sliding Friction on Moment Curvature Relation

effect is dependent onthe beam length; and for this reason there is no constituative relation which exists at every point of the beam. In a textile structure, however, which under certain cases may be considered as a number of multilayer beams in series, there is a constituative relation that exists when the size of each element of the structure is much smaller than the length of the sample under test.

The slope of the moment-curvature relation will be referred to as the "elastic rigidity" and the additive amount of moment which must be applied to overcome frictional effects will be referred to as the "frictional moment". For this case the elastic rigidity is merely the sum of the individual layer rigidities and the frictional moment is a term related to the friction force, the number of layers, and the geometry. During unloading the direction of slip changes and the sign of the friction moment becomes negative. The hysteresis curve produced is shown on figure 1-17.

The type of behavior predicted here corresponds to that observed for textile materials.[7] There is a stiffening effect due to friction, an energy loss due to relative motion and a non-recoverability from bending due to friction.

Propagation of Slip in Beam with Constant Bending Moment. The solution of this loading situation was made with the assumption that the individual layers are free to slide. This limits the results to the behavior beyond the transition region during which the slip is propagating through the structure. The transition region can be investigated in greater detail by determining the magnitude of imposed shear stress at every point of the beam and comparing it to the stress that can be resisted by static friction.

In performing this computation an apparent paradox arises. On the basis of classical considerations of beams there is no shear stress in the central region of a four-point loaded beam because the shear force is zero. This is true for most of the

length of the beam. However, in a small region near the ends, a shear stress develops because of the discontinuous strain distribution imposed on the beam section. This was discussed previously and it was shown that the maximum shear force per unit width imposed is given by equation 39. To use this equation the strain discontinuity must be computed at the beginning of the constant moment region. This can be done by integrating equation 18 with the boundary condition of zero strain at the free end and the appropriate values of friction force in each region. The result for an interior layer within the range of slip propagation is,

$$b_{i-1} - b_i = kh \tag{1-63}$$

From the curvature function of equation 60 this can be evaluated in terms of position along the beam.

$$b_{i-1} - b_i = \begin{cases} \dfrac{hM}{aNEI_\ell}\, x & 0 < x < a \\ \dfrac{-h^2(N-1)f_k(x-a)}{NEI_\ell} + \dfrac{Mh}{NEI_\ell} & a < x < L_s \end{cases} \tag{1-64}$$

Where:

L_s = extent of slip

This equation is valid for any length of slip propagation into the beam. From equation 39 the imposed shear stress per unit width at the end of slip ($x = L_s$) can be computed. At this point the imposed shear stress just equals the shear stress that can be resisted by the static frictional forces. The extent of slip can then be calculated from equations 39 and 64.

$$\text{at} \quad x = L_s$$

$$f_{d_j i} = f_s$$

$$L_s - a = \frac{Mh - \dfrac{Nf_s\pi h^3}{12}}{h^2(N-1)\, f_k} \tag{1-65}$$

The extent of slip into the region of constant moment increases with the imposed moment as expected. The slip region will start propagating when sufficient moment is applied to cause initial interlayer motion and will grow linearly with imposed moment until the slip has propagated throughout the beam. To characterize this transitional region, the point of initial slip and the point at which slip has propagated throughout will be computed. This is done by evaluating the bending moment at the appropriate values of $L_s - a$.

Point of Slip Initiation:

$$L_s - a = 0$$

$$M_{\substack{1st \\ slip}} = \frac{N f_s \pi h^2}{12} \tag{1-66}$$

Point of Complete Slip Propagation:

$$L_s - a = \frac{L_B}{2}$$

$$M_{\substack{end \\ of\ slip}} = \frac{N f_s \pi h^2}{2} + \frac{h(N-1) f_k L_b}{2} \tag{1-67}$$

It is convenient to put these computed values in terms of the friction moment that has been determined for the constant moment beam in equation 62.

$$M_F = \frac{1}{4}(N-1) f_k h L_B \tag{1-68}$$

$$\frac{M_{1st\ slip}}{M_F} = \left(\frac{N}{N-1}\right)\frac{\pi h f_s}{3 L_b f_k} \approx \frac{h}{L_b} \tag{1-69}$$

$$\frac{M_{end\ of\ slip}}{M_F} = 2 + \left(\frac{N}{N-1}\right)\frac{\pi h f_s}{3 L_b f_k} \approx 2 \tag{1-70}$$

This transition region is shown on figure 1-17. For the static and kinetic coefficient of frictions about equal and for beam lengths much greater than the layer thickness the slippage

begins propagating at very low levels of moments. When the imposed moment equals about twice the value of the friction moment, the slip will have propagated throughout the beam. Before the first slip, the beam behaves as a solid and after the completion of slip, the behavior follows equation 62.

The important difference between the transition region of the constant moment beam and that of the constant shear force beam is that in this case the slip propagates along the length of the beam, whereas in the other case it propagates through the section of the beam. Furthermore, the development of shear stress in this case is a result of a discontinuous strain distribution while in the other case it is the result of the imposed shear force.

Recovery from Constant Curvature Band--Theoretical and Experimental. In the previous applications of the multilayer beam theory the emphasis was placed on the loading cycle. The unloading behavior in each case could be predicted by reversing the direction of the friction force. In this section bending recovery will be considered in greater detail and the specific case in question will be a multilayer beam under constant pressure bent to a constant curvature and then allowed to recover.

During bending it will be assumed that the slip has been complete. Then, when the load is released, the layers will reslip an amount dependent on the relative effects of friction and elasticity. The extent of the reslipping will determine the bending recovery.

Let:

k_i = imposed curvature (in^{-1})
k_r = residual curvature (in^{-1})
L_b = total length of beam (in)
u_b = slippage during bending (in)
u_r = slippage after recovery (in)

e_i = strain during bending

e_r = strain during recovery

x = coordinate along beam measured from left edge (in)

x_r = point where final slip equals original slip (in).

From the assumption of complete slip during bending, the initial strain distribution on the interior layers can be found from equation 18 to be,

$$e_i = ky - ky_i \tag{1-71}$$

The relative slippage can be computed from equation 21 and the symmetry condition which states that the slip is zero at the center of the beam.

$$u_b = kh\left(\frac{L_b}{2} - x\right) \tag{1-72}$$

Upon release of the load, the layers will reslip from edges inward. This will continue until the reslip is zero. At this point (denoted by x_r) the relative layer motion will be equal to that originally imposed. Within the region of the beam where no reslippage occurs, the residual curvature will be equal to that imposed. Considering only the left side of the beam, this may be written as,

$$k_R = k_I \qquad x_R < x < \frac{L_b}{2} \tag{1-73}$$

Within the reslip region the relation between geometry and load may be expressed by equation 16. The friction force will be negative due to the reverse direction of slip and the shear force zero because there are no externally applied loads.

$$\frac{dk_R}{dx} = \frac{h(N-1)f_k}{NEI_\ell} \qquad 0 < x < x_R \tag{1-74}$$

Since the residual curvature is zero at $x = 0$, equation 74 can be integrated and combined with equation 73 to give the result,

$$k_R = \begin{cases} \dfrac{h(N-1)f_k}{NEI_\ell}\, x & 0 < x < x_R \\ k_I & x_R < x < \dfrac{L_b}{2} \end{cases} \tag{1-75}$$

The remaining portion of the strain distribution can be calculated for an interior layer from equations 5 and 74. The result is,

$$b_i = \frac{-h(N-1)f_k y_i x}{NEI_\ell} \qquad 0 < x < x_R \qquad (1\text{-}76)$$

From this equation the slip distribution after recovery can be computed using the results of equations 76 and 21.

$$u_R = \begin{cases} \dfrac{-h(N-1)f_k h(x^2 - x_R^2)}{2NEI_\ell} + k_I h\left(\dfrac{L_b}{2} - x_R\right) & 0 < x < x_R \\ k_I h\left(\dfrac{L_b}{2} - x\right) & x_R < x < \dfrac{L_b}{2} \end{cases} \qquad (1\text{-}77)$$

Plotting equations 72 and 77 on figure 1-18 for the full beam length shows the distributions of slip before and after release of load.

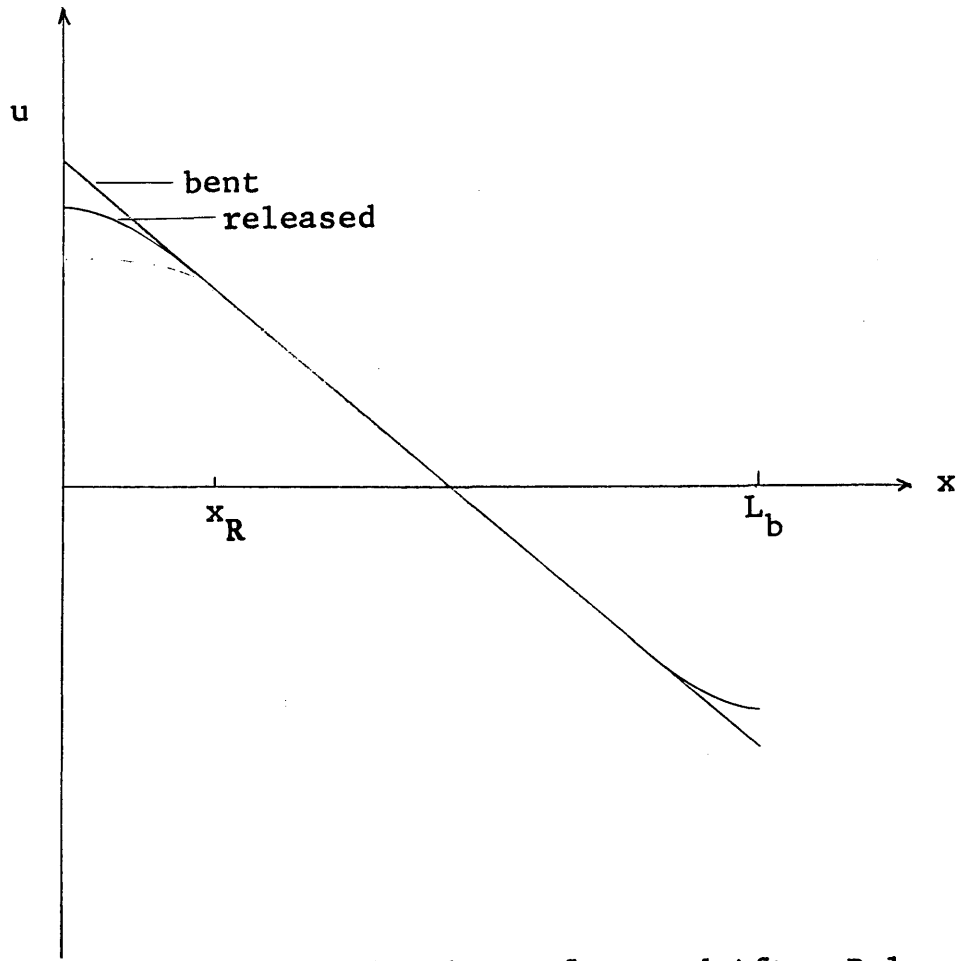

Fig. 1-18 Slip Distribution Before and After Release of Load

The point at which the final slip equals the original slip can be obtained from the strain distributions. At this point the strains will be equal and it can be shown that,

$$x_R = \frac{NEI_\ell}{h(N-1)f_k} k_I \tag{1-78}$$

This equation can be used to determine the residual curvature distribution by substituting into equation 75. Then, averaging the residual curvature over the length of the beam gives,

$$\bar{k}_R = \begin{cases} k_I \left[1 - \frac{k_I NEI_\ell}{h(N-1)f_k L_b}\right] & 0 < \frac{k_I NEI_\ell}{h(N-1)f_k} < \frac{L_b}{2} \\ \frac{h(N-1)f_k L_b}{NEI_\ell 4} & \frac{L_b}{2} < \frac{k_I NEI_\ell}{h(N-1)f_k} \end{cases} \tag{1-79}$$

This can be written in dimensionless form by multiplying each of the curvatures by the half-thickness of the beam. The resulting dimensionless curvature represents the maximum strain that would occur in a solid beam bent the same amount. The result is,

$$k_R^* = \begin{cases} k_I^* \left(1 - \frac{k_I^*}{4F}\right) & 0 < k_I^* < 2F \\ F & 2F < k_I^* \end{cases} \tag{1-80}$$

Where,

$$k_I^* \equiv k_I \frac{Nh}{2} \tag{1-81}$$

$$k_R^* \equiv \bar{k}_R \frac{Nh}{2} \tag{1-82}$$

$$F \equiv \frac{L(N-1)f_k L_b}{4NEI_\ell} \left(\frac{Nh}{2}\right) \tag{1-83}$$

Equation 80 is plotted on figure 1-19 for several values of the dimensionless parameter F. This quantity represents a measure of the relative amount of friction to elasticity in the beam. Note that it is composed of terms previously introduced in

Fig. 1-19 Residual Curvature vs Imposed Curvature for Multi-Layer Beam

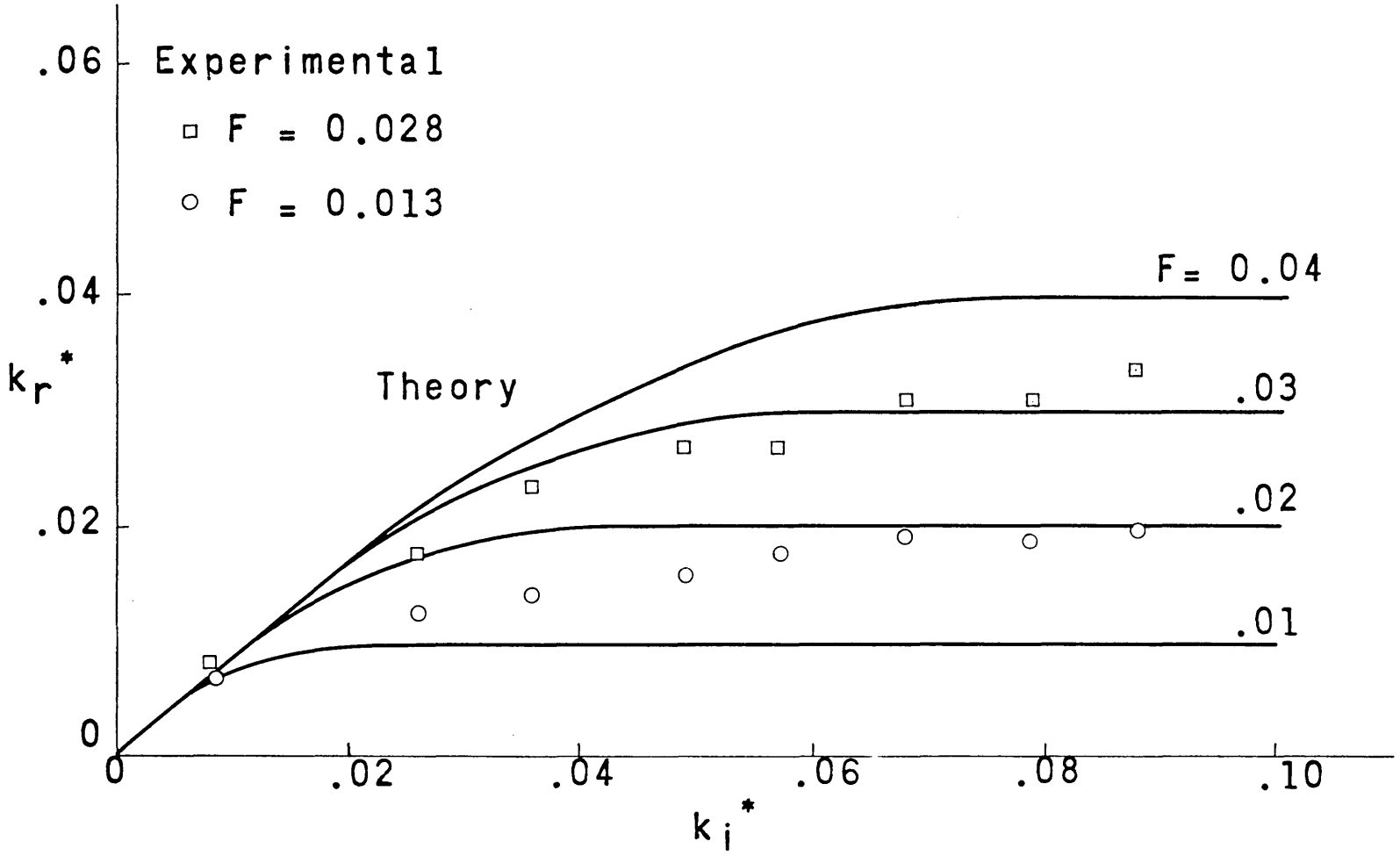

the analysis: the friction moment; the elastic rigidity for complete slip; and the half thickness of the beam.

The results of the recovery prediction show quantitatively how a multilayer beam with friction displays a non-recoverability from bending even though none of the individual components have been permanently deformed. This structural non-recoverability is also found in textile structures as will be shown in Chapter III.

Experimental. Two multilayer beams subjected to constant pressure were prepared as in the previously described experiment. They were bent around mandrels of varying curvature and permitted to recover. The average residual curvature was measured from the difference between tangent angles at the ends of the bent beam. And, the friction parameter F of each beam was determined from preliminary measurements as in the previous experiment. Since there was some stress relaxation during the test, the times of bending and recovery were held fixed at 20 seconds each. The amount of relaxation was then measured in a separate test and a correction (about 20%) was applied to the elastic rigidity of the structures. The measured values are plotted on figure 1-19 together with the theoretical predictions.

The theory and experiment appear to be in reasonable agreement, although the residual curvature increases slightly where the theory predicts it should remain constant. This discrepancy is probably due to a slight yielding of the material--which was evidenced in the stress relaxation determinations. This may also account for a generally greater than predicted residual curvature.

DISCUSSION OF CHAPTER I

This chapter involved the formulation of a theory of bending of multilayer beams with frictional interactions. This theory consists of a beam theory approach to the problem with suitable modifications to account for frictional effects. With a number of simplifying assumptions it was possible to solve the general

equations for several special cases. Then, a number of experiments were conducted to establish the validity of the proposed theory and reasonable agreement was obtained with the measured values.

The important qualitative conclusions that were reached are that the effect of friction in a multilayer beam is to require additional loads to be applied to achieve a certain deformation. This occurs because friction either prevents the relative motion of the layers or else provides a restraint against this motion for which additional input energy must be supplied. When the layers slide against a restraint, the load deflection behavior is non-linear, energy is lost in the structure, and recovery is not complete even when the individual layers behave elastically.

A number of interesting effects were observed theoretically and experimentally. The most striking of these is the reverse curvature that occurs in a cantilever which is under a normal pressure and loaded by a point load between the wall and its free edge. In this effect the region of the beam between the load and the free edge curves in a direction opposite to that of the main portion of the beam. A beam without relative motion against a frictional restraint would be straight in this region.

Another interesting effect is that the behavior of a beam with friction may be dependent on the length of the beam. This means that a constituative relation cannot be established between moment and curvature at each point such as is done in classical beam theory. For example, in the case of a beam bent with a constant bending moment, the curvature will vary along the length of the beam and the extent of this variation will depend on the beam length as well as the frictional force.

The applications of the work presented here may be applied to a number of situations that arise in engineering technology. Examples of this would be such things as laminated structures, devices for generating unusual motions, structures for damping vibrations, and combination spring-dampers.

As mentioned in the introduction, there are a number of

aspects of the mechanical behavior of multi-layer beams that correspond to observable phenomena in textile materials. In both cases friction between the elements causes a stiffening of the structure; a non-linearity in the bending behavior energy loss due to structural interactions; an increased level of strain; and a non-recoverability of the structure.

In textile materials, it is possible, under certain circumstances, to consider the structure to be composed of series of multi-layer beams. Then, even though no constituative relation may be established for a point on the elemental beam, one can be established for the textile structure provided there are a large number of elemental beams in the length of bend. This is in effect a continuum approach to the bending mechanics of textiles.

When considering a textile to be composed of a series of beams, the curvature of the textile depends on the angular deflection of each sub-unit. Since average curvature provides a measure of angular deflection between the ends of a beam, this quantity was utilized in the analysis, even though it is not usually of interest in engineering problems.

The analyses presented in this chapter represent one of the first approaches to the problem of the mechanics of multi-layer beams with frictional interactions. Additional research in this area with fewer simplifying assumptions would undoubtedly be fruitful in the development of a complete understanding of this type of structure. It is hoped that the material presented here will provide a useful starting point for such investigations.

CHAPTER II

THE EFFECT OF FRICTION ON THE BENDING OF TEXTILE STRUCTURES

In this chapter the effects of friction on multi-layered structures will be extended to include textile materials. The generalizations established for multi-layered beams will be utilized wherever possible and new approaches will be developed when they are needed.

In the first section several classical methods of analyzing the bending behavior of textiles will be discussed. These analyses consider only the limiting cases of frictional interactions. The next section contains a mostly qualitative discussion on the intermediate frictional effects that are actually found in many textiles. In this section a conceptual mathematical model is developed from which the bending behavior of textiles can be described by two parameters.

In the sections that follow, computations and experimental results are presented to establish these parameters for a number of different types of textile structures. In addition, some general formulations are presented which pertain to the relative motion of fibers and yarns in textiles that may be useful for areas of textile technology not related to bending.

LIMITING ANALYSES FOR THE PREDICTION OF BENDING BEHAVIOR OF TEXTILE STRUCTURES.

A number of investigations have been conducted with the aim of predicting the bending behavior of textile structures[7,8,17,18] . The goal was to relate the bending behavior of a particular structure to the properties of the component fibers and their geometric arrangement.

As a first approach to the problem, the classical method has been to compute the limiting situations that can exist. These limiting cases can be established by considering two

possible forms of fiber interactions: complete freedom of fiber motion, and no freedom of fiber motion. In both cases it is generally assumed that the fibers deform as linear elastic elements. Then, for small deflections, the moment-curvature behavior will be linear and can be described by the slope of the curve which is, of course, the rigidity.

For the case of complete freedom of fiber motion, the overall behavior of a structure is determined by assuming that there is no interaction between the fibers which will cause them to develop axial stresses. Then, the total moment acting on a structure can be computed by vectorially summing the individual bending and twisting moments on each of the fibers. If all the fibers are aligned perpendicular to the axis of bending, the total rigidity for this case will merely be the sum of the individual fiber rigidities.

In the case of no freedom of fiber motion, it is assumed that the interactions between the fibers are of sufficient magnitude to prevent any relative fiber motion or fiber buckling. Then, the structure will deform as a solid material and have a linear strain distribution across the section perpendicular to the axis of bend. These strains will develop stresses in the fibers which can be computed by considering the orientation of the fibers relative to the axis of bend, and assuming that each fiber carries only axial loads. This was done for the case of a twisted yarn by Backer [17]. The rigidity of the structure can then be determined by integrating the stress distribution at a fixed curvature. If all the fibers are perpendicular to the axis of bend, the rigidity will be approximately that of a solid material having the same modulus as the fibers.

Clearly, the rigidity computed by each of the two limiting analyses depends on the number of fibers in a section of

the structure, the rigidity of each fiber, and the geometry of the system. The result for the assumption of no freedom of fiber motion will be considerably greater than that for the assumption of complete freedom of motion and this is illustrated qualitatively on Fig. 2-1. The magnitude of rigidity will be computed for the limiting cases of certain structures in this section. Then, in later sections, the intermediate cases of frictional interaction will be considered to determine the actual moment-curvature relation for certain structures.

Limiting Rigidities for Zero Twist Yarn. The rigidity of a zero twist yarn can be computed for the two cases of freedom of fiber motion using the above methods. It is assumed that the yarn cross section is round and that the packing of fibers is constant. Let,

D_f = fiber diameter (in)
D_y = yarn diameter (in)
E = tensile modulus (lb/in^2)
I_i = moment of inertia of fiber (in^4)
I_y = moment of inertia of yarn (in^4)
N_f = number of fibers in yarn
γ_y = packing factor
M = bending moment on yarn (in/lb)
k = yarn curvature (in^{-1})

For the case of complete freedom of motion, the bending moment on the yarn will be the sum of the individual fiber bending moments. If the radius of curvature is small relative to the diameter of the yarn, then all of the fibers will be bent approximately the same amount and they will each have approximately the same bending moment. The moment-curvature for this case can be written as,

$$M = N_f EI_i k \text{ (complete freedom of motion)} \quad (2\text{-}1)$$

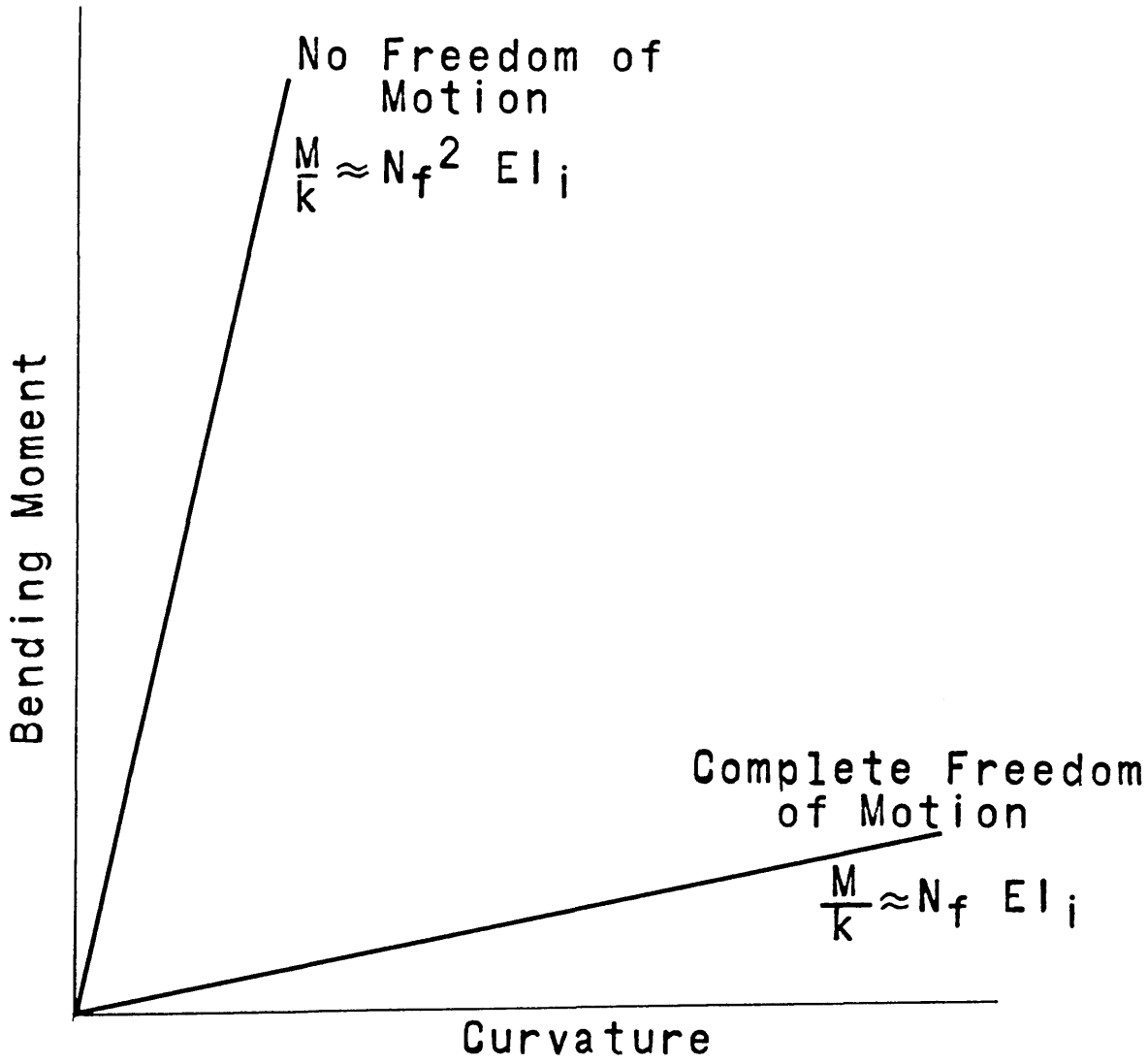

Fig. 2-1 Limiting Conditions of Freedom of Relative Fiber Motion

Since this equation can be used to give a good estimate of the bending rigidity of a large number of textile materials, it is useful to rewrite it in terms of quantities commonly used in textile terminology.

$$\frac{M}{k} = (3.02)(10^{-11}) \frac{N_f E_g \omega_f^2}{\rho} \qquad (2\text{-}2)$$

Where:

E_g = fiber modulus (gms/denier)
ω = fiber linear density (denier)
ρ = fiber density (gm/cc)
M/k = yarn rigidity ($lb\text{-}in^2$)

For the case of <u>no freedom of motion</u> the rigidity can be determined from the rigidity of a solid rod corrected for the packing of the fibers. Since all the fibers lie perpendicular to the axis of bend, orientation effects need not be considered. The moment-curvature relation for this case is,

$$M = EI_y k \qquad (2\text{-}3)$$

The yarn moment of inertia can be written in terms of the yarn diameter and packing factor. The result can then be rewritten in terms of the fiber diameter and packing factor.

$$I_y = \frac{\gamma_y \pi D_y^4}{64} = \frac{N^2 \pi D_f^4}{\gamma_y 64} \qquad (2\text{-}4)$$

This equation can be used to determine the final relation in terms of the individual fiber rigidity,

$$M = \frac{N_f^2}{\gamma} EI_i k \quad \text{(no freedom of motion)} \qquad (2\text{-}5)$$

From equations 1 and 5 it is clear that the rigidity for no freedom of motion is about N_f times as great as that for complete freedom of motion. Since N_f is of the order of 100 for many yarns, there is considerable difference between the rigidity in both cases. Note that in the multi-layered beam

analysis of Chapter I, the results indicated a factor of N_Q^2 between the rigidities of the limiting cases. The difference arises because in one system fibers are the individual elements and in the other, layers.

Limiting Rigidities of a Twisted Yarn. The limiting cases of rigidity of a twisted yarn can be computed by considering an idealized yarn made of helically arranged fibers. The complete freedom of motion rigidity can be determined by vectorially summing the moment contributions on the individual fibers at one cross section. The no freedom of motion rigidity can be determined by integrating the tensile stress distribution across the section and correcting for the inclination of each of the fibers.

Both limiting cases were solved by Platt[8] in an analysis which was quite involved because of the complex geometry of the structure. Nevertheless, he was able to solve the equations by making suitable approximations, and he obtained results which are valid up to helix angles of about 30°. These results may be written in the same form as used in the previous section:

$$M = N_f \, EI_i \, f_1(Q) \, K \quad \text{Complete Freedom of Motion} \quad (2\text{-}6)$$

$$M = \frac{N_f^2}{\gamma_y} \, EI_i f_2(Q) \, K \quad \text{No Freedom of Motion} \quad (2\text{-}7)$$

Where,

Q = outside helix angle

$$f_1(Q) = \left[\frac{2 \ell n_e \sec^2 Q - 3 \sin^2 Q + (1 - \cos^4 Q)}{2 (1 - \cos Q)}\right]\left[\frac{\tan^2 Q \cos Q}{2(1 - \cos Q)}\right] \quad (2\text{-}8)$$

$$f_2(Q) = \left[\frac{2\ell n_e \sec^2 Q - 2\sin^2 Q}{\tan^4 Q}\right]\left[\frac{\tan^2 Q \cos Q}{2(1 - \cos Q)}\right] \qquad (2\text{-}9)$$

It can be shown that the values of both functions $f_1(Q)$ and $f_2(Q)$ are unity for zero helix angle and the results reduce to the solution of the zero twist yarn. As the helix angle increases, both functions fall slightly, and each reaches a magnitude of about 0.75 at 30°. This means that the effect of the helical configuration of the fiber is small on the bending rigidity of the yarn. The maximum change of rigidity due to this effect is about 25%, whereas the change of rigidity due to differences in freedom of motion can easily be a factor of 100.

A similar result was found by Owens[7] for the case of complete freedom of motion. His approach was considerably different from that of Platt, but the results are in surprisingly good agreement[19].

In addition to a direct geometric effect on rigidity, the twist can also influence the degree of relative fiber motion. Since the geometric effect is small, it is probable that the major effect is the change of internal yarn pressure and relative fiber motion with change of twist.

Limiting Rigidities of a Bonded Fabric. Although bonded fabrics have a considerably different structure from the yarns considered in the previous sections, it is possible to compute their limiting rigidities by the same general procedures. This was done by Platt and Freeston[18] for a bonded fabric having an arbitrary angular distribution of the fiber orientations. When the equations are applied to the case of a random laid non-woven, the results can be written in the same form as before. The conversion of Platt's equations to the form used here is shown in Appendix B.

$$M = N_f EI_i \frac{3}{8} \zeta k \quad \text{Complete Freedom of Motion} \qquad (2\text{-}10)$$

$$M = N_f^2 EI_i \frac{\pi}{8\gamma_B} k \quad \text{No Freedom of Motion} \qquad (2\text{-}11)$$

Where,

N_f = number of fibers in section having a width equal to the fabric thickness.

ζ = factor dependent on fiber torsional properties (between about 1.2 and 1.3)

γ_B = approximate packing factor of bonded fabric.

Note the similarities between the limiting rigidities for the bonded fabric and the yarn structure. For this material, there is an additional factor of about 0.5 in the equation and this accounts for the fact that the fibers are not all perpendicular to the axis of bend. The ratio of rigidity for the limiting cases is almost the same as before.

Experimental investigations have shown[18,20] that the behavior of bonded fabrics approaches the predicted values for no freedom of motion. This results from the bond points between fibers which act to restrict relative fiber motion.

Twisted yarns and most fabrics on the other hand behave very close to the predictions of complete freedom of motion. This can be demonstrated qualitatively by applying treatments such as starch and observing large increases of rigidity.

QUALITATIVE EFFECTS OF FRICTION ON BENDING BEHAVIOR

In the preceding section, predictions of bending behavior were made for the limiting cases of fiber interaction. The results indicated that there are large differences between these cases and the problem at hand is the determination of

the bending behavior for intermediate values of frictional interaction.

This was done in Chapter I for multi-layered beams. It was found that inter-element friction produced: a stiffening of the structure; a non-linearity in the moment-curvature relation; an energy loss in bending; and a non-recoverability from bending. Quantitative determinations of these effects were made by an analysis of the equilibrium requirements of the structure. The results indicated that friction affects the bending of multi-layer structures in two ways; it prevents the elements from sliding by each other as much as they would if there were no friction; and it requires that energy be lost where sliding takes place.

In Chapter I it was also found that friction could restrict sliding by either preventing slip propagation throughout the cross-section of the structure, or by preventing its propagation throughout the length of the beam. This lack of slip produced an increase in rigidity but had no energy loss associated with it.

It was also found that friction had an effect in the region of the beam where sliding did occur. The sliding friction forces required an additional moment to be applied to the structure during bending. This is illustrated on Fig. 1-16 as is the energy loss associated with this frictional effect.

On the basis of these results a conceptual model can be constructed which is useful for analyzing the bending behavior of textile structures. This model, which is shown on Fig. 2-2, consists of an elastic element in parallel with a dry-frictional element. The load-deflection or moment-curvature relation for this model is shown by the straight lines on Fig. 1-16. The elastic term increases linearly with load while the friction

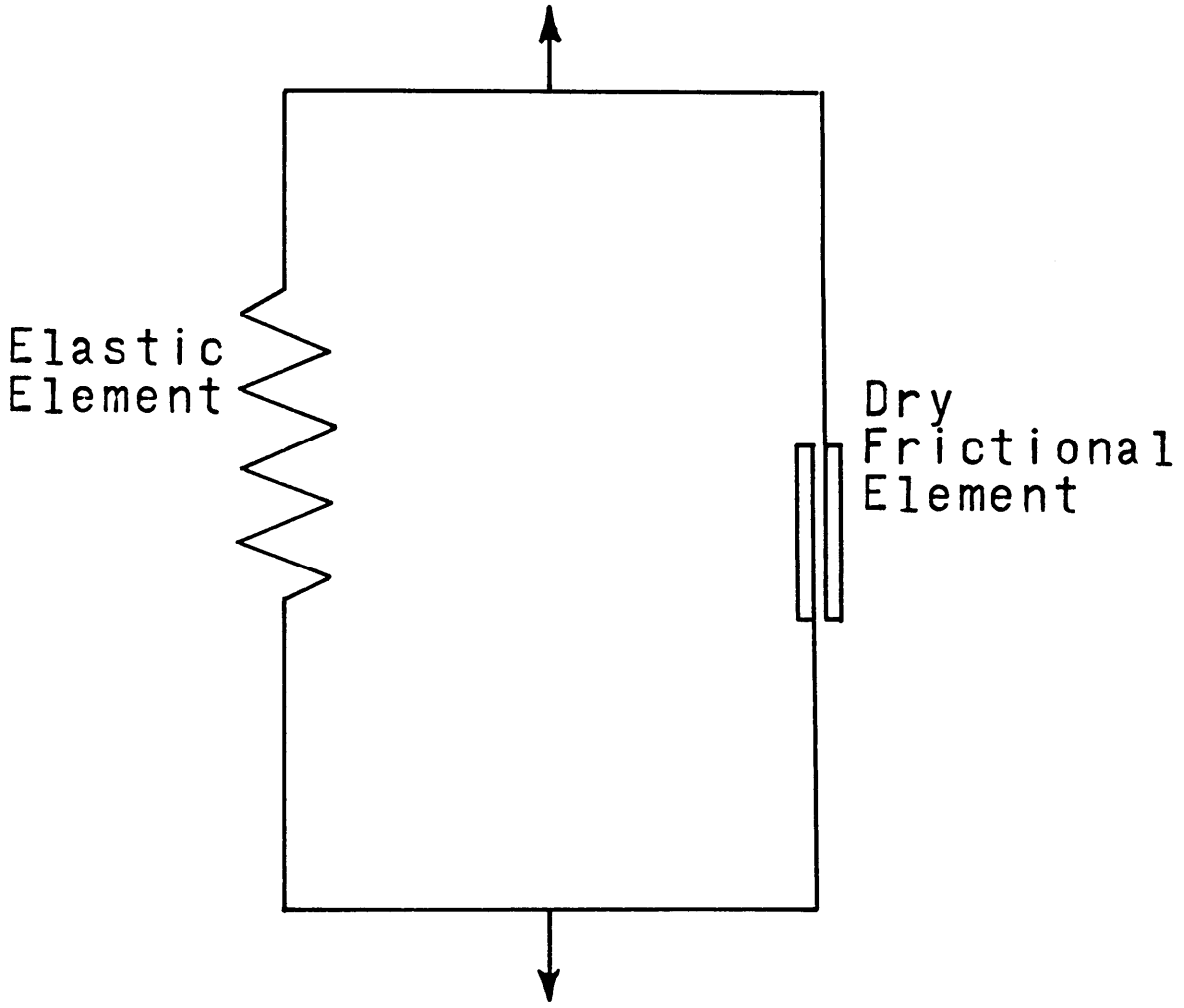

Fig. 2-2 Conceptual Model of Frictional Effect

term is constant and always acts opposite to the direction of loading.

This conceptual or mathematical model requires two parameters for its description: an elastic parameter which will be called the elastic rigidity; and a frictional parameter which will be called the friction moment. The magnitude of these quantities are functions of the geometry and properties of the elements of a structure. The elastic rigidity depends on the degree of freedom of fiber motion and the friction moment depends on the amount of energy lost due to sliding friction. One method of computing the friction moment which has been found convenient for the analysis of textile structures is shown in the following equation,

$$M_f = \frac{\partial \omega_f}{\partial \bar{k}} \qquad (2\text{-}12)$$

Where,

M_f = friction moment

$\bar{k}$ = average curvature

ω_f = energy loss per length of material due to sliding friction.

This equation can be solved when both the slip distribution and the friction force distribution is known in a structure being bent. Upon integration, these functions determine the energy loss per length.

Previous investigators have found the existence of a friction moment in the bending of textiles. Eeg-Olofsson[12,21] found a hysteresis in the moment-curvature relation which may have been due to frictional effects. In similar measurements Isshi[11] found a relation close to that shown on Fig. 1-16 for cotton yarns and fabrics. Owens[7] also observed frictional moments on a number of textile fabrics.

In addition to direct observations of friction moments in textiles, Zorowski and Chen[10] found non-linearities in the deflection behavior of gravity loaded cantilevers made of ply yarns. Their results could be explained in terms of a friction moment. Similar measurements were also made by Swami and Grossberg[13], using fabric samples. They determined friction moments by both cantilever and buckling tests and related the measured values to certain properties of the materials.

Since friction can effect bending behavior by either preventing complete slip or by producing a restraining force against slip, it will effect both the elastic and the frictional parameters of this model. At low frictional effects there will be both low elastic rigidity and low friction moment. At very high frictional effects,which are close to the case of no freedom of motion, the elastic rigidity will be high, but the frictional moment will again be low. In the first case the friction moment will be low because the frictional forces are low; and, in the second case, it will be low because the relative fiber motion is small. At intermediate friction effects, the elastic rigidity will be moderate and the frictional moment will reach its maximum value.

A number of modifications can be applied to the fundamental model of Fig. 2-2. For example, combinations of this type of element can be used to account for such effects as variability of properties or frictional interactions. Or, it is possible to include time dependent elements in the model to account for the visco-elastic properties of fibers. This will not be done in this investigation but would certainly be of value for further research on frictional effects on bending.

FIBER MOTIONS DURING BENDING

In the preceding section it was shown that the frictional effects in textiles are directly connected with the relative fiber motions. The extent of these relative motions depends on the amount of frictional interaction and the amount of motion required to map out the bent configuration of the fiber assembly. In this section two analyses will be presented from which it is possible to determine the relative fiber motions for a number of situations. The results will be applied in the later sections of the thesis.

In Chapter I two methods were derived for computing relative motion between the layers of a multi-layer beam. (Equations 21 and 28.) These methods are based on strain discontinuities of parallel layers in intimate contact. Although the results are useful for fiber systems having layered arrangements, they cannot be applied to more complicated cases such as twisted yarns or randomly arranged fibers. Consequently, additional methods were established and will be included in this section.

The equations which describe the relative motions of fiber have applications in fiber technology not necessarily related to bending. Examples of this are drafting, fiber migration, fabric abrasion, and jaw penetration during tensile testing. Perhaps the equations developed here can later be applied in some of these areas of research.

Continuity Equation for Fiber in a Deforming Structure. When a textile structure deforms, the component fibers are rearranged or distorted in some manner. The fibers may either strain, move relative to the structure, or buckle. These actions can occur separately or in combinations.

As an example, consider a yarn bending. There are a number of possible changes of fiber configuration that can take place. If all the fibers are cemented together, the fibers will undergo tensile deformations but will not slip or buckle. If, on the other hand, the fibers are free to slide, they will not develop a net tension or compression, but will slide relative to the structure and possibly buckle. Here, the term buckling refers to a departure of the fiber from the assumed geometric configuration. For example, the fiber may follow a helical path before bending and then deviate into a non-helical path after bending. The particular type of fiber rearrangement occurring in any situation clearly will depend on the interactions between the fibers. However, from the condition of continuity there are only a limited number of possible fiber rearrangements for any situation. And this may be expressed mathematically in the form of a continuity equation.

The continuity equation will be written in terms of a coordinate system defined by the yarn axis. It can easily be rewritten in terms of a coordinate system defined by a line in the center of a fabric or any other convenient system. Let,

s = coordinate measured along yarn axis.

L_1 = fiber length in length of yarn from 0-S at state 1.

L_2 = fiber length in length of yarn from 0-S at state 2.

u_y = fiber length moving through yarn cross-section in change from state 1 to 2.

e_f = fiber strain.

Consider a control volume defined by two planes perpendicular to the yarn axis at locations s and s + ds. As the yarn axis deforms from state 1 to state 2, the fibers will in

general move through these planes by a certain amount. This movement will be referred to as fiber motion relative to the structure. The motion of two fibers relative to each other can then be computed by taking the difference between their motions relative to the structure.

The relation between slip and strain of a fiber can be found by a conventional continuity approach for the control volume shown on Fig. 2-3. Note that a partial derivative is used to avoid confusion with the change of slippage with curvature.

$$\frac{\partial u_y}{\partial s} = (1 + \varepsilon_f) \frac{dL_1}{ds} - \frac{dL_2}{ds} \qquad (2\text{-}13)$$

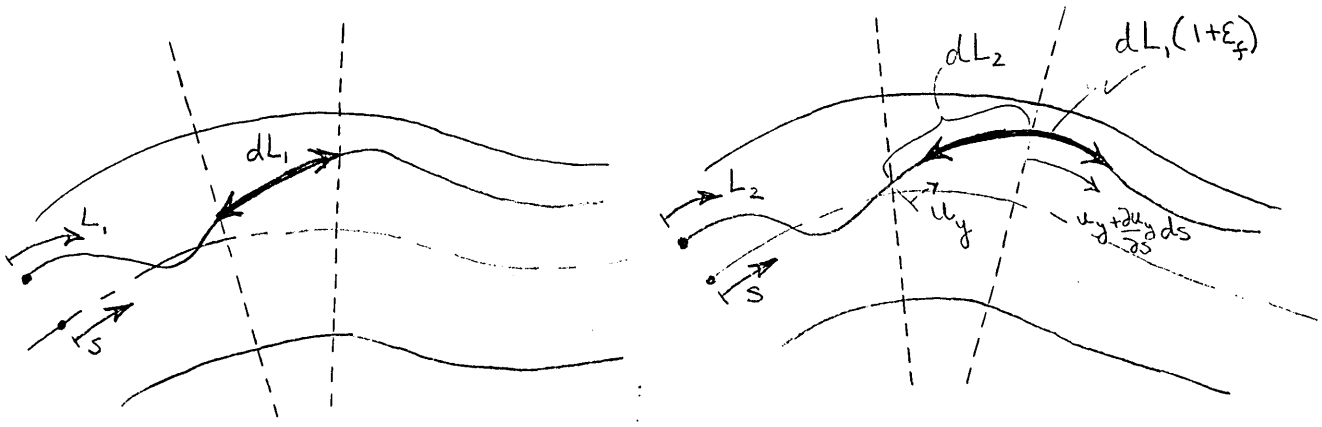

State 1 State 2

Fig. 2-3 FIBER SLIP AND STRAIN IN DEFORMING STRUCTURE

The continuity equation can be specialized for certain cases to obtain solutions. This is done by specifying the geometric states of the system in terms of functional relations between L_1, L_2 and s. This will be demonstrated for two types of systems, a bent twisted yarn and a bent layered structure.

Twisted Yarn. In this case it is assumed that the fiber geometry is helical (with constant rate of rotation around yarn axis) in both the straight and bent yarn. A coordinate system can be defined from the yarn axis with,

s = coordinate along yarn axis

r = fiber radial position

θ = fiber angular position measured from inside of bend

L_t = yarn length per turn of twist.

Now the fiber length functions can be written for the case of a yarn straight in state 1 and bent to a curvature k in state 2. It will be assumed that the fibers do not buckle and that their path around the yarn axis remains helical.

$$\frac{dL_1}{ds} = \sqrt{1 + \left(\frac{dr}{ds}\right)^2 + r^2\left(\frac{d\theta}{ds}\right)^2}$$

$$\frac{dL_2}{ds} = \sqrt{(1 - rk\cos\theta)^2 + \left(\frac{dr}{ds}\right)^2 + r^2\left(\frac{d\theta}{ds}\right)^2} \qquad (2\text{-}14)$$

For a yarn with no migration and a constant fiber rotation about the axis,

$$r = \text{constant} \qquad (2\text{-}15)$$

$$\theta = \frac{2\pi}{L_t}\, s \qquad (2\text{-}16)$$

For this idealized yarn, the continuity equation is obtained

from equations 13 -16.

$$\frac{\partial u_y}{\partial s} = (1 + \varepsilon_f)\sqrt{1 + \left(\frac{dr}{ds}\right)^2 + r^2\left(\frac{d\theta}{ds}\right)^2} - \sqrt{(1-rk\cos\theta)^2 + \left(\frac{dr}{ds}\right)^2 + r^2\left(\frac{d\theta}{ds}\right)^2} \qquad (2\text{-}17)$$

This equation relates the fiber slippage to the strain. It can be integrated directly for the two limiting cases of freedom of fiber motion. When there is no freedom of fiber motion, there will be no slippage and the equation reduces to the following form,

$$\varepsilon_f(r,\theta) = \sqrt{\frac{(1-rk\theta)^2 + (2\pi r/L_t)^2}{1 + (2\pi r/L_t)^2}} - 1 \quad \text{No Freedom of Motion} \qquad (2\text{-}18)$$

This strain distribution has previously been established by Backer[17,42] for fibers at different radial positions and for varying twist. He used a method based on differential geometry.

When there is complete freedom of fiber motion, there will be no strain and the continuity equation reduces to,

$$\frac{\partial u_y}{\partial s} = \sqrt{1 + \left(\frac{2\pi r}{L_t}\right)^2} - \sqrt{(1 - rk\theta)^2 + \left(\frac{2\pi r}{L_t}\right)^2} \quad \begin{matrix}\text{Complete} \\ \text{Freedom of} \\ \text{Motion}\end{matrix} \qquad (2\text{-}19)$$

This equation can be solved using the boundary condition of no slippage at the inside of the bend, $\theta = 0$, which is a point of symmetry. The result for radii of curvature much greater than the yarn radius is approximately,

$$u_y = \frac{rkL_t}{2\pi} \sin\theta \qquad (2\text{-}20)$$

The result reduces to that derived by Backer for low values of twist.

The slippage is greatest at the sides of the bend and falls to zero at the top, $\theta = \pi$, which is also a point of symmetry. Since the conditions of symmetry require that slip be zero at this point, it can be concluded that an idealized yarn can bend with complete freedom of fiber motion and no strains. Alternatively stated, an ideal yarn which bends with no fiber strain maintains a fixed fiber length between inside and outside of the bend. This length of fiber moves relative to the structure but does not have to strain or buckle to map out the geometry of the bent yarn. This finding corresponds to derivations in differential geometry of the constancy of the path length of a single loop of a yarn before and after bending[17,22].

An interesting observation can be drawn from equation 20. From this expression it can be shown that the points of fibers lying on a plane perpendicular to the yarn axis before bending will not lie on that plane after bending. In fact, these fiber points will lie approximately on a plane that has rotated from the original plane. This is illustrated in Fig. 2-4. Note that this situation differs considerably for the case of no freedom of fiber motion where the points on individual fibers always remain in the plane perpendicular to the yarn axis.

Another interesting observation can be drawn from the fiber motions of a bent yarn that may have some practical significance. When two equally twisted yarns are side-by-side, during bending, there will be a considerable relative motion between the surface fibers. This effect does not occur for yarns with opposite direction twist.

In more complex cases the conditions of symmetry cannot be satisfied without fiber strain or buckling. For example, in a yarn having fiber migration so that individual fibers

form a helix of varying radius, it can be shown that the length of the fiber path between two symmetry points is not constant during bending. This means that the fibers will have to alter their path around the yarn axis during bending and buckle; or they will have to strain at some points along their length.

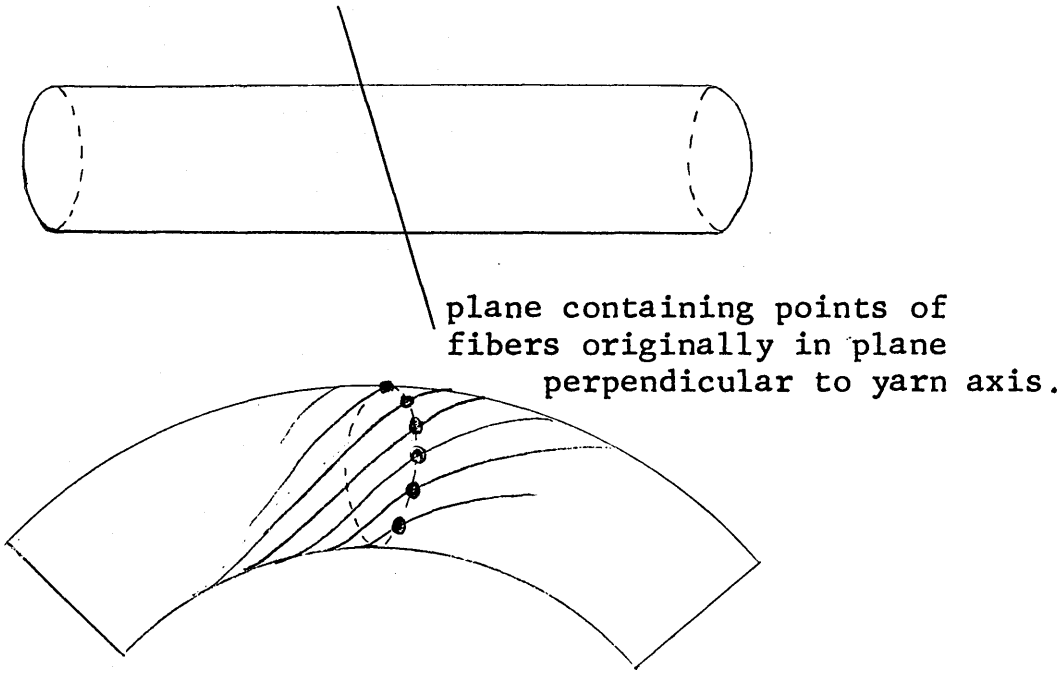

Fig. 2-4 FIBER MOTION IN A BENT TWISTED YARN

The same situation holds true in structures of higher order such as ply yarns and cables. In these systems the fibers may have to strain to map out the bent configuration merely because there is no available path by which they can slide. This phenomenon represents a <u>geometrically induced strain or buckling</u>. It can also occur in simple layered structures under certain conditions. One such case is a multi-layer beam that is cemented or clamped at the ends so

that no relative motion can occur at these points. Then, even if the interlayer friction approaches zero, there will be no relative layer motion within the structure as it is bent. This results from the boundary conditions of no slip at the ends which corresponds to the case of no slippage at the symmetry points of a textile structure. The bent configuration of this multi-layer beam will then of necessity involve tensile strains and/or buckling of the layers; and the beam will be much stiffer than a similar beam without an end restraint.

From these considerations, it may be concluded that the bending behavior of a multi-element structure depends not only on the frictional interactions between the elements, but also on the geometric restrictions to relative motion between the elements.

Two-Dimensional Layered Structure. The continuity equation may also be applied to layered structures which deform from one state to another. The length functions can be determined from a knowledge of the shapes of each state and from the distance between the centerline of the structure and the element in question. Again, for the purpose of illustration the structure will be assumed to be a yarn, but this time composed of parallel layers of fibers. An example of the deformation of this structure from one state to another would be the bending of a yarn in a fabric. State one would correspond to the original crimped path of the yarn and state two would be the crimped and bent path of the yarn in the bent fabric. Let,

$k_{1,2}(s)$ = curvature function describing path of yarn axis in state 1 or 2.

$r_{1,2}$ = distance of fiber to yarn axis in state 1 or 2.

Other variables as before.

The differential relation between fiber length and yarn length can be written as follows for the two states,

$$\frac{dL_1}{ds} = 1 + r_1 k_1 (s) \qquad (2\text{-}21)$$

$$\frac{dL_2}{ds} = 1 + r_2 k_2 (s) \qquad (2\text{-}22)$$

Substituting into equation 13 gives the result,

$$\frac{du_y}{ds} = r_1 k_1 - r_2 k_2 + \varepsilon_f(1 + r_1 k_1) \qquad (2\text{-}23)$$

This equation may be specialized as before for limiting cases of fiber interactions. These specialized forms of the continuity equation illustrate how the change in geometric states can be accomplished by fiber strains, fiber slippage, fiber buckling, or combinations of the three.

$$\varepsilon_f = \frac{r_1 (k_2 - k_1)}{1 + r_1 k_1} \qquad (2\text{-}24)$$ Only strain, no slip, no buckling.

$$\frac{du_y}{ds} = r_1 (k_1 - k_2) \qquad (2\text{-}25)$$ Only slip, no strain, no buckling.

$$r_2 = r_1 \frac{k_1}{k_2} \qquad (2\text{-}26)$$ Only buckling, no strain, no slip.

Relative Fiber Motion. The slippage term of the continuity equation is based on the relative motion between individual fibers and the planes perpendicular to the yarn axis. This motion represents the relative motion of the fibers to the yarn structure. For certain cases this motion will be the governing factor in the description of frictional effects. In others, the relative motion between two adjacent fibers will

be of importance. The solution for the first case can be obtained by a direct application of the derived equation and that of the second case can be computed by taking the difference between the values of relative motion of two adjacent fibers.

The results for the two cases will be quite different and generally differ by a factor on the order of the ratio of fiber to yarn diameter. This difference can have a great effect on the overall behavior of a yarn or a textile structure in general.

When the arrangement of fibers in a yarn or fabric is highly disoriented, the motion of one fiber can be thought of as occurring through a medium composed of a random fiber mass. In this case the relative fiber motion can best be calculated by considering fiber motions with respect to the yarn structure. This is because the adjacent fibers will be different at every point and will not necessarily move in the same manner as the fiber in question. The relative fiber motions computed in this way will be large and will result in large frictional effects if they occur against a frictional restraint. This probably takes place in some needled fabrics.

If the fibers are arranged in a highly oriented manner,as would be the case in an idealized twisted or layered yarn, the relative fiber motion is much less than in the previous case for a given amount of change of curvature. This is because the relative fiber motion involves the movements of two adjacent fibers. Although the individual fibers may move considerable amounts relative to the yarn axis, they will move only small amounts relative to each other. For this reason, the frictional effects for this type of system are much smaller than those of the previous effects when the internal pressures are the same. On the other hand, highly disoriented fiber systems often have a greater opportunity

for fiber buckling and in those cases there may be small amounts of relative motion.

Effect of Friction on One-Dimensional Slip and Strain. In addition to the continuity equation developed in the previous section, another fundamental relation may be obtained by considering the propagation of slip into an infinite medium. This will be done for the case of a fiber which is held in such a medium by frictional forces and displaced a fixed amount at the point of entry into the medium. To compute the slippage and strains that take place in this case, it will be necessary to go beyond the point of using the conditions of continuity and utilize the equations of force equilibrium.

Consider a rectangular fiber extending into a semi-infinite medium as shown on Fig. 2-5. Using the coordinate system shown, let,

u = relative fiber motion during loading

v = relative fiber motion during unloading

x_s = extent of slip into medium during loading

x_r = extent of reslip during unloading

f_k = sliding frictional force per length on each side of fiber

f_s = static frictional force per length that can be exerted on each side of fiber

u_o = imposed displacement on end of fiber

v_o = residual displacement at end of fiber after unloading

E = fiber tensile modulus

w = fiber width

h = fiber thickness.

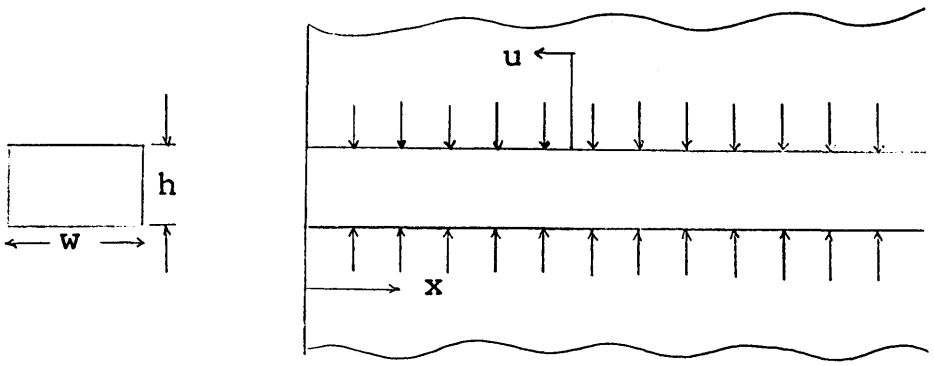

Fig. 2-5 ONE-DIMENSIONAL SLIP AND STRAIN PROPAGATION INTO SEMI-INFINITE MEDIUM.

The problem in this case is to determine the nature and extent of slip and strain propagation into the infinite medium when a force or displacement is applied to the fiber end. Qualitatively, it can be reasoned that the fiber will both strain and slip only a finite distance into the medium. Then, when the load is released, the fiber will slip back into the medium, but it will not do so completely and thereby leave a residual deformation. This deformation will depend on the counterbalancing of elastic and frictional forces and will be analagous to the residual bending deformation computed for the multi-layer beam in Chapter I.

During the loading cycle, a differential equation may be written for the displacement at a point of the fiber. This equation is obtained from the continuity equation for this case, the stress-strain relation, and the force balance for an infinitesmal element,

$$\varepsilon_f = -\frac{du}{dx} \tag{2-27}$$

$$T = Ewh\,\varepsilon_f \tag{2-28}$$

$$2f_k + \frac{dT}{dx} = 0 \qquad 0<x<x_s \tag{2-29}$$

$$\frac{d^2u}{dx^2} = \frac{2f_k}{Ewh} \tag{2-30}$$

The boundary equations for this equation are,

$$u(o) = u_o \tag{2-31}$$

$$u(x_s) = 0 \tag{2-32}$$

$$\frac{du}{dx}(x_s) = -\frac{\pi f_s}{Ew} \tag{2-33}$$

Note that one extra boundary condition is given and this permits calculation of the extent of slip propagation. The boundary condition which gives the strain at the point x_s is obtained by computing how much shear stress is developed in a solid wall of material subjected to a step distribution of strain. When this shear stress equals that which the material can just withstand by static friction, the step distribution of strain will correspond to the strain used in the boundary condition. The intermediate steps leading to this conclusion are not shown, but they follow the same general procedure used in Appendix A.

During unloading, a similar differential equation can be written for the region in which reslippage occurs. In this case, the sliding frictional force will act in the opposite direction. The boundary conditions for this equation are based on zero tension at the fiber end and no reslip beyond the

point x_r. At this point the tension drop due to resliding will produce shear stresses which can just be maintained by the static friction forces. The magnitude of the strain at the point is computed by a superposition of strain distributions and a method similar to that used for loading.

$$\frac{d^2v}{dx^2} = \frac{-2f_k}{Ewh} \tag{2-34}$$

$$\frac{dv}{dx}(o) = 0 \tag{2-35}$$

$$v(x_r) = u(x_r) \tag{2-36}$$

$$\frac{dv}{dx}(x_r) = \frac{du}{dx}(x_r) + \frac{\pi f_s}{Ew}(1 + \nu) \tag{2-37}$$

The solutions to the differential equations can be obtained by considerable algebraic manipulation. They are,

$$u = (u_o - x_s F)\left(\frac{x}{x_s}\right)^2 - (2u_o - x_s F)\left(\frac{x}{x_s}\right) + u_o \tag{2-38}$$

$$v = -(u_o - x_s F)\left(\frac{x}{x_s}\right)^2 + \frac{u_o}{2} + \frac{(x_s F)^2(2\nu + \nu^2)}{8(u_o - x_s F)} \tag{2-39}$$

Where,

$$\frac{x_s}{h} = \frac{\pi}{2\nu}\left[\sqrt{1 + \frac{4\nu}{\pi F}\frac{u_o}{h}} - 1\right] \tag{2-40}$$

$$\frac{x_r}{h} = \frac{x_s}{h}\left[\frac{1}{2} - \frac{\nu}{4}\left(\frac{x_s F}{u_o - x_s F}\right)\right] \tag{2-41}$$

$$F = \frac{\pi f_s}{Ew} \tag{2-42}$$

$$\nu = \frac{f_k}{f_s} \tag{2-43}$$

The results are plotted on Fig. 2-6 for slip and reslip as functions of position.

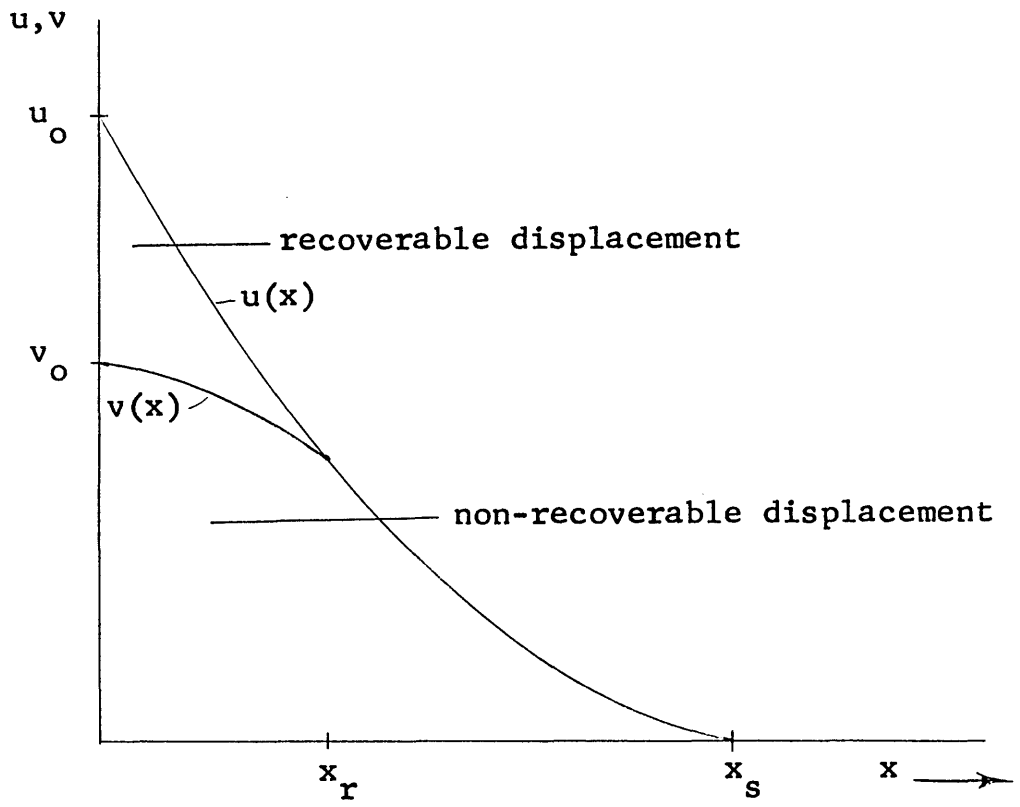

Fig. 2-6 SLIP AND RESLIP IN ONE-DIMENSIONAL PROPAGATION

Two variables are of particular interest in this result: the length of slip propagation and the residual displacement. The length of slip propagation can be represented in terms of the parameters of the system and the imposed displacement. The result is plotted on Fig. 2-7 for $\gamma = 1$. This result shows that the greater the friction is relative to the elastic forces, the less propagation. It also illustrates the nature of the dependence of imposed displacement on the propagation length. Another relation of importance is the residual

Fig.2-7 SLIP PROPAGATION LENGTH vs END DISPLACEMENT

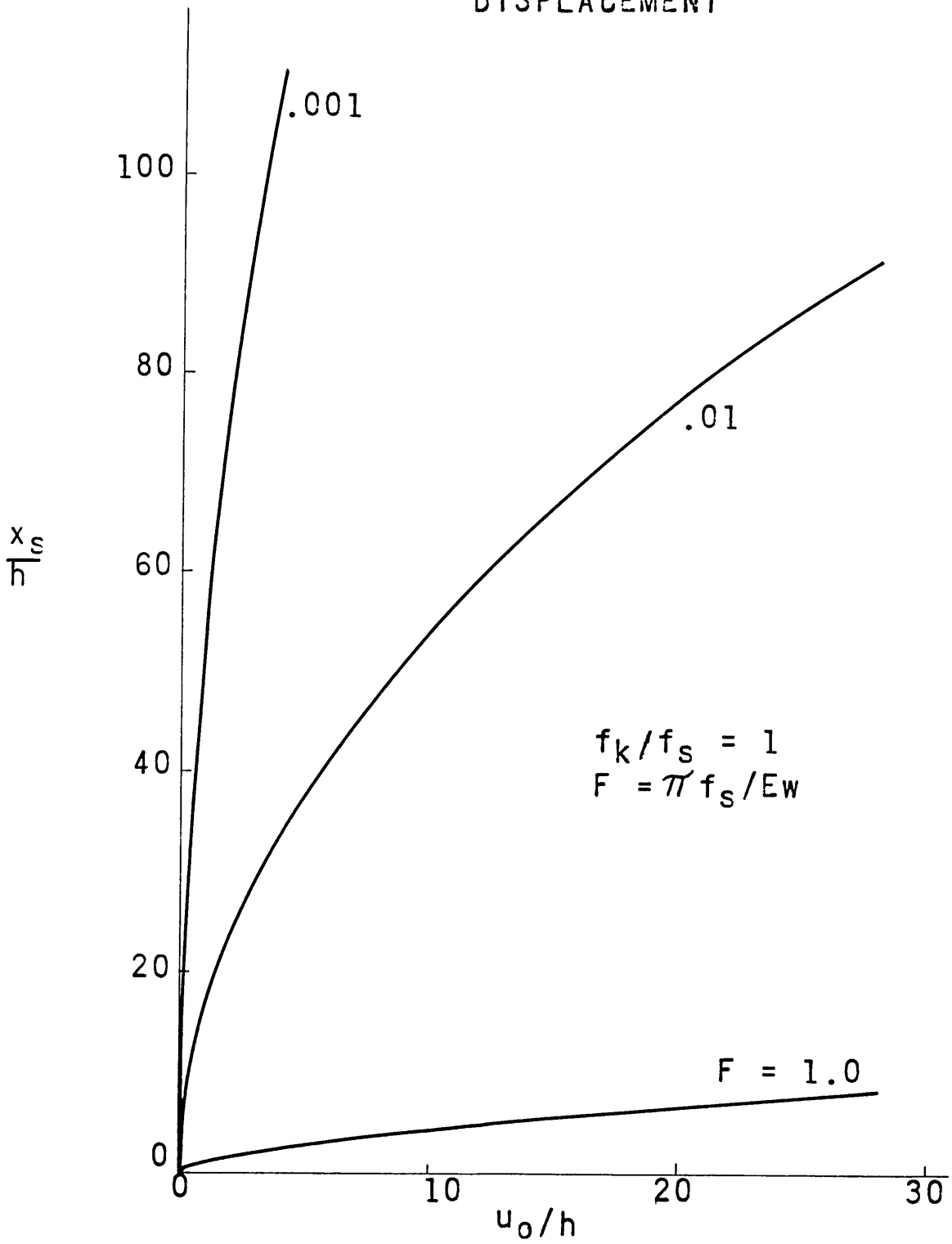

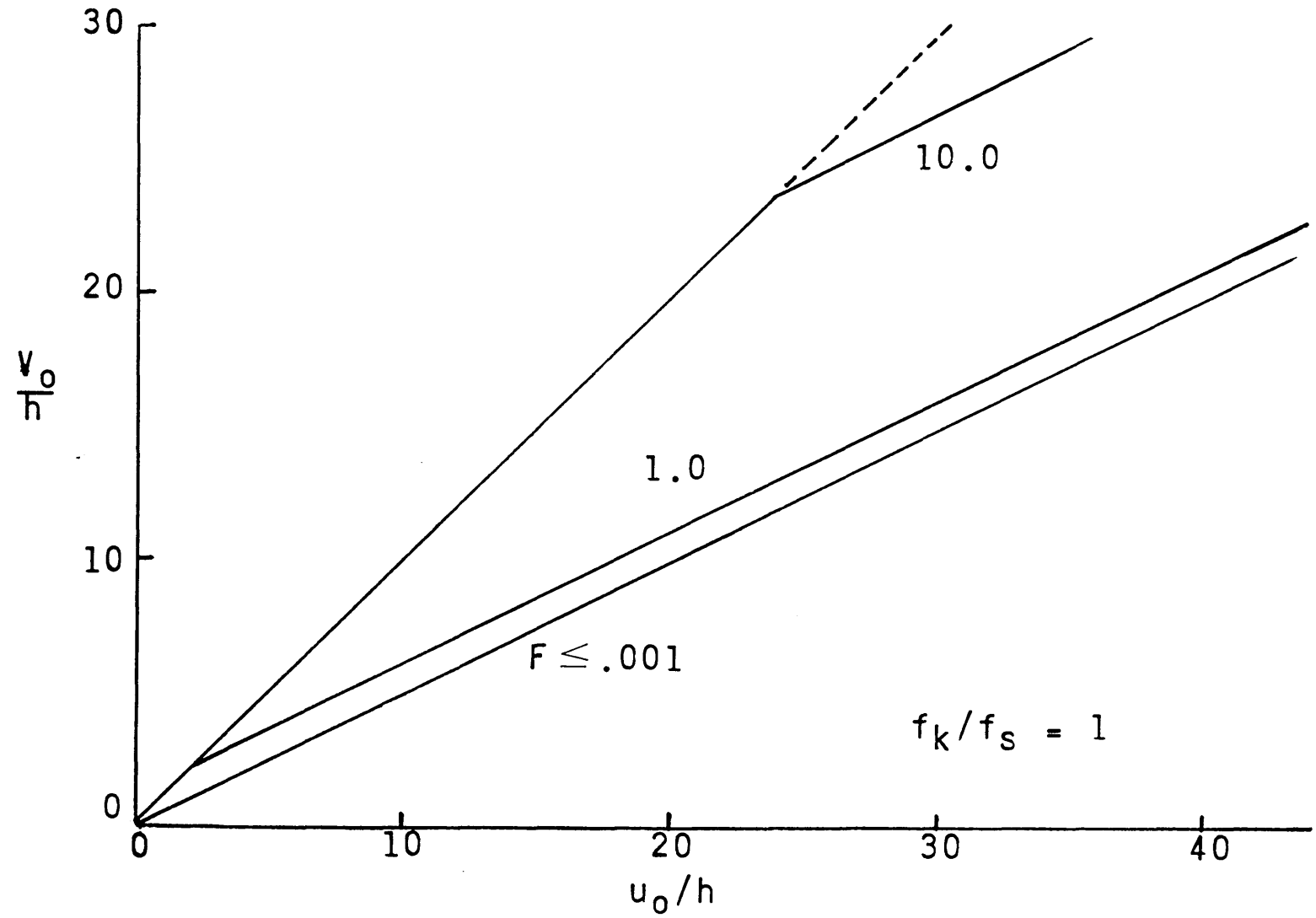

Fig. 2-8 Residual Displacement vs Imposed Displacement

displacement that remains after the load has been removed. This variable is plotted on Fig. 2-8 in terms of the same variables as before and for $\nu = 1$. Note that the residual displacements equal the imposed displacement when the elastic restoring force is not great enough to cause reslipping into the matrix. Beyond this point the residual displacement is close to one-half the imposed displacement.

The analysis presented here was done in conjunction with Mr. Harvey Plonsker, who is using the results in connection with a research project on fiber drafting. In addition to being of interest in connection with that problem, these results may have application in the problem of slip and stretching that takes place in a stretch fabric garment during wearer motion. They could also be used to predict the degree to which materials will slip into the jaws of a tensile testing machine. Or alternatively how much pressure must be applied to confine the propagation length to a fixed space.

Although the results do not give any direct information on bending behavior, they do give a better insight into the question of slip during bending and reslip during recovery. Moreover, the results may be applied directly to the problem of bending by considering the infinitesmal element at the top and bottom of a layer in a multi-layer system. This infinitesmal strip will behave as the fiber in this analysis if the curvature changes are small. The strain variable can then be replaced by the local change of curvature if the layer bends with no tension.

FRICTIONAL EFFECTS IN YARNS

Zero Twist Yarn. In most uses of textiles the yarns used have at least some twist inserted for either strength or geometry requirements. However, the length of one turn of twist is usually considerably greater than the length of the

repeating unit of the fabric. For this reason, it is often possible to assume that the yarns have a negligible twist and that fabrics behave as though the fibers were arranged in a simple layered form.

For a yarn of this type the frictional behavior is similar to that of the multi-layered beam discussed in Chapter I. There it was shown that once the slip had propagated throughout the structure, the bending behavior could be characterized by an elastic rigidity and a friction moment. This can be done readily for a zero twist yarn if it is assumed that the structure is under a constant normal pressure. This pressure can develop from such things as cross yarn interlacings in a woven fabric or fiber tensions in a bent yarn.

Assuming that the yarn is bent by a pure moment and that slip has propagated throughout the yarn length, the elastic rigidity will be the sum of the individual fiber rigidities and the friction moment can be computed from equation 12. Let,

n = normal force per length at each fiber interface

D_f = fiber diameter

k = curvature of the yarn centerline

u = relative fiber motion

W_i = frictional energy loss at each interface in yarn length L

W_t = total frictional energy loss in yarn length L

L = yarn length

s = position coordinate measured along fiber from center of bend

N_i = total number of fiber interfaces between layers

N_f = total number of fibers

r = yarn height to width ratio.

The relative displacement between two fibers stacked on top of one another can be determined from the strain discontinuity between the fibers and the condition of symmetry at the center of the bend as in Chapter I, equation 25. (Note that a correction may be applied to account for close packing effects.)

$$u = D_f k s \tag{2-44}$$

Since the fibers move relative to each other against an assumed constant frictional restraint, the work lost at each element of fiber interface can be computed by

$$dW_i = \mu n\, u\, ds \tag{2-45}$$

After integrating, this becomes,

$$W_i = 2\int_0^{L/2} \mu n\, D_f k\, s\, ds = \frac{\mu n D_f k L^2}{4} \tag{2-46}$$

Note that the integration was broken into two parts because of the change in direction of the frictional force on either side of the bent yarn. This same procedure will be used in subsequent calculations. Summing the frictional work loss over all the fibers gives,

$$\frac{W_t}{L} = \frac{N_i \mu n\, D_f L_k}{4} \tag{2-47}$$

This equation can be differentiated as in equation 12,

$$M_f = \frac{1}{4} N_i \mu n\, D_f\, L \tag{2-48}$$

If the fibers are arranged in an open packed rectangular section, the number of fiber interfaces will be equal to the number of fibers less the number of fibers in one layer.

This can be expressed in terms of the height to width ratio of the yarn

$$N_i = N_f - \sqrt{N_f r} \tag{2-49}$$

$$M_f = \frac{1}{4} N_f \left(1 - \sqrt{\frac{r}{N_f}}\right) \mu n D_f L \tag{2-50}$$

This equation relates the frictional effect in zero twist yarns to the parameters of the system. Note that the result is identical to that of equation 62 in Chapter I. In this case the number of fibers is used in place of the number of layers; and, the force per length on each fiber is used in place of the force per length on each layer. Note also that the computation made here utilized the energy equation rather than the method of Chapter I which involved the equations of force equilibrium.

In the section on the bending of woven fabrics, the imposed pressure will be evaluated in terms of the structure and properties of the system and it will no longer be necessary to include this unknown quantity in the equations.

Twisted Yarn. The frictional effect in twisted yarns can be determined for situations in which the fibers are free to slide, but do so against a frictional restraint. In this case the elastic rigidity will be given by equation 6 and the frictional moment can be computed by the energy method of equation 12.

In order to establish this frictional bending moment, it will first be necessary to determine the relative fiber motions that occur as the yarn bends. If the yarn is assumed to consist of cylindrical layers of twisted fibers, there will be relative motion both between fibers of different

layers and fibers of the same layer as bending takes place. These relative motions can be computed from the geometry of the bent twisted yarn.

Relative motions of fibers in adjacent layers can be computed by first determining the relative motion of the individual fibers to the yarn matrix and then computing the relative motions of these fibers to each other. Using the results of equation 20 and considering two fibers at radial positions differing by one fiber diameter, the result is found to be,

$$u_r = \frac{D_f k}{2\pi T} \sin \theta \qquad (2\text{-}51)$$

where,

u_θ = relative motion between fiber of the same layer

u_r = relative motion between fibers in adjacent layers

D_f = fiber diameter

k = yarn curvature

T = yarn twist

r = fiber radial position

θ = position angle of point on fiber measured from inside of bend

Q_o = helix angle before bending

Q = helix angle after bending

L_t = yarn length in one turn of twist

w_i = frictional energy loss per length at one fiber interface.

The pattern of relative motion of equation 51 indicates that there will be a sinusoidal distribution of slip which is zero at both the inside and outside of the bend. The amplitude of this distribution depends on the yarn twist, fiber

diameter, and yarn curvature as shown. It is independent on the radial position of the fiber.

Relative motion between fibers of the same layer results from a change in the local helix angle as bending progresses. The magnitude of this change has been computed by Backer and found to vary with fiber position as follows,

$$\cot Q = (1 - rk \cos \theta) \frac{1}{2\pi rT} \qquad (2\text{-}52)$$

This equation has been rewritten in terms of the variables used in this treatment. (See Appendix C). It indicates that all fibers except those at the sides of the bend change their helix angle; and that the maximum increase is at the inside of the bend while the maximum decrease is at the outside. When two adjacent fibers of the same layer experience this change in helix angle, they will slide by each other as shown in Fig. 2- .

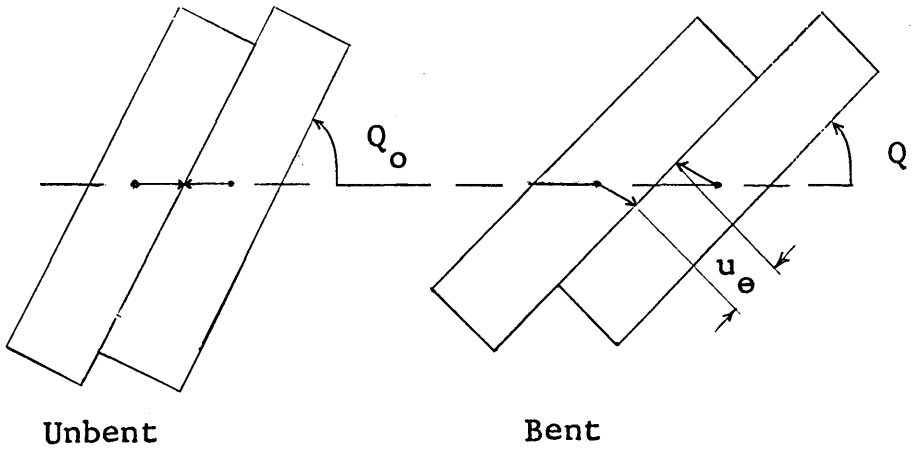

Fig. 2-9 RELATIVE FIBER MOTION DUE TO CHANGE IN LOCAL HELIX ANGLE

The magnitude of this relative motion can be shown to be related to the change in helix angle as follows,

$$u_\theta = D_f \, (\cot Q_o - \cot Q) \tag{2-53}$$

Combining equations 52 and 53 gives the slippage distribution for this effect.

$$u_\theta = \frac{D_f k}{2\pi T} \cos \theta \tag{2-54}$$

This relative motion is quite similar to that of equation 20. In this case, however, the relative motion is zero at the sides of the bend and reaches a maximum at the inside and outside positions.

Since the relative motion of fibers is readily observable, an experiment was conducted to determine the validity of equation 54. This was done with a large scale model of a seven-ply yarn (each model fiber being about 1/8 inch in diameter). In order to facilitate the interpretation of the variables in the slippage equation, it was rewritten in dimensionless form.

$$\frac{u_\theta}{D_f} = R_y k \cot Q_o \cos \theta \tag{2-55}$$

In this notation the slippage is measured in units of fiber diameters. The curvature is given in a dimensionless form which corresponds to the maximum amount of strain that would occur in a solid elastic rod of equal size bent the same amount. This dimensionless curvature was used in Chapter I and will again be used in Chapter III.

Measurements were made to determine the relationship between slip and curvature, and slip and fiber position. The results for both theoretical and measured values are given on Figs. 2-9 and 2-10. Note that there is generally good agreement for low curvatures. The deviations at the higher

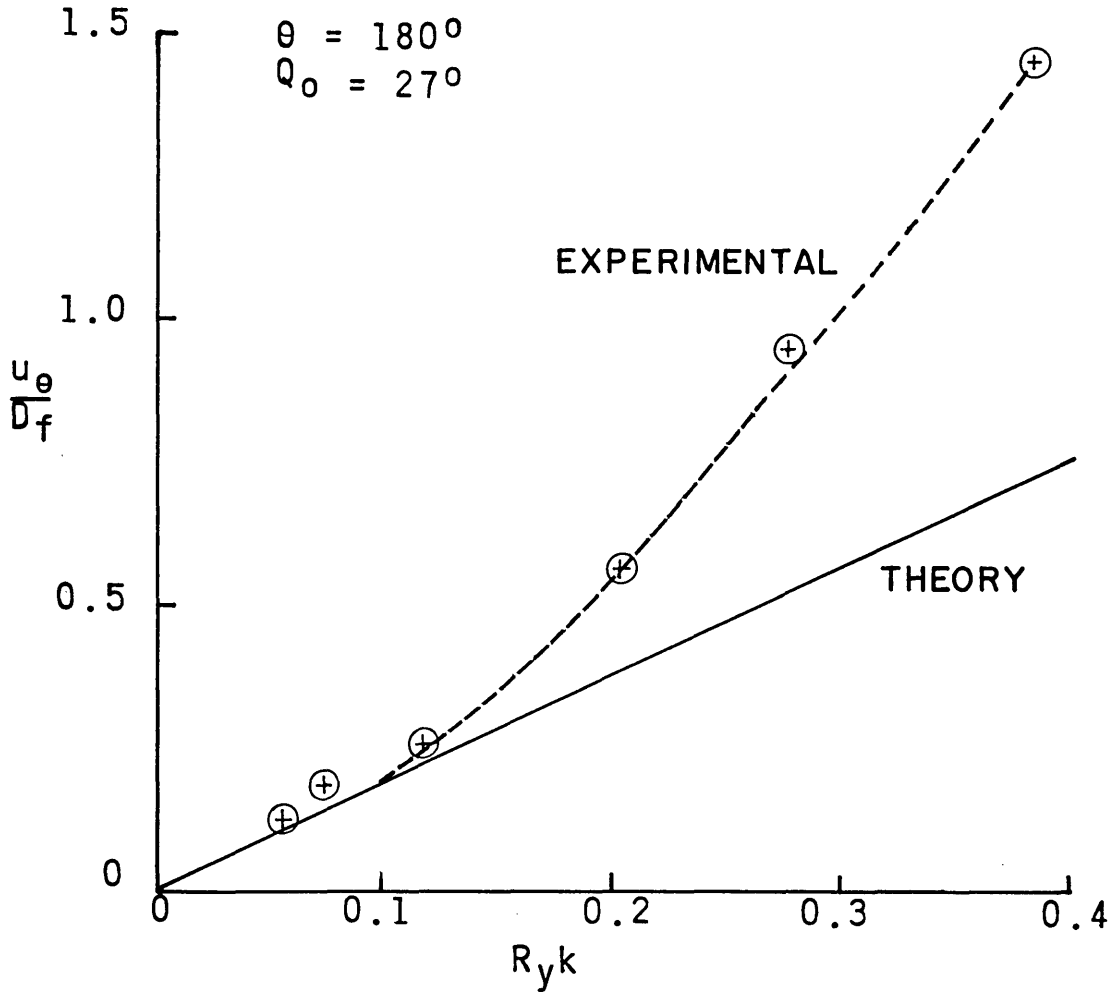

Fig.2-10 RELATIVE MOTION BETWEEN FIBERS OF ONE LAYER OF A BENT YARN

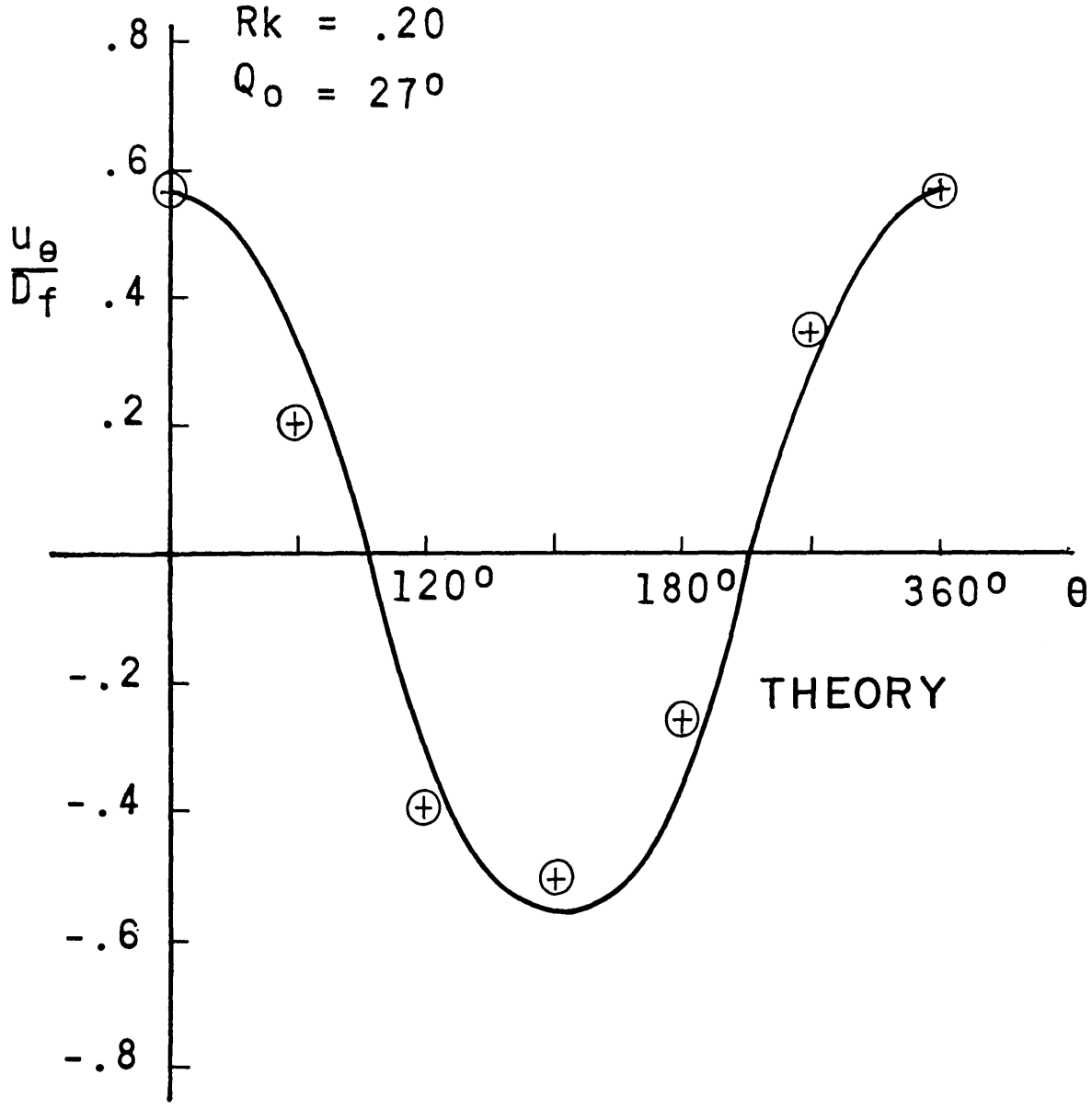

Fig. 2-11 RELATIVE MOTION VS FIBER POSITION

curvatures probably occur because of the mathematical simplifications made in the analyses.

The relative fiber motions that take place in a bent twisted yarn are given by equations 51 and 54. When the interfiber friction resisting these motions is known, then it is possible to compute the friction moment by applying equation 12. This will be done for two cases: in the first the internal pressure distribution will be assumed constant; and in the second it will be assumed to be the distribution resulting from a constant tension. In both cases the analyses will assume that the fibers are able to slip to the full extent and that frictional forces act against the motions rather than act to prevent them. In this case the elastic rigidity will be as given by the result of the complete freedom of motion case. If the frictional forces are sufficiently high to prevent complete slip, then the continuity equation must be used to determine the effects of partial slip on elastic rigidity and friction moment. The case of partial slip will be considered later for the woven fabric and those results can be applied here.

Friction Moment in Twisted Yarn under Constant Pressure. Under the assumption of constant pressure the normal force per length at each fiber interface will be constant. Then the frictional energy loss per length of yarn at one interface, "w_i", can be computed. This is done by integrating the force-displacement behavior over one-half turn of twist. A half turn is used because this length represents a repeating unit of the structure.

$$w_i = 2T \int_0^{1/2T} \mu n_i u \, ds \qquad (2\text{-}56)$$

Note that the yarn length of one-half turn of twist is 1/(2T) and the length of fiber in this amount of yarn is taken

to be approximately $L_t/2$. Since the normal force is assumed constant, equation 56 may be rewritten as:

$$w_i = 2T\mu n_i \frac{L_t}{2} u_{avg} \tag{2-57}$$

$$u_{avg} = \int_0^{L_t/2} u(s)\, ds \tag{2-58}$$

Since the slippage distributions between and within layers differ only in phase, the average values will be the same. It should be noted that the integration of equation 58 must be performed in such a way as to average the slippage over a region in which the frictional force remains the same. This must be done because the direction of this force changes so that it always opposes motion. The result may be substituted into equation 57 to give:

$$w_i = \frac{2}{\pi^2}\mu n_i D_f \frac{L_t}{2} k \tag{2-59}$$

Summing over all the fiber interfaces N_i and differentiating with respect to curvature gives the friction moment,

$$M_f = \frac{2}{\pi^2}\mu n_i N_i D_f \left(\frac{L_t}{2}\right) \tag{2-60}$$

This equation corresponds closely to the friction moment predicted for a zero twist yarn by equation 50. In this case the characteristic length of the system corresponds to the average length of fiber in one-half turn of twist, whereas in the other it corresponds to the sample length.

If it is assumed that each fiber contacts two fibers in its layer, two fibers in adjacent layers, and the number of fibers in the yarn is large, then:

$$M_f = \frac{4}{\pi^2} N_f \mu n_i D_f \frac{L_t}{2} \tag{2-61}$$

Equation 61 gives the functional relation predicted within the assumptions of this analysis. The normal force between fibers has been left in general terms. It will depend on the equilibrium configuration of the fibers, the yarn tension, any lateral loading which may exist, and the yarn twist.

It should be noted that this equation assumes that the length of yarn being bent is much greater than the twist length. If the test length is smaller than the twist length, then the yarn will behave as predicted by the zero twist analysis previously presented. In that case the effect of twist will be to change the normal force. If the test length is greater than the twist length, then equation 61 holds and the twist will serve to reduce the required relative fiber motion. This indicates that twist not only reduces rigidity because of the fiber inclinations to the yarn axis, but also because it reduces the required relative fiber motion.

Friction Moment in a Twisted Yarn under Constant Tension. The friction moment developed in a twisted yarn under tension can be computed by a method similar to that used in the constant pressure case. In this case, the pressure will vary radially and its magnitude will depend on the tension and geometry of the system. For the purpose of this analysis it will be assumed that the assumptions of the previous case hold and that the pressure distribution is as computed by Machida[23].

$$p_A = 2\pi F T^2 \left(1 - \frac{r^2}{R_y^2}\right) \qquad (2\text{-}62)$$

Where,

r = fiber radial position

R_y = yarn radius

γ_y = packing factor

μ = coefficient of friction

T = twist (turns/length)

F = yarn tension

p_A = internal pressure (force/area)

This pressure distribution can be translated into a normal force per length on each fiber interface and this can be combined with the relative fibers motions to give the energy loss. The essential difference between this analysis and that of the previous section is that in this case the energy loss varies with radial position. For this reason, the total energy loss involves summing, or integrating, the energy losses throughout the structure after correcting for the differences in number of interfaces at each radial position.

The details of the calculation are shown in Appendix D and the resulting friction moment is approximately,

$$M_f = 4 R^2 \gamma_y \mu F T \qquad (2\text{-}63)$$

The results of this analysis can be applied to twisted materials that are bent while under tension. Examples of this are found in yarns running over guides and twisted structures being wound on drums or packages.

FRICTIONAL EFFECTS IN WOVEN FABRICS

As in the case of multi-layer beams and yarns, the elements of a woven fabric slide by one another as the structure bends. The extent to which sliding occurs will determine the elastic rigidity of the material and the energy lost during the process will determine the frictional moment. These two quantities, which describe the bending behavior, were investigated analytically and experimentally. The results will be given in terms of the fabric geometry and the properties of the component fibers.

The frictional moment will be investigated for two different types of energy losses that can occur--one due to relative fiber motion and one due to relative yarn motions. Following this, the elastic rigidity of the fabric will be related to the geometry of the system and the extent of slip propagation.

Frictional Moment due to Relative Fiber Motion. As a fabric bends, the fibers slide by each other as do the individual layers of a multi-layer beam. This relative motion is resisted by frictional forces which develop as a result of the internal pressure of the fabric. From a knowledge of the distribution of fiber slip and internal pressure, it is possible to compute the energy lost during bending and this can be used to compute the frictional moment by means of equation 12.

In the analysis it will be assumed that: the fibers are not restricted from sliding by friction in a fixed region of the structure; the fibers are linearly elastic; the fibers are arranged in layers and have no twist; and, the pressure distribution does not change during bending. Furthermore, the analysis will be restricted to cases of low curvature bends where the radius of curvature is much greater than the thickness of the fabric and to fabrics having moderate crimp. Let,

s = coordinate along fiber

T_s = length coordinate fiber at start of slip region

D_f = fiber diameter

k = fabric curvature

n_j = normal force per length acting between fibers in layer j-1 and j

n_d = net downward force on fiber

N_f = number of fibers per yarn

N_p = number of fibers per layer

r = height to width ratio of yarn

ℓ = number of layers of fibers

EI_f = fiber rigidity

x, y = rectangular coordinates

h_b = wave height of bent yarns

p_c = spacing of cross yarns

μ = coefficient of friction between fibers

c_b = crimp of bent yarns

w_j = frictional work loss per length of fabric at fiber interface j-1, j

w_t = total frictional work loss per length of fabric

u = relative fiber motion at each point.

The slippage distribution can be estimated from the strain discontinuity in the fibers using the method of Chapter I equation 25 just as in the case of the zero twist yarn considered earlier. Referring to Fig. 2-12, if relative fiber motion starts at the point $s = T$, and if every element of fiber between $s = T$ and $s = p_c$, changes its curvature by an amount equal to the curvature of the fabric, then the slippage distribution can be shown to be,

$$u = D_f k (T - s) \qquad (2\text{-}64)$$

The fibers located at the inside crowns of the fabric will experience some buckling and lateral motion to satisfy the continuity requirements of bending. This effect will be neglected in the present discussion.

The internal pressure distribution can be computed from a knowledge of the geometry of each of the fibers in the fabric and their equilibrium geometry. For a first approximation it will be assumed that the fibers are originally straight and that their geometry in the fabric is sinusoidal. Furthermore, it will be assumed that the fiber deflections in the

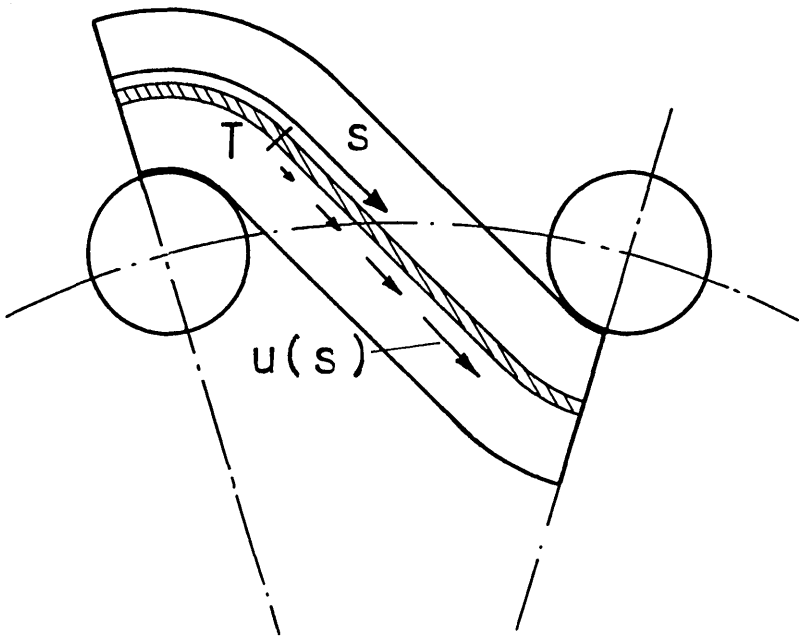

Fig. 2-12 Relative Fiber Motion in Woven Fabric

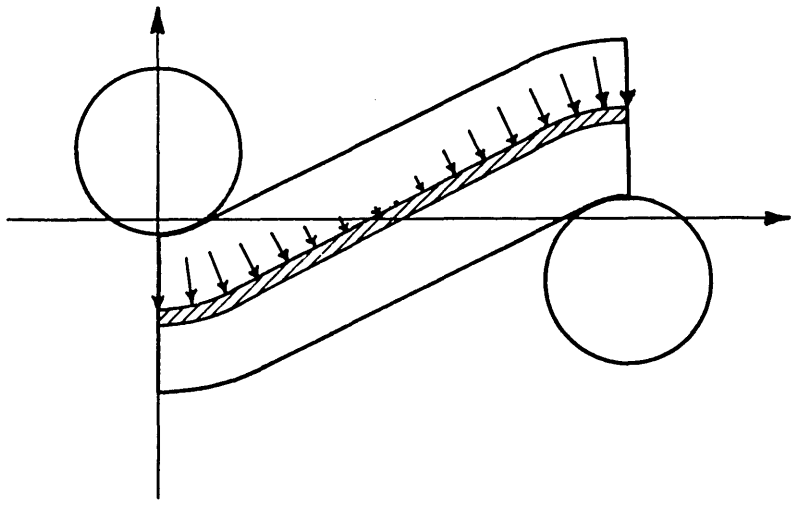

Fig. 2-13 Pressure Distribution in a Woven Fabric

fabric are small and that the conventional beam theory formulations can be used. Referring to Fig. 2-13 the fiber shape can be represented as,

$$y = -h_b \cos \frac{\pi}{p_c} x \tag{2-65}$$

The net normal force per length acting downwards on each fiber can be determined from the classical relation of beam theory which relates deflected shape to loading.

$$n_d = EI_f \frac{d^4 y}{dx^4} \tag{2-66}$$

Solving equations 65 and 66 gives,

$$n_d = EI_f \, h_b \left(\frac{\pi}{p_c}\right)^4 \cos \frac{\pi x}{p_c} \tag{2-67}$$

The net downward force on each fiber element represents a difference between the normal forces on either side of the fiber. Since the normal force on the outside of the fiber on the exposed side of the yarn is zero, it is possible to solve for the normal force at each fiber interface by a difference equation type approach. The result for the j-th fiber, counting from the bottom, on Fig. 2-13 becomes;

$$n_j = j \, EI_f \, h_b \left(\frac{\pi}{p_c}\right)^4 \cos \frac{\pi x}{p_c} \tag{2-68}$$

From symmetry arguments the same reasoning holds for fibers in the next crown. However, in the coordinate system being used, a correction must be made for the fact that the next element is inverted and out of phase by ninety degrees. After performing this manipulation, the pressure distribution can be found to be,

$$n_j = \begin{cases} jEI_f\, h_b \left(\frac{\pi}{p_c}\right)^4 \cos\frac{\pi x}{p_c} & 0 < \frac{\pi x}{p_c} < \frac{\pi}{2} \\ -(\ell - j)\, EI_f\, h_b \left(\frac{\pi}{p_c}\right)^4 \cos\frac{\pi x}{p_c} & \frac{\pi}{2} < \frac{\pi x}{p_c} < \pi \end{cases} \qquad (2\text{-}69)$$

This equation gives the pressure at any location along the fiber length for a fiber in any layer.

Since the pressure distribution is assumed constant, the frictional work lost at each fiber element is merely the friction force times the relative fiber displacement. This energy loss is obtained by integrating over the length of fiber in a length of fabric and dividing by the length of fabric considered.

$$w_j = \frac{1}{p_c} \int_{s=T}^{p_c} u(s)\, n_j(s)\, ds \qquad (2\text{-}70)$$

This integral may be evaluated by using equations 64 and 69, and assuming that x = s and T is small. (The second assumption will be dropped in a later section.) The result is,

$$w_j = \mu EI_f\, h_b \left(\frac{\pi}{p_c}\right)^3 D_f \left[\frac{2}{\pi} j + \left(\frac{1}{2} - \frac{1}{\pi}\right)\ell\right] k \qquad (2\text{-}71)$$

In order to find the total work per length done on the fabric, it is necessary to sum over all the fiber interfaces in a cross-section. This can be done by assuming a rectangular yarn cross section with N_f fibers per yarn and ℓ layers of fibers.

$$w_t = \frac{N_f}{\ell} \sum_{j=1}^{\ell} w_j \qquad (2\text{-}72)$$

$$w_t = \mu\, EI_f\, h_b \left(\frac{\pi}{p_c}\right)^3 D_f N_f \left(\frac{1}{2} + \frac{\ell}{\pi}\right) \qquad (2\text{-}73)$$

This result can now be differentiated with respect to curvature to obtain the frictional moment per yarn. Written in terms of the number of fibers per yarn and the height to width ratio, the result is,

$$M_f = \mu E I_f h_b \left(\frac{\pi}{p_c}\right)^3 D_f N_f \left(\frac{1}{2} + \frac{\sqrt{N_f r}}{\pi}\right) \tag{2-74}$$

The relation between wave height, spacing and crimp established by Pierce[24] can be used to express the result in more convenient terms.

$$\frac{h_b}{p_c} = \frac{4}{3}\sqrt{C_b} \tag{2-75}$$

$$M_f = \frac{4}{3}\pi^2 (N_f E I_f) \sqrt{N_f r}\, D_f \mu \frac{\sqrt{C_b}}{p_c^2} \tag{2-76}$$

The frictional moment predicted by this equation can be seen to depend on geometric structure of the fabric as well as the fiber properties. Since this moment can have an important effect on the bending, and, as will be shown later, the recovery, it is felt that this analysis will be useful, although not completely rigorous.

Experiments were conducted on two series of fabrics to determine the validity of the predicted relation between frictional moment and fabric structure. Both series involved fabrics constructed of yarns with varying spacings and crimps. One set was made of cotton and the other of nylon. The specifications of these fabrics are given in Appendix E.

The moment-curvature relation of each fabric sample was measured on a specially designed instrument which is described in detail in Chapter IV. From this test it was possible to determine a friction moment and an elastic rigidity for each sample. The measured friction moments are plotted on

Figs. 2-14 and 15 as functions of the structural variable $\sqrt{C_b}/p_c^2$ which is a measure of the fabric tightness in the direction of bending. Equation 76 predicts a linear relation between friction moment and this variable which passes through the origin. The measured values of friction did increase with the structural parameter $\sqrt{C_b}/p_c^2$ but the agreement between experiment and theory is <u>not</u> good. In both the cotton and nylon fabrics, the extrapolated value of friction moment for zero structural parameter is greater than zero. This is probably due to additional friction losses that occur due to yarn twist or adjacent yarn rubbing (discussed in the next section).

In the theory which was developed it was assumed that the equilibrium configurations of the fibers is straight. However, in both sets of fabrics a major portion of the residual stresses had relaxed between the time of weaving and measurement. The fiber equilibrium configurations were changed from straight to crimped and the actual internal pressures were far less than those predicted on the basis of no stress relaxation. For this reason it was expected that the measured value of slope of the friction moment vs. structural parameter relation would be considerably smaller than that predicted on the basis of no stress relaxation. This was found to be the case. The ratios of theoretical to measured slope for the cotton and unset nylon fabrics were approximately 100 and 6 respectively. These values are in line with estimates of stress relaxation which were determined from comparisons of the crimp spacing of yarns withdrawn from the fabrics to yarns in the fabrics.

An additional consequence of fiber stress relaxation was found in the difference in measured values of the unset and heat set nylon samples. As expected, the heat setting altered

Fig.2-14 FRICTION MOMENT vs STRUCTURAL PARAMETER

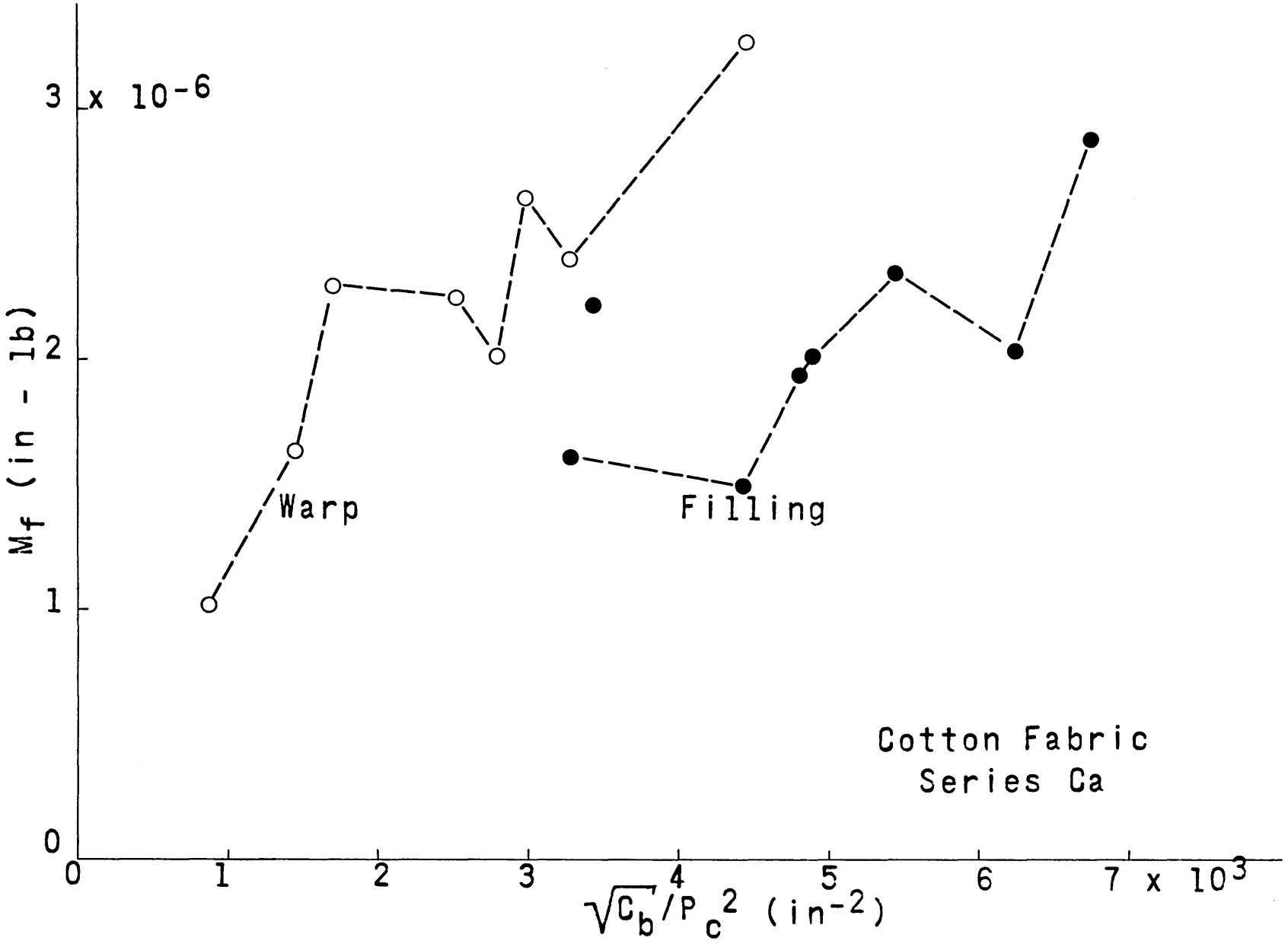

Fig. 2-15 Friction Moment vs Structural Parameter for Nylon Fabrics

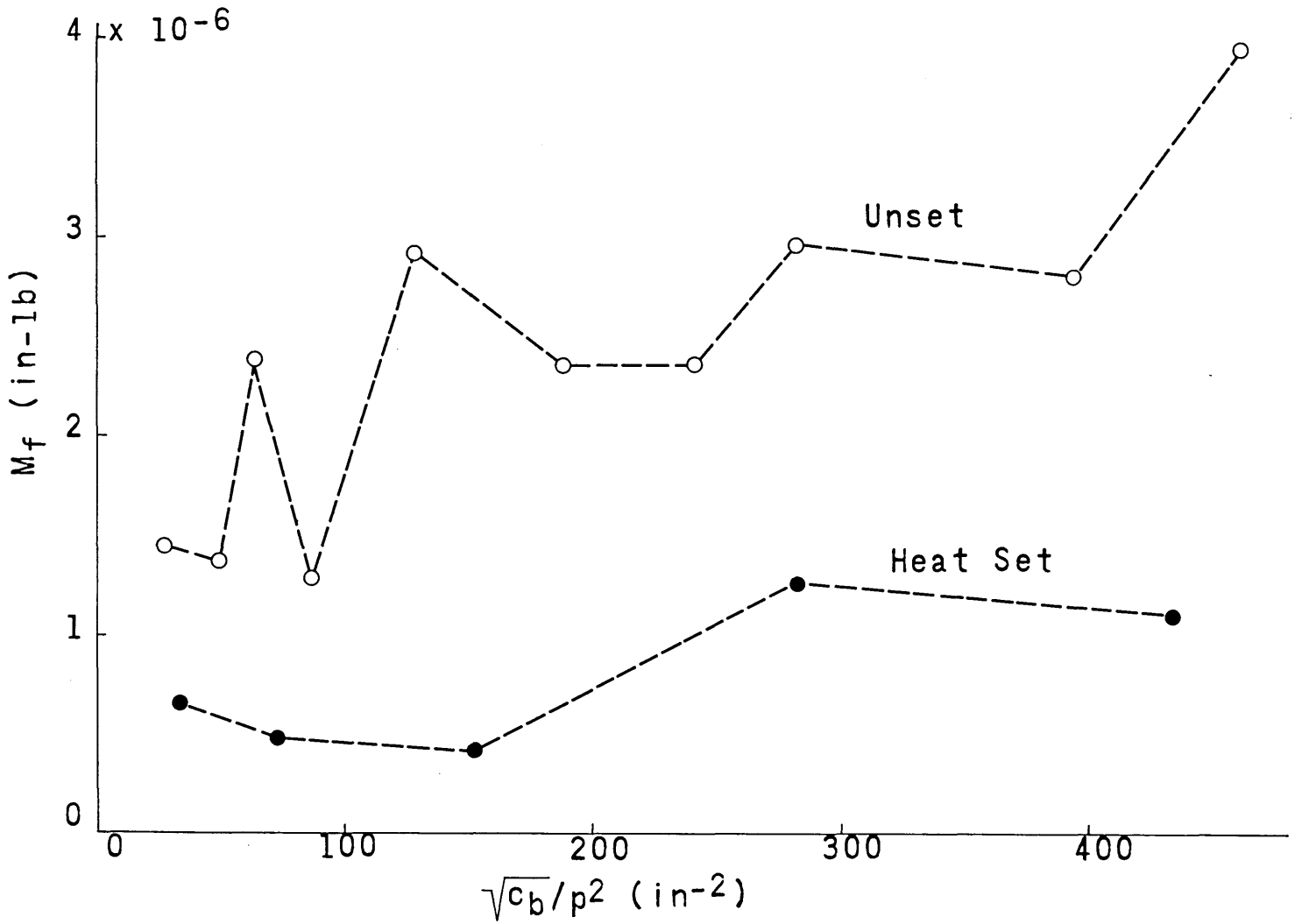

the equilibrium configuration of the fibers, lowered the internal pressure distribution, and resulted in fabrics with considerably reduced friction moments[7] .

It is probable that a more rigorous mathematical treatment which includes the effects of stress relaxation and partial slip propagation would be useful in obtaining a more precise prediction of the effects of fabric structure on the friction moment. Nevertheless, it is felt that the analysis and experimental results presented here do indicate the general trend of the important interrelations between fiber properties, fabric geometry, and friction moment. In a later section the question of partial slip propagation will be discussed in detail.

Parallel Yarn Rubbing in a Woven Fabric. The previous section dealt with the frictional moment that develops in a woven fabric due to energy losses between the fibers. This type of frictional effect appears to be the most significant in most materials at low curvature bends. However, experimental investigations of a number of large scale fabric models have shown that another mode of frictional behavior is possible in some asymmetric fabrics. This mode of frictional effect, which does not appear to have been observed previously, involves a rubbing together of two adjacent yarns as the fabric bends. When the rubbing is done against a frictional force, energy is lost and a frictional moment will develop.

This yarn rubbing is illustrated in Fig. 2-16. There it can be seen that as the fabric bends, the yarns will move relative to the structure (as shown by the arrows) and consequently relative to each other. If these yarns are in contact (as they are in some fabrics), energy will be lost to friction as the material bends. An illustration of

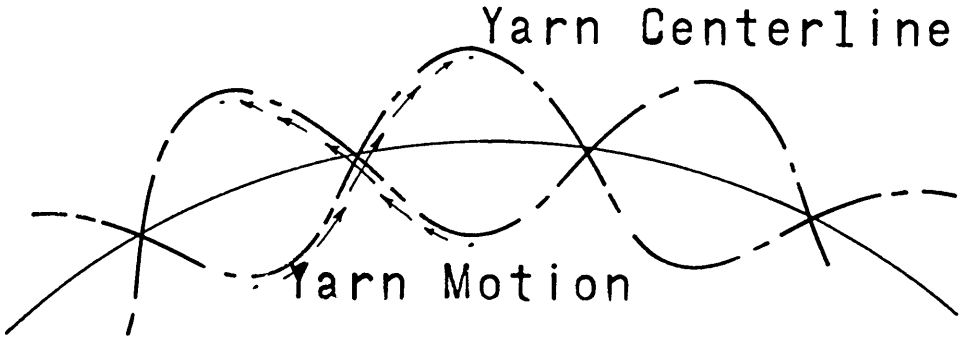

Fig. 2-16 Yarn Motion During Fabric Bending

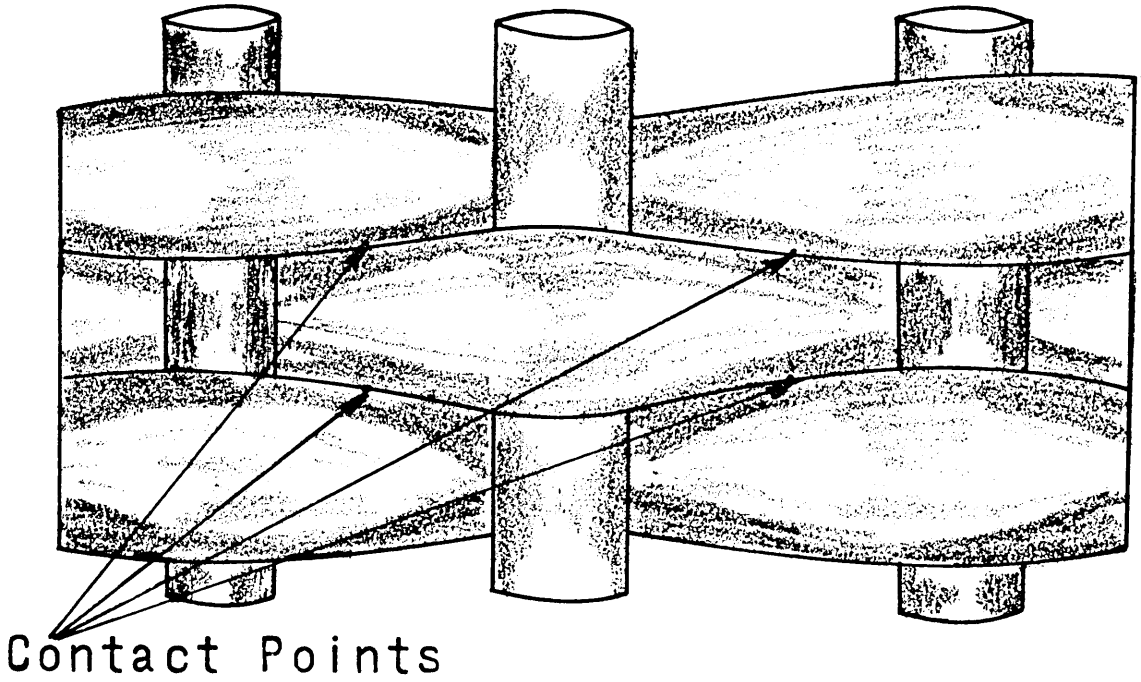

Fig. 2-17 Illustration of Adjacent Yarn Rubbing

adjacent yarns in contact is given in Fig. 2-17.

An approximate analysis will now be presented with the aim of computing the frictional moment for this effect.

Let:

u = relative motion between yarns and fabric matrix at crossing point

u_R = relative motion between adjacent yarns at crossing point

h_b = wave height of bent yarns

c_b = crimp of bent yarns

p_c = spacing of cross yarns

k = fabric curvature

m = number of bent yarns weaving together

F = force between adjacent yarns at crossing point

M_f = frictional moment per yarn of fabric

w = energy loss per length of fabric per yarn

μ = sliding coefficient of friction between yarns.

If it is assumed that the shape of each yarn axis is sinusoidal relative to the fabric centerline before and during bending, it is possible to compute the relative motion between the yarns and the body of the fabric, using the previously derived continuity equation. This relative motion can be shown to be zero at the top and bottom of each crown and a maximum at the crossing point between adjacent parallel yarns. At this point it has a magnitude equal to,

$$u = \left(\frac{p_c}{\pi}\right)^2 \left[\ln \left(\frac{\pi h_b}{p_c} + \sqrt{1 + \left(\frac{\pi h_b}{p_c}\right)^2} \right) \right] k \qquad (2\text{-}77)$$

The relative motions between the yarns can be computed vectorially from this equation and the yarn geometry. It is

$$u_R = \frac{\ln\left(\frac{\pi h_b}{p_c} + \sqrt{1 + \left(\frac{\pi h_b}{p_c}\right)^2}\right)}{\sqrt{1 + \left(\frac{\pi h_b}{p_c}\right)^2}} \frac{2}{\pi^2} p_c^2 k \qquad (2\text{-}78)$$

If a constant force acts between the adjacent yarns at each crossing point, then the work done against friction can easily be computed from the above equation. Assuming that there are m yarns weaving together, the frictional work per length that must be done per yarn in order to achieve a given curvature may be written as,

$$w = \frac{\mu F u_R}{m p_c} \qquad (2\text{-}79)$$

The frictional moment can be found by combining equations 78 and 79 and differentiating with respect to curvature. Furthermore, it is possible to make a simplification by introducing the relation between crimp and wave height to spacing ratio as in equation 75. The frictional moment can then be found in terms of the cross spacing, the crimp, the number of yarns weaving together and the frictional force.

$$M_f = \frac{2}{\pi^2} \frac{F}{m} p_c \frac{\log_e\left(\beta + \sqrt{1 + \beta^2}\right)}{\sqrt{1 + \beta^2}} \qquad (2\text{-}80)$$

$$\beta \equiv \frac{4}{3}\pi\sqrt{c_b} \qquad (2\text{-}81)$$

Fabrics in which adjacent yarns do not touch have a zero value of F and, clearly, there is no frictional loss due to this mechanism. However, in some fabrics this effect can be considerable. This is especially true in certain elastic type fabrics where stretch yarns are left in the material with high residual stresses. These stresses pull the cross yarns together and thereby develop a normal force F. In more

conventional fabrics that have internal yarn rubbing without residual stresses, a normal force develops as the yarns compress each other laterally. The magnitude of these forces depends on the amount of this compression and the lateral properties of the yarns.

Since the relative yarn motions that occur in this situation are of considerable magnitude, large losses can be obtained by this mode of frictional behavior. This may be desirable for certain types of industrial applications such as damping devices or schrapnel protective materials.

Although the effect of internal yarn rubbing was developed in connection with fabric bending and recovery, it should be pointed out that this action may be important in internal fabric abrasion and fiber migration.

Structural Effect on Elastic Rigidity. The bending behavior of woven fabrics was studied by both microscopic examination and by means of large scale models. It was found that as the fabric bends there is a change of curvature produced in the yarns perpendicular to the axis of bending. However, the sections of these yarns that form the outer crowns of the bend are restricted from bending by the cross yarns and they retain their original curvature. This is illustrated in Figs. 2-18 and 2-19. This means that the lengths of yarn in the unrestricted regions will have to undergo larger changes of curvature to conform to the curvature of the fab ric. From this consideration the rigidity of a yarn in a fabric will be greater than that of the yarn before it was woven. On the other hand, the yarn in a fabric follows a crimped path and this would tend to reduce the rigidity of a yarn in a fabric over what it was originally. Both of these factors will be considered in the following analysis in an attempt to predict

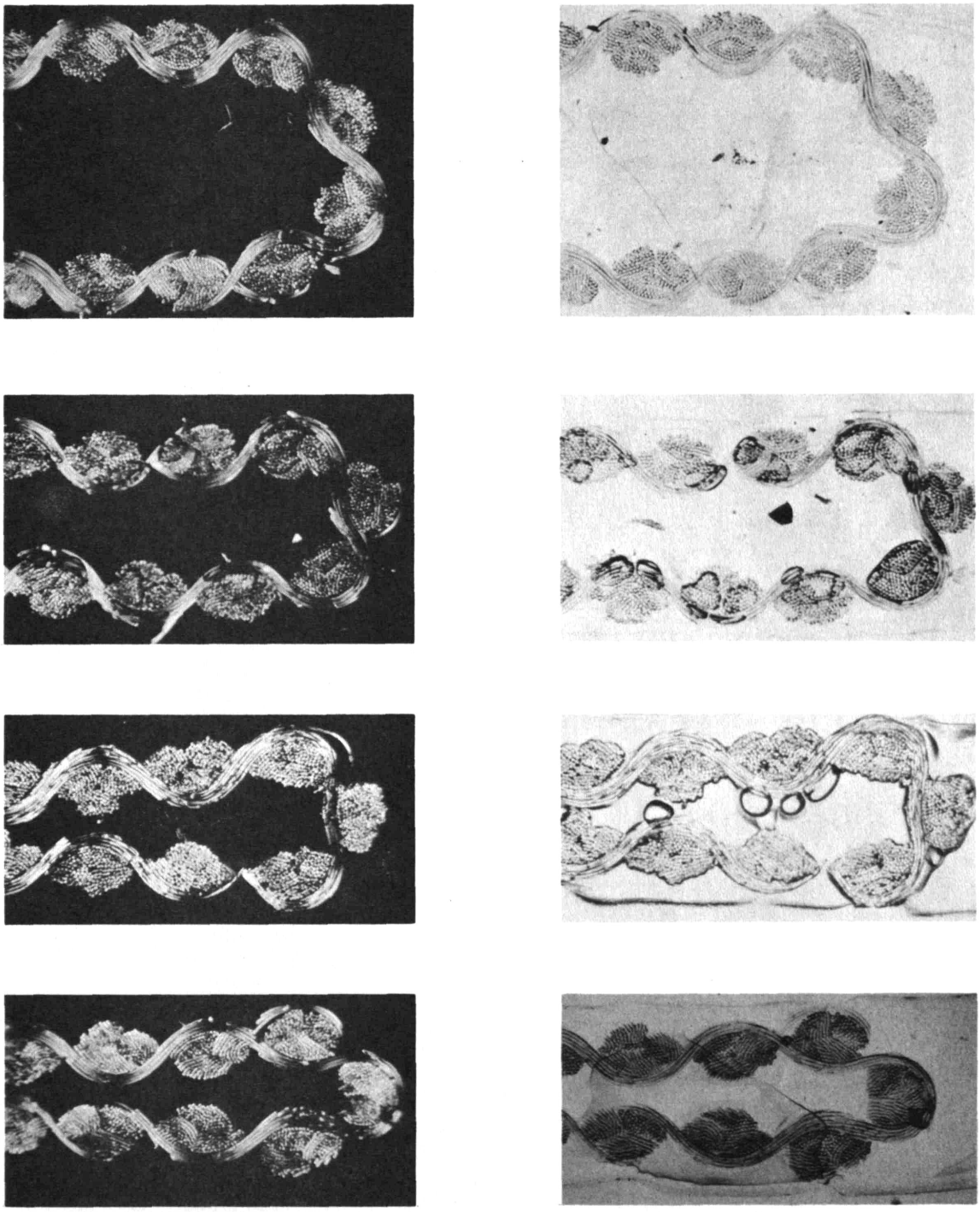

Fig 2-18 CROSS SECTIONS OF FABRIC BENT TO VARIOUS CURVATURES

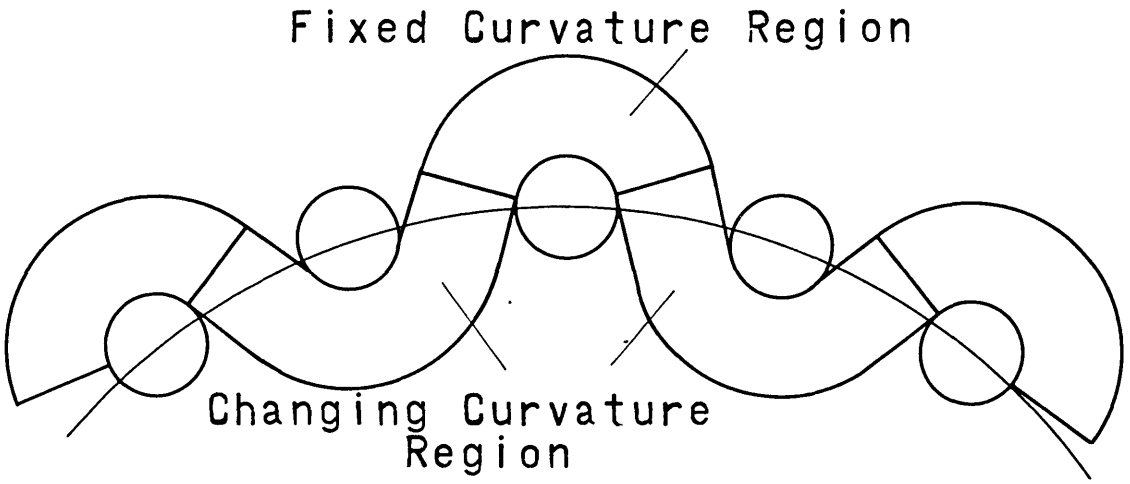

Fig. 2-19 Effect of Fabric Structure on Rigidity

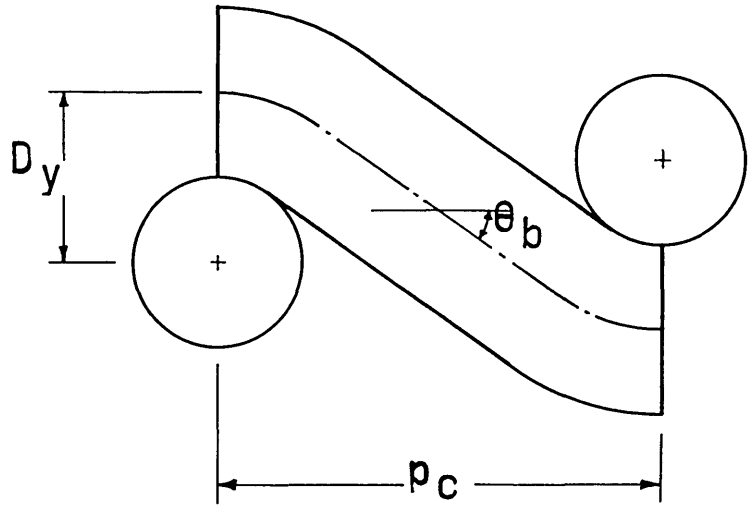

Fig. 2-20 Idealized Geometry of Woven Fabric

the elastic rigidity of a woven fabric.

Let,

R_{yf} = rigidity of a yarn in a fabric
R_y = rigidity of a yarn before weaving
s = coordinate along yarn axis measured from center of outside crown
ϕ_o = tangent angle of yarn axis--original
ϕ_B = tangent angle of yarn axis--bent
S_r = length of restricted region
S_t = total yarn length between crowns
p_c = spacing of cross threads
M = moment per yarn applied to fabric
c_b = crimp of bent yarns = $S_t/L - 1$
q = S_r/S_t
D_y = yarn diameter
k_f = fabric curvature
θ_b = inclination angle of bent yarns.

If a pure moment is applied to the fabric, then it can be shown that each element of yarn length not touching a cross yarn is also under a pure moment. These elements of yarn length will then change their curvature ($d\phi/ ds$) by an amount M/R_y. On the other hand, each element of yarn in the restricted region will retain its original curvature.

Referring to Fig. 2-18 this can be expressed mathematically as,

$$\frac{d\phi_b}{ds} = \begin{cases} \frac{d\phi_o}{ds} & 0 < s < S_R \\ \frac{d\phi_o}{ds} + \frac{M}{R_y} & S_R < s < S_T \end{cases} \qquad (2\text{-}82)$$

Integrating this equation and assuring that ϕ is continuous,

gives,

$$\phi_b = \begin{cases} \phi_o & 0 < s < S_R \\ \phi_o + \frac{M_s}{R_y} - \frac{MS_R}{R_y} & S_R < s < S_T \end{cases} \tag{2-83}$$

This equation makes it possible to compute the fabric curvature. If it is assumed that the yarn spacing remains fixed, then the fabric curvature becomes,

$$k_f = \frac{\phi_b\,(S_T)}{p_c} \tag{2-84}$$

With the aid of equation 83 this may be written as

$$\frac{M}{k_f} = R_{yf} = \frac{p_c\, R_y}{S_T - S_R} \tag{2-85}$$

This result can be written in terms of the crimp and fractional length of the restricted region.

$$\frac{R_{yF}}{R_y} = \frac{1}{(1 + C_b)(1 - q)} \tag{2-86}$$

Equations 85 or 86 can be used directly, or else they can be converted to a more useful form. This conversion can be made in terms of the usual idealized model of a plain weave as shown on Fig. 2-20. From this model it is possible to evaluate the quantities in equation 86. The result is,

$$\frac{R_{yf}}{R_y} = \frac{\frac{p_c}{D_y}\cos\theta_b}{\theta_b \cos\theta_b + \frac{p_c}{D_y} - 2\sin\theta_b} \tag{2-87}$$

$$2\sin\theta_b < \frac{p_c}{D} < \frac{2}{\sin\theta_b}$$

The limits placed on the cross spacing result from considerations of yarn jamming. Equation 87 is plotted on

Fig. 2-21. It illustrates the relation between fabric rigidity per yarn and looseness of the fabric. As tighter fabrics are considered (lower p_c/D_y), the rigidity predicted will remain approximately equal to the original yarn rigidity for a range of p_c/D_y and then the rigidity will increase sharply. This effect was found by Chadwick[25] in his research on a variety of fabrics. It was also found to be the case in experiments conducted in this research. The cotton and nylon fabric series described in Appendix E were evaluated on the moment-curvature instrument and the results of elastic rigidity are plotted on Figs. 2-22, 23 and 24. The measured relation between elastic rigidity and cross yarn spacing follows the trend predicted by equation 87 for both series. The leveling off of this relation at high spacings is more apparent in the nylon series since those fabrics cover a considerably wider range of constructions.

The increase of elastic rigidity with decreasing spacing was more pronounced in the unset than in the heat set nylon fabrics. This occurred because of the higher internal pressures present in the unset fabrics which apparently caused a reduction in the extent of slip propagation. Superimposed on this effect was the cross yarn restriction which occurred in both sets of fabrics. As a result both sets had higher elastic rigidities for the tighter constructions due to the geometric effect considered in this section, and the unset fabrics had additional increases in rigidity due to incomplete slip propagation. (The degree of slip propagation will be discussed in a later section.) The measured results also indicate that the asymptotic complete freedom of motion rigidity is the same for both sets of nylon fabrics as expected.

An additional relation regarding the effect of geometric

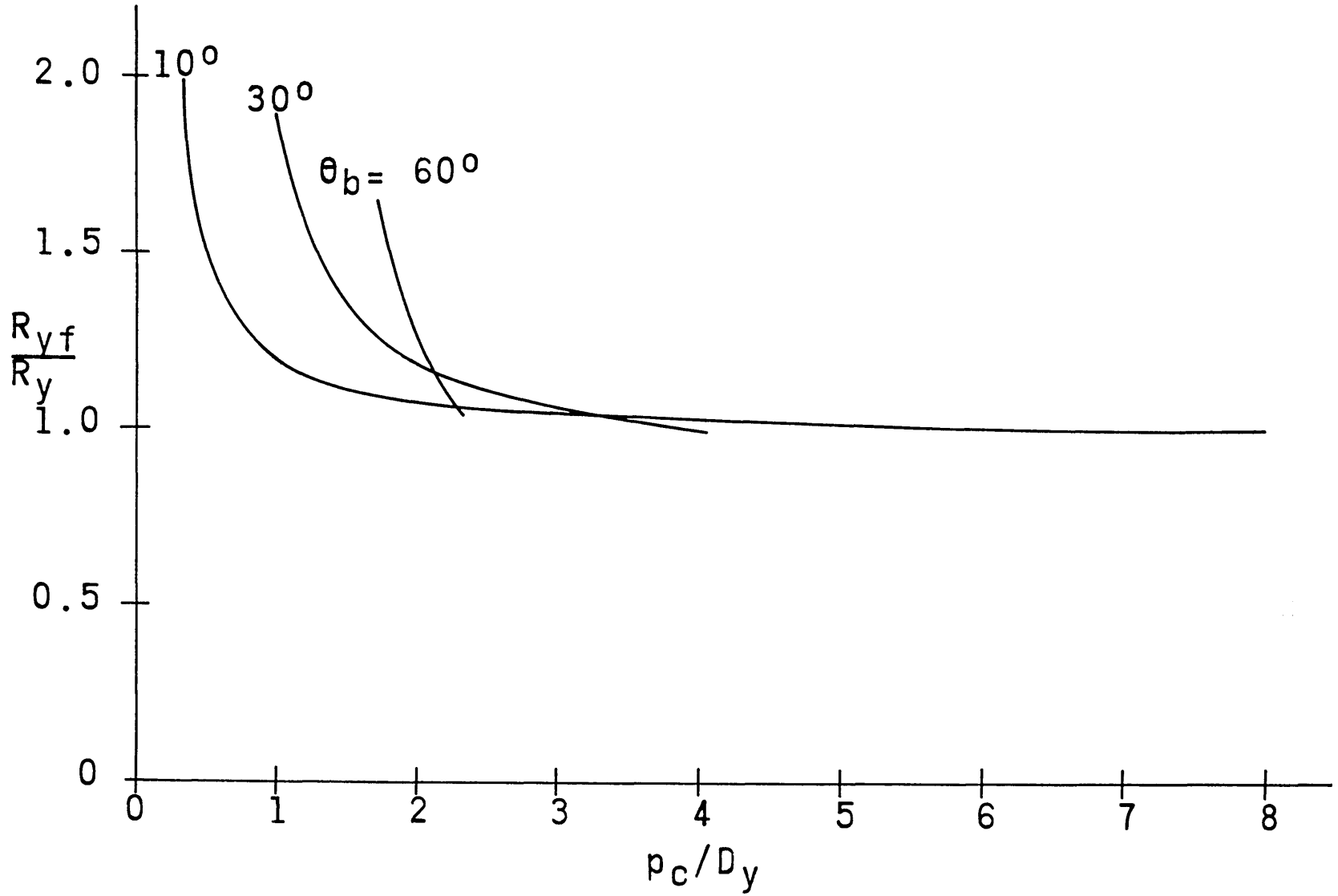

Fig. 2-21 Elastic Rigidity of a Woven Fabric

Fig. 2-22 ELASTIC RIGIDITY VS YARN SPACING

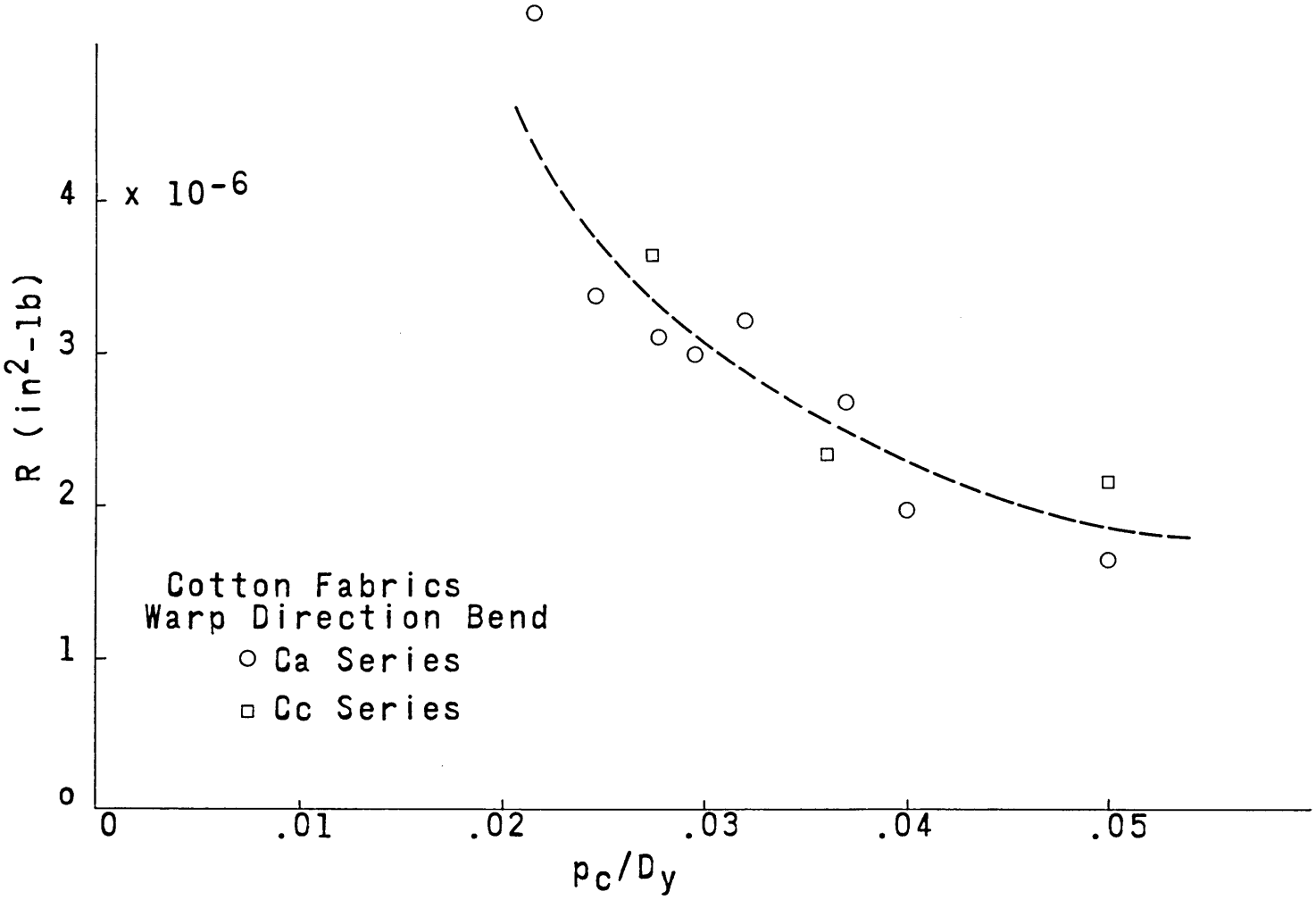

Fig.2-23 ELASTIC RIGIDITY vs YARN SPACING

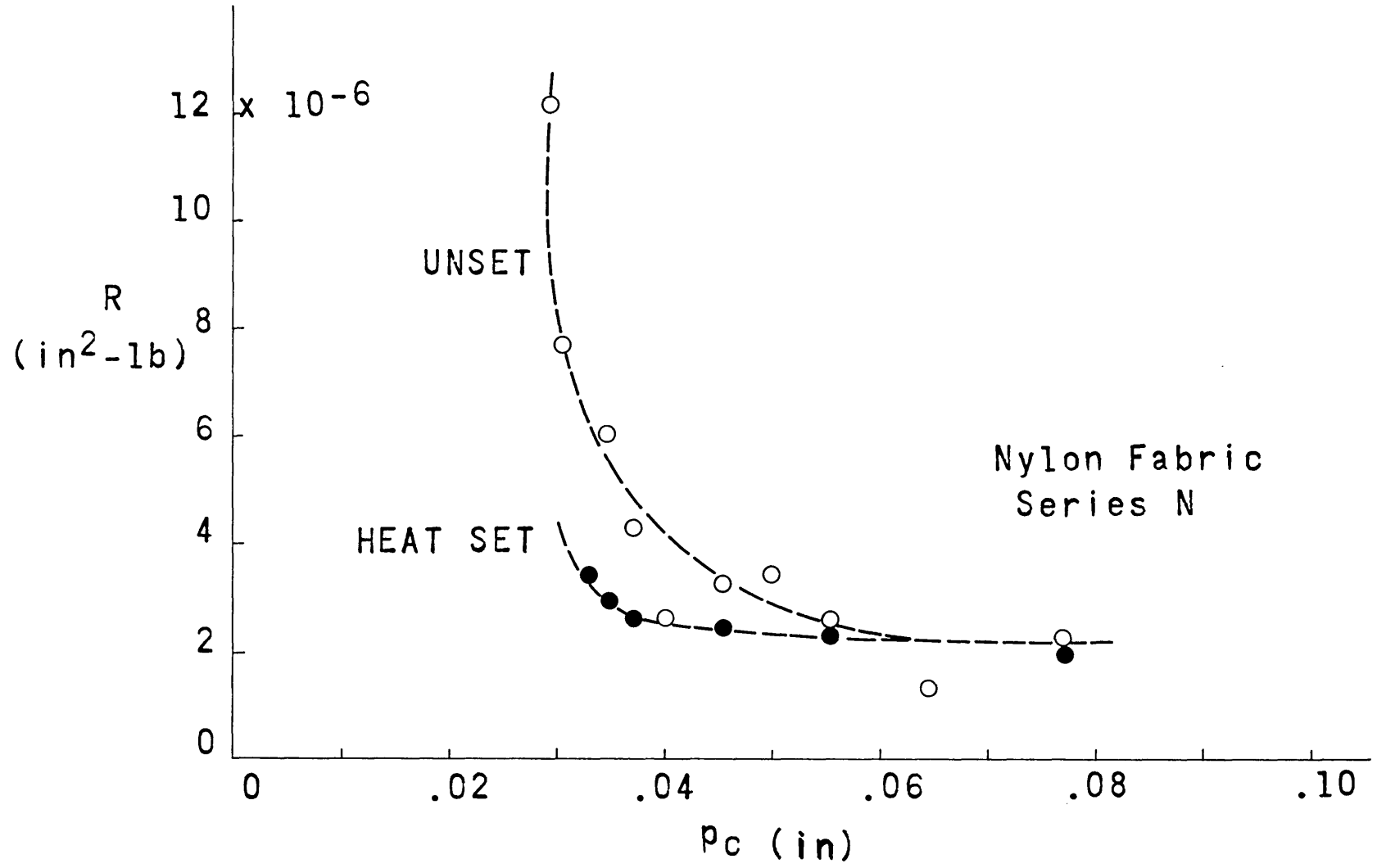

restrictions was observed for the cotton fabric series bent in the filling direction. In this experiment the cross yarn spacing of each sample was approximately constant, but the crimp of the bent yarns varied considerably. The measured values of elastic rigidity of these samples showed a definite increase with crimp. This is shown on Fig. 2-24 , together with an extrapolation to the complete freedom of motion rigidity at zero crimp.

The measured effect of crimp on elastic rigidity is as predicted by the theory. As originally stated, crimp tends to reduce rigidity by providing excess yarn length for bending; and, it also tends to increase the rigidity by increasing the relative size of the regions of fixed curvature of the yarns. According to the results of the analysis which are shown on Fig. 2-21 the latter effect of crimp predominates and rigidity increases with crimp at a fixed value of cross yarn spacing. (Note that the parameter used on this figure is the yarn inclination angle, which is a measure of crimp.) This effect of crimp on rigidity is independent on the ability of the fibers to slide by one another and is caused by a geometric interaction between the yarns in a fabric.

When structures, either of a non-plain weave, or else plain weave with highly flattened yarns are considered[21,26], then this analysis must be modified. This is due to the fact that in these cases geometric changes occurring in the cross yarns will not hold the bent yarn at a fixed curvature. There will be a region of slightly changing curvature rather than one of fixed curvature. This can be seen in some of the open fabric sections on Fig. 3-11.

Relation Between Friction and Extent of Slip Propagation. The previous sections dealt with the relations between friction

Fig. 2-24 Elastic Rigidity vs Yarn Crimp

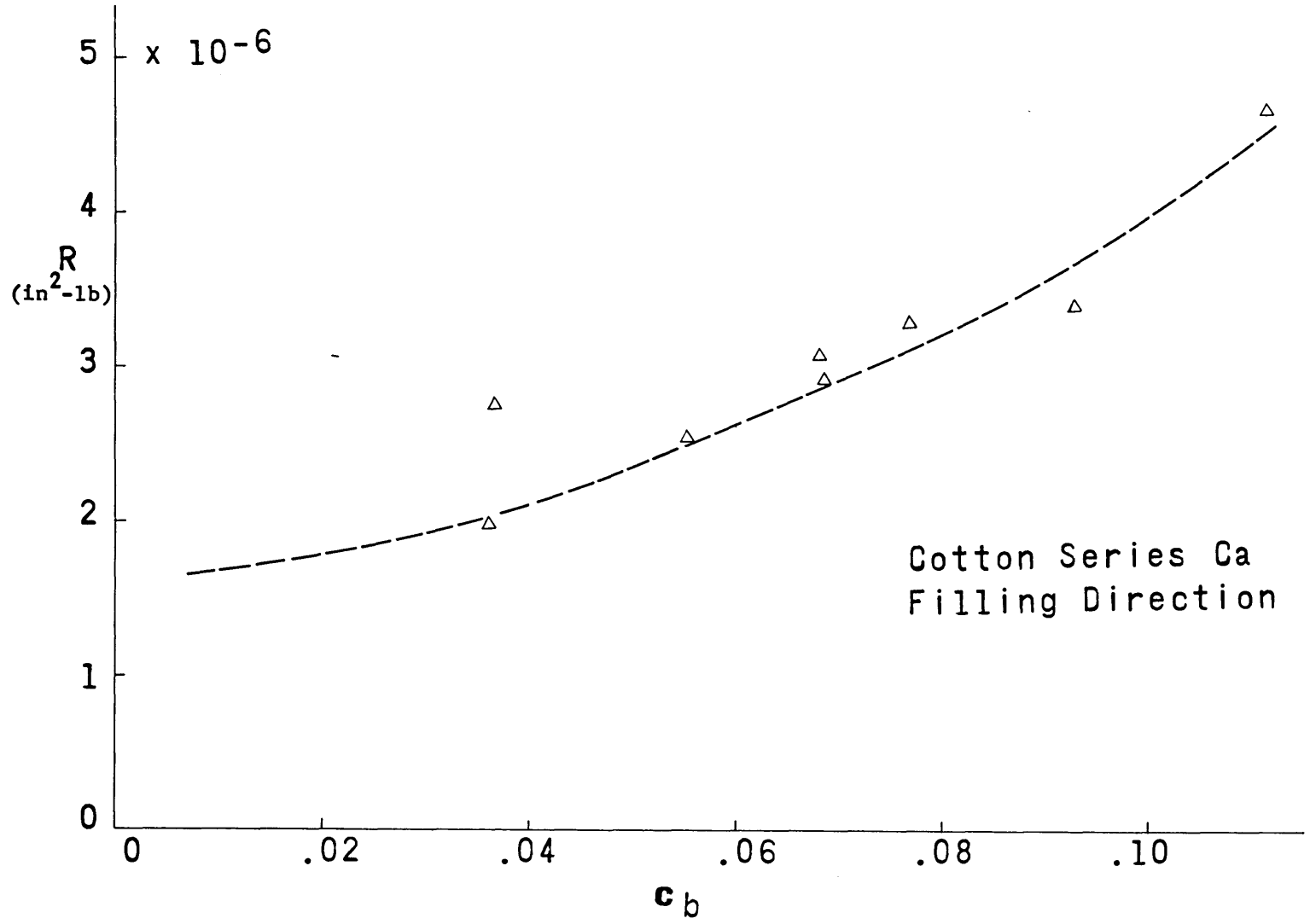

moment, elastic rigidity, and fabric structure. It was assumed that slip had propagated throughout the structure and that the effect of friction was to provide a restraint against slip rather than to prevent it from occurring. Under this assumption, the elastic rigidity corresponds to the complete freedom of motion case corrected for geometric restrictions.

In this section, partial slip propagation will be considered and it will be shown that the assumptions made previously hold only for low levels of friction. It will be assumed that slip propagates lengthwise through each yarn element and that the extent of this propagation depends linearly on the frictional interaction. If the friction is low, the propagation is complete and if the friction is above a critical value, there will be no slip at all.

In the case of bending under a pure moment, it was shown in Chapter I that slip propagated lengthwise through the structure. The extent of the propagation was shown to depend on both the frictional interaction and the level of applied load. Here, it is assumed that the extent of propagation depends only on the frictional restraint and not on the load. The justification for this assumption is found in the fact that the internal fabric pressure changes as the material is bent. This means that while the slip is propagating into the structure, the tendency for increased propagation due to increased level of load will be offset by the increased resistance to propagation caused by the pressure. In this way the extent of propagation will be fixed even though the load increases.

The effect of the extent of slip on elastic rigidity can be predicted by considering the yarns in the fabric to be composed of sections of fibers having no freedom of motion and sections having complete freedom of motion against a

frictional restraint[9] . The fractional length of each of these sections can be expressed in terms of the properties and geometry of the fabric using the indicated assumption.

$$L_s = L\ (1 - \frac{f}{g}) \tag{2-88}$$

Where,

L_s = length of yarn within propagation region
L = total length of yarn in one element
f = frictional force per length at one fiber interface
g = frictional force per length at one fiber interface required to prevent all relative motion
R = elastic rigidity

When a fabric composed of a series arrangement of the two types of elements is subjected to a pure bending moment, the net change of curvature can be found by computing the change in each section and then averaging. Assuming that the fibers are in an idealized square layered form, the section having no freedom of motion will bend with a rigidity of $N_f^2\ EI_f$ and the section having complete slip against friction will bend as the zero twist yarn previously analyzed (equations 1 and 50). Note that this involves the further assumption that the pressure distribution is constant in the latter region and that the number of fibers is large. On this basis, the moment curvature relation can be shown to be,

$$M = \frac{NEI_i}{(1 - \frac{f}{g})(1 - \frac{1}{N}) + \frac{1}{N}}\ k + \frac{(1 - \frac{f}{g})^2\ \frac{f}{g}\ D_f\ N_f\ gL/4}{(1 - \frac{f}{g})(1 - \frac{1}{N}) + \frac{1}{N}} \tag{2-89}$$

From this equation, the friction moment and the elastic rigidity can be related to the friction force and to each other. This has been done for the case of fabric with a

large number of fibers in each yarn with the following results,

$$M_f = \frac{D_f N_f g}{4} \frac{L}{} \left(\frac{f}{g}\right)\left(1 - \frac{f}{g}\right) \tag{2-90}$$

$$\frac{R}{NEI_i} = \frac{1}{1 - \frac{f}{g}\left(1 - \frac{1}{N}\right)} \tag{2-91}$$

$$M_f = \frac{D_f N_f g}{4} \frac{L}{} \left(1 - \frac{NEI_i}{R}\right)\left(\frac{NEI_i}{R}\right) \tag{2-92}$$

These equations are plotted on Fig. 2-25 in dimensionless terms. Note that the length term corresponds to twice the cross yarn spacing for the case of a plain weave fabric.

These equations show that the elastic rigidity increases with friction from the case of complete freedom of motion to the case of no freedom of motion as the friction force varies from zero to g. If the value of f/g is small, the change of elastic rigidity will be small for low values of friction force and the result reduces to that found in the previous sections where the elastic rigidity was assumed to be the sum of the individual fiber rigidities independent of friction.

Equation 90 indicates the relationship between friction moment and interfiber friction force. This quantity varies approximately parabolically with friction force. It first increases, goes through a maximum, and then falls to zero. The physical interpretation of this effect is that the friction moment increases with friction force until the reduction of slip length becomes significant. Then, when the slip length approaches zero the friction moment falls to zero. For the case of small values of f/g, the results of the analysis reduce to those of the zero twist yarn. In that analysis the effect of partial slip propagation was neglected.

The relation between friction moment and elastic rigidity is given by equation 92 and Fig. 2-25b. It is useful for the

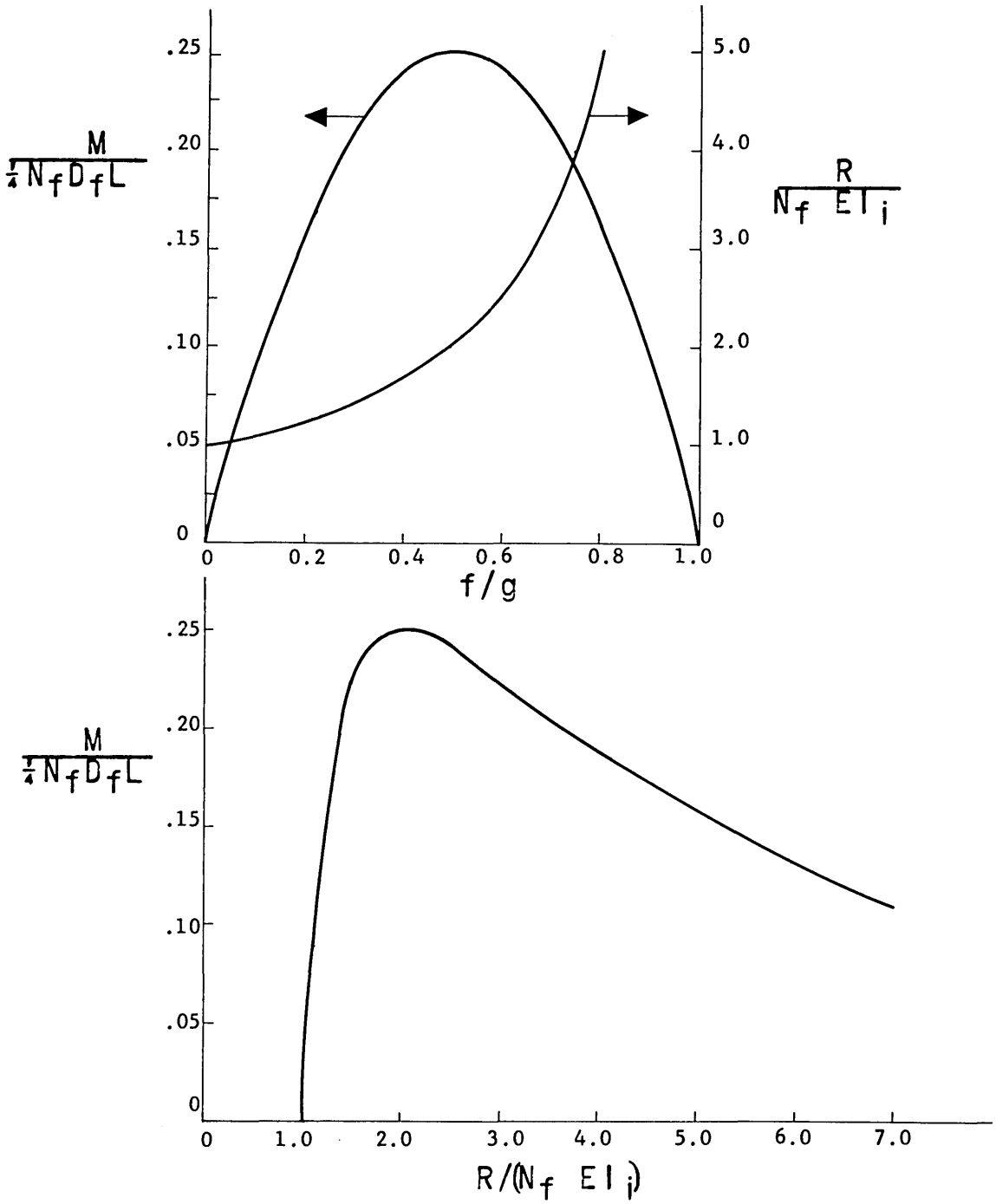

Fig. 2-25 Relation Between Friction Moment, Elastic Rigidity, and Friction Force

evaluation of fabrics in which it is difficult to measure the interfiber friction force. The functional relation exists for values of elastic rigidity between the limiting cases. It increases rapidly at first, goes through a maximum and then drops to zero gradually.

Although equation 89 has been written for the bending of a fabric, it can also be applied to other situations. In a twisted yarn, for example, the effect of changing the friction force will also effect the length of slip propagation and thereby cause changes in both the elastic rigidity and the frictional moment. In that case, the nature of the extent of propagation will be more complex. Fibers will begin slipping on the sides of the bend and the slip will propagate towards the outside and inside of the bend. Again, the elastic rigidity will increase with friction from the case of complete freedom of motion to that of no freedom of motion and the friction moment will increase, go through a maximum, and then fall to zero.

An experiment was conducted to determine the effect of frictional changes on the elastic rigidity, the friction moment, and the bending recovery behavior. One cotton and one nylon fabric was used and treatments were applied to each for the purpose of both increasing and decreasing the interfiber friction. For each fabric seven samples were scoured and then three samples were treated with softening agent (commercially available type) of varying concentration and three were treated with a "frictionizer" (Monsanto's Syton) of varying concentration. The seventh sample was used as a control. (See Appendix E for the sample descriptions.)

The bending parameters were measured on the moment-curvature instrument described in Chapter IV and the results are plotted on Figs. 2-26 to 2-29. For the nylon series,

Fig.2-26 FRICTION MOMENT vs INTERFIBER FRICTION FORCE

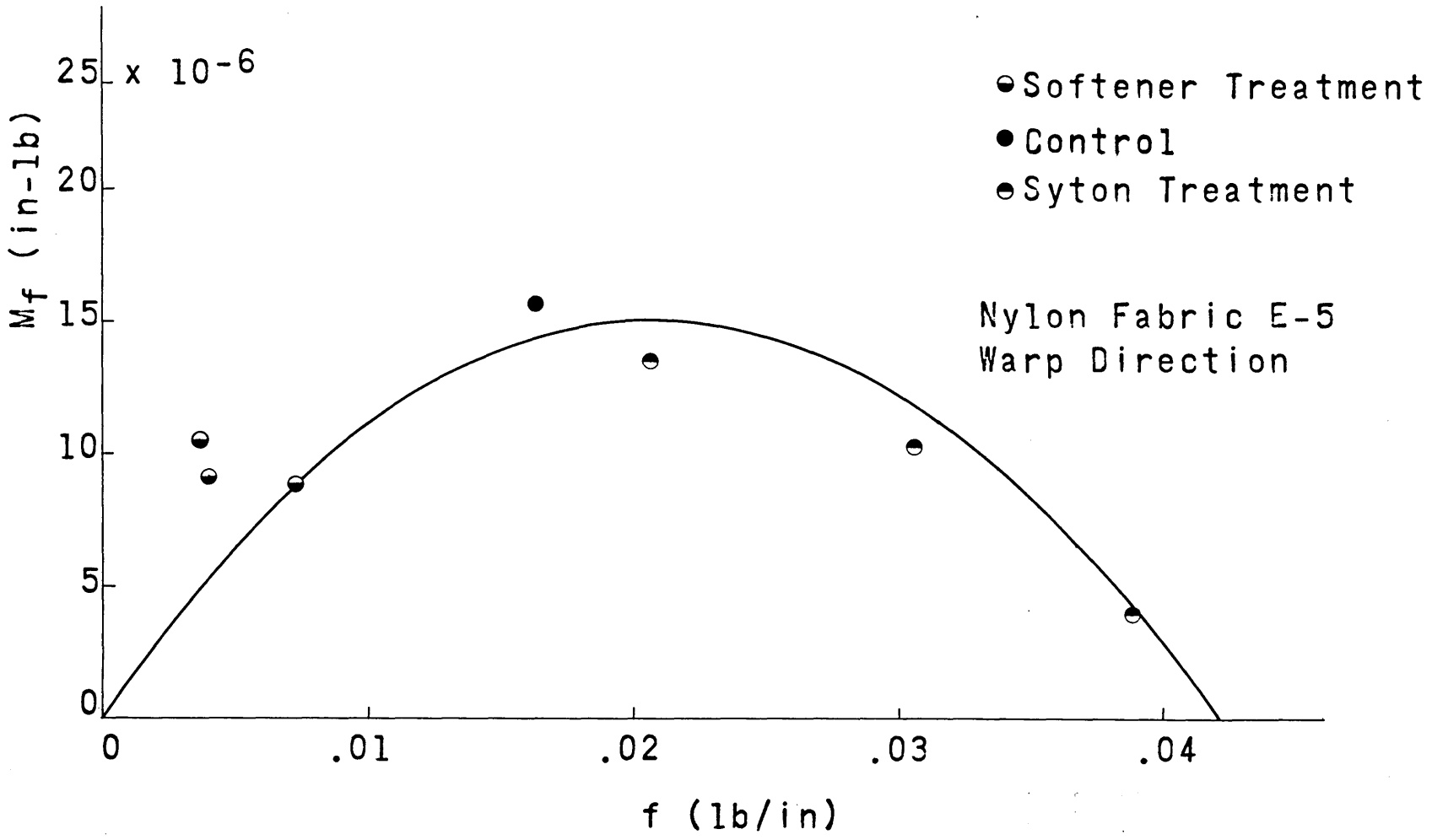

Fig.2-27 ELASTIC RIGIDITY vs INTERFIBER FRICTION

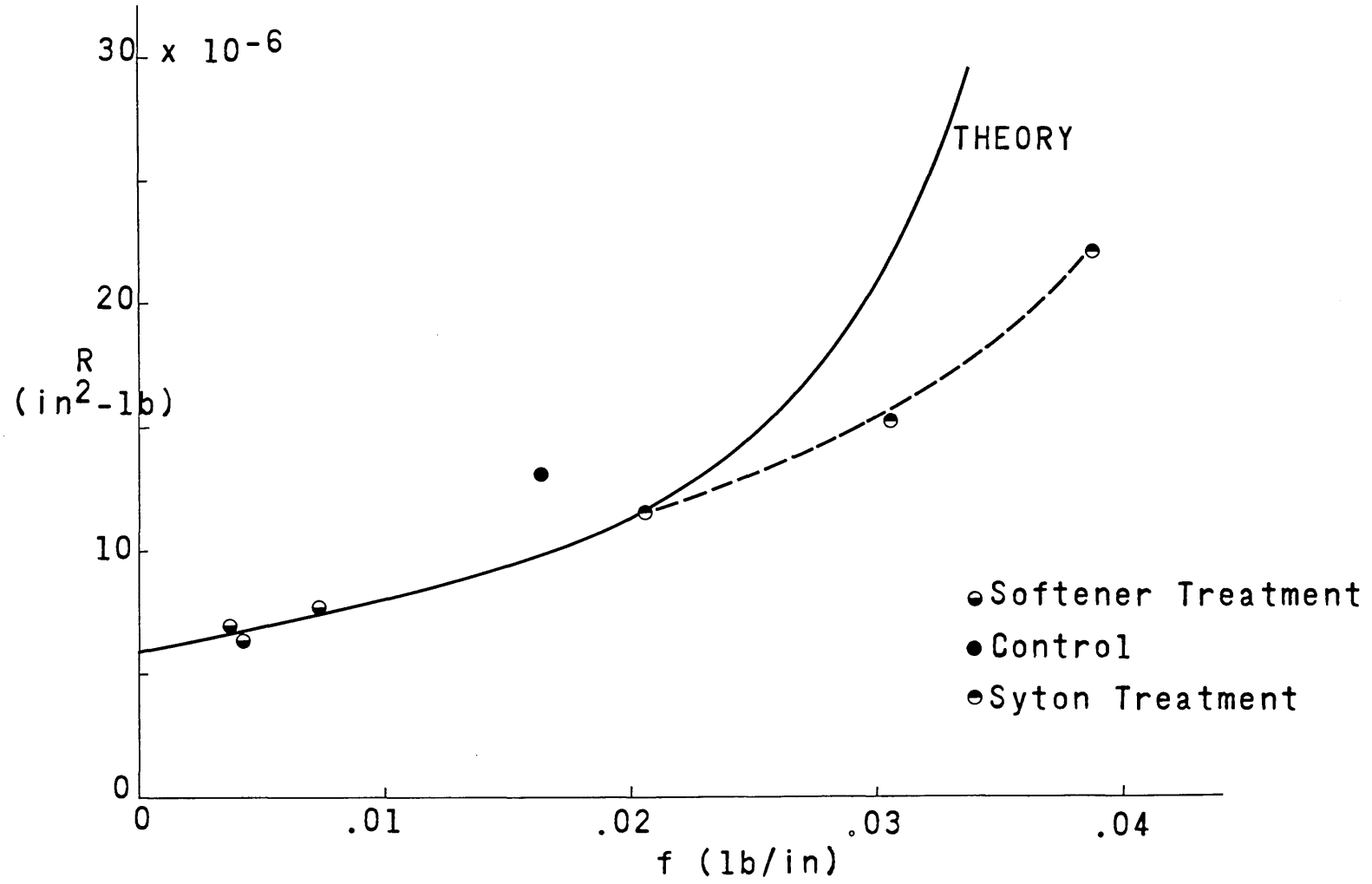

both the elastic rigidity and the friction moment are plotted against the interfiber friction force. This quantity was determined by means of the pull out test described in Chapter IV. The bending parameters of the nylon series are also given in crossplotted form. For the cotton series, it was found unfeasible to measure the fiber pull out force and the bending parameters are given only in cross plotted form.

The results of the nylon series show good qualitative agreement with the theory. The elastic rigidity increases monotonically with interfiber friction while the friction moment increases and then falls. In order to compare the theoretical relations with those measured, it was necessary to graphically determine the parameter "g" from the friction moment plot. Then, the value of $D_f N_f L/4$ was determined from the fabric specifications and also from the maximum of the friction moment plot. The two values thus obtained differed by a factor ot two, and the value obtained from the second method was used to plot the theoretical curve on Fig. 2-26. On this basis, the a greement between theory and experiment was good. The discrepancy between the two values of $D_f N_f L/4$ obtained is probably due to the effect of a varying pressure distribution within the fabric which was not considered in this section.

The measured relation between elastic rigidity and friction force for the nylon series also showed good qualitative agreement with the proposed theory (Fig. 2-27). The extrapolation of rigidity to a zero value of friction force on this plot represents the complete freedom of motion rigidity of the material and the value thus obtained was within 5% of that determined from the tensile properties of the yarns. This value was used in conjunction with the previously determined

Fig.2-28 FRICTION MOMENT vs ELASTIC RIGIDITY

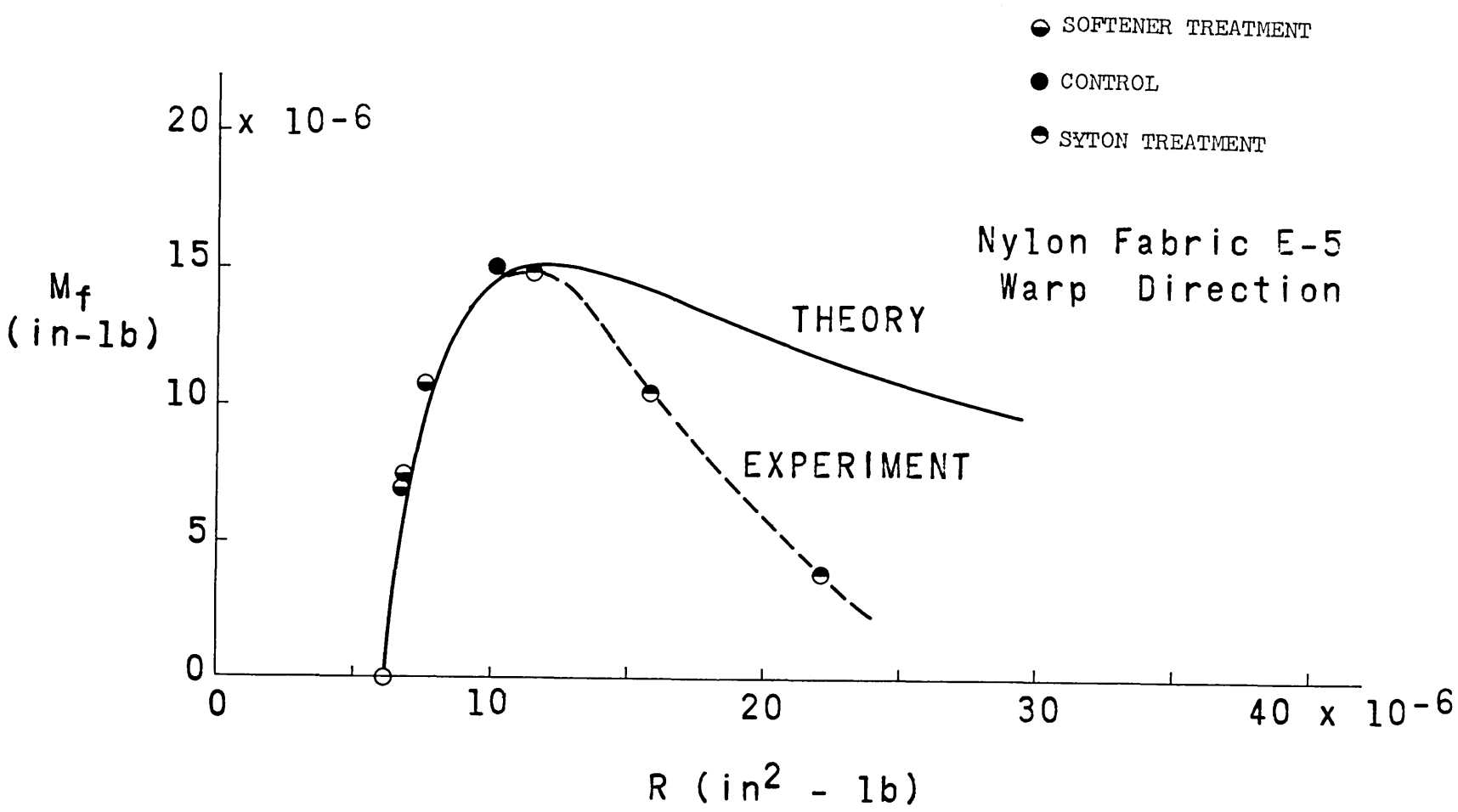

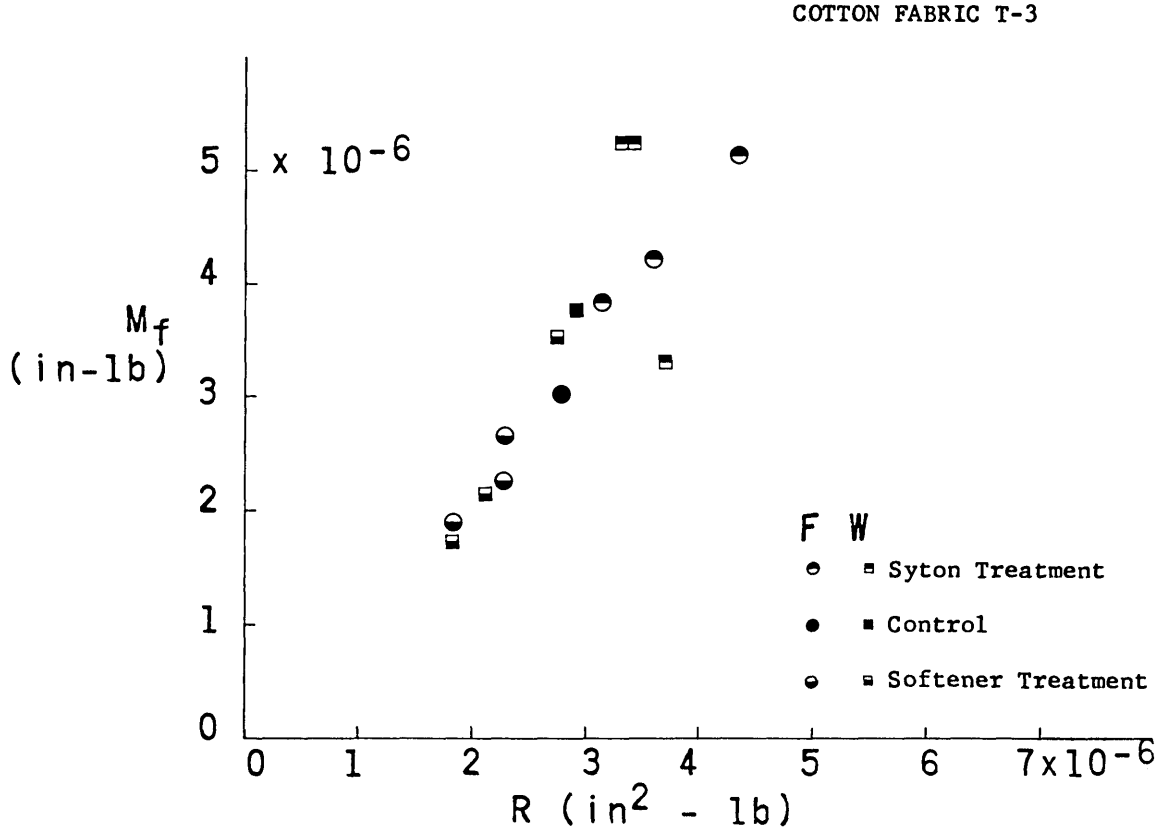

Fig.2-29 FRICTION MOMENT vs ELASTIC RIGIDITY

value of "g" to establish the theoretical relation for this measurement. The comparison between theory and experiment is quite good for moderate values of friction. At the higher levels the predicted elastic rigidity is considerably higher than that measured. This discrepancy is probably due to the effect of yarn flattening which was not included in this analysis and which has the effect of changing the ratio of the complete freedom of motion rigidity to the no freedom of motion rigidity. This ratio was taken to be $1/N_f$ in equation 91.

The relation between friction moment and elastic rigidity is plotted on Fig. 2-28 for the nylon series. The measured values on this graph have been corrected from the original ones by adjusting each point to the value lying on the best smooth curve through the original data. Then the theoretical relation was plotted based on the parameters used previously. The agreement between theory and experiment is excellent for the lower values of elastic rigidity, then at the higher values the agreement becomes poor because of the previously discussed discrepancy between theoretical and measured elastic rigidity at high friction levels. Note that the samples treated with the friction reducing treatments fall in the initial region of the curve and they are followed by the control sample and the samples treated with the frictionizer.

The measured results of the cotton series are shown on Fig. 2-29 . The qualitative relation between the variables is as expected although it appears that the levels of inter-fiber friction force was insufficient to extend the measured values beyond the point of maximum friction moment. As in the case of the nylon series, the data points are identified by the type of friction treatment applied. Again, the low friction fabrics lie in the initial region of the curve while those with high friction lie at the end.

CHAPTER III

BENDING RECOVERY OF TEXTILE STRUCTURES

Since the bending recovery behavior of fabrics plays an extremely important role in the performance of textile materials for clothing purposes, a great deal of research has been done in this area[28,29]. It has been shown that the individual fiber properties determine recovery behavior to a great extent and that fibers with good recovery from tensile strains generally have good recovery from bending[30]. A number of investigations have demonstrated however[14,15,31] that the bending recovery also depends on the frictional interactions of the fibers. Although this effect is generally of secondary importance, it certainly warrants careful investigation because of the great importance of bending recovery in user acceptance of new materials and finishes.

In the first section of this chapter a bending recovery relation will be established which can be used to characterize the performance of any material or structure. This relation involves the use of dimensionless variables and permits the evaluation of materials independent of their size.

In the sections to follow, the recovery behavior will be given for the limiting cases of fiber motion. Then, following the procedure of Chapter I, the intermediate cases of fiber motion will be considered. It will be shown that friction not only produces an intermediate behavior, but also introduces an entirely different type of behavior in certain cases.

REPRESENTATION OF BENDING RECOVERY

Bending recovery is defined as the fractional amount of curvature recovered to that imposed on a specimen. In standard tests the imposed curvature is usually[32] determined by the curvature a fabric experiences when it is bent around a slab approximately 10 mils thick. Since the thickness of fabrics varies, the imposed curvature of such a test will vary for different materials. Also, the severity of a given imposed curvature will depend on the thickness of the fabric. For these reasons a standard test which involves bending a material around a slab of fixed thickness is not always satisfactory. This was demonstrated by Bostwick in an investigation of a number of test procedures[33]. A better measure of bending recovery is to bend a fabric to a radius of curvature that is a fixed fraction of the fabric thickness. The magnitude of the imposed curvature in this case can be expressed in dimensionless form by multiplying it by the half thickness of the material as is done in Chapter I. The physical significance of this dimensionless curvature is that it is the same as the maximum strain that would exist in a solid material of equal thickness bent to the same curvature. For example, the dimensionless curvature of a fabric bent around a thickness equal to itself is one-half.

For a complete representation of bending recovery, the recovery at every possible value of imposed curvature must be known. This functional relation has been used in a number of previous investigations[14,15] and will be used here and referred to as the recovery curve. Both variables on this curve range from zero to one; and, on this representation it is possible to plot the recovery of any one or two dimensional structures such as fibers, wires, ropes, films, fabrics, and other materials.

BENDING RECOVERY OF A SINGLE FIBER

As mentioned before, the most important single factor that determines the bending recovery of textile structures is the bending recovery behavior of the individual fibers. It has been shown in a number of investigations that this recovery depends largely on the tensile recovery of the fibers[30]. In particular, Platt and Freeston[34] found the mathematical relation between residual fiber curvature and imposed curvature based on the fiber stress strain behavior. For a fiber with an idealized tensile curve as shown on Fig. 3-1, the residual curvature was shown to be,

$$k_r = k_i \left(1 - \frac{\sigma}{E}\right)\left(1 - \frac{4\varphi^3\psi}{3\pi} - \frac{2\varphi\psi}{\pi} - \frac{2}{\pi}\sin^{-1}\psi\right) \qquad \psi < 1 \qquad (3\text{-}1)$$

Where,

D_f = fiber diameter

k_r = residual curvature

k_i = imposed curvature

$\varphi^2 = 1 - \psi^2$

$\psi = \frac{2e^*}{D_f k_i}$

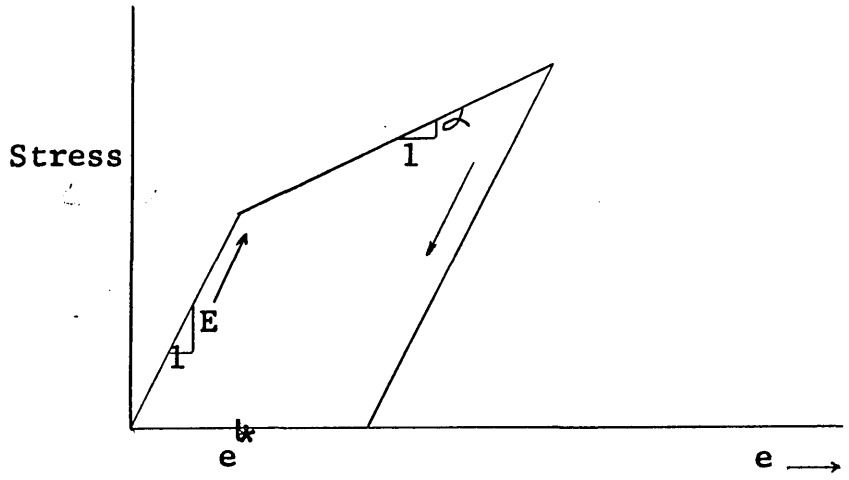

Fig. 3-1 IDEALIZED TENSILE BEHAVIOR FOR BENDING RECOVERY PREDICTION

$$t_f = 2D_f\sqrt{\frac{N_f r}{\gamma_y}} \tag{3-2}$$

Where,

t_f = fabric thickness
N_f = number of fibers in yarn
r = height to width ratio of yarn section
γ_y = yarn packing factor
k^*_i = dimensionless curvature of fabric
B = bending recovery

From the definition of dimensionless curvature,

$$k_i^* = k_i D_f - \sqrt{\frac{N_f r}{\gamma_y}} \tag{3-3}$$

This equation can be used in conjunction with equation 1 which defines the recovery of individual fibers. For fibers which do not follow the assumptions on which equation 1 is based, it is possible to use any other formulation which describes the recovery of individual fibers. For example, experimental results can be used at this point[35] to give this information. If, however, equation 1 is assumed to hold, then the result for the recovery behavior of a fabric with complete freedom of fiber motion can be obtained by rewriting the equation in terms of bending recovery and substituting equation 3.

$$B = \begin{cases} 1 & 0 < k_i^* < P \\ (1 - \frac{\alpha}{E})(\frac{4}{3\pi}^3\psi + \frac{2}{\pi}\psi + \frac{2}{\pi}\sin^{-1}\psi) + \frac{\alpha}{E} & k_i^* > P \end{cases} \tag{3-4}$$

The recovery behavior predicted by equation 1 has been measured by Platt and Freeston for a number of metallic fibers and for viscose rayon with good agreement between theory and experiment.

In the following sections this formulation will be used to predict the recovery of fiber assemblies. Then frictional effects will be included to determine how this factor affects recovery. It should be noted that the residual curvature predicted by equation 1 applies to fibers whose stress-strain and recovery behavior can be characterized by the idealization of Fig. 3-1. For other materials, the individual fiber recovery must either be recomputed or measured directly.

LIMITING CASES OF FRICTIONAL INTERACTION

Just as in the case of the bending of textile structures, it is possible to estimate the recovery from bending by considering the limiting cases of frictional interaction. This can be done for the case of a woven fabric bent by assuming that the change of curvature of the centerline of the fabric is the same as that of the individual fibers. This assumption can be applied most satisfactorily for yarns with moderate crimp and for moderate imposed curvatures.

For the case of <u>complete freedom of motion</u>, the fibers will bend independently and on the basis of the stated assumption, equation 1 can be applied directly. However, to express the result in terms of the dimensionless curvature imposed on fabric, it is necessary to express the fabric thickness in terms of the fiber diameter. This can be done for a yarn of elliptical cross section in a fabric with a thickness of two yarns. The result is,

$$\psi = \frac{P}{k_i^*}$$

$$\varphi^2 = 1 - \psi^2$$

$$P = 2\, e^{*\sqrt{\frac{N_f\, r}{\gamma_y}}} \qquad \text{(Complete Freedom of Motion)} \qquad (3\text{-}5)$$

For the case of no freedom of fiber motion, the fibers will not slip and the fabric will be assumed to be made of yarns which behave as monofilaments. In that case, the diameter term of equation 1 must be replaced by the yarn diameter. The resulting recovery equation is the same as equation 4, but the parameter "P" is replaced by,

$$P = 2\, e^{*} \qquad \text{(no freedom of motion)} \qquad (3\text{-}6)$$

This means that the recovery behavior for the case of complete and no freedom of motion follow the same form but have different values of a parameter which is a measure of the non-recoverability of the fibers. This recovery relation is plotted for several values of this parameter on Fig. 3-2. These curves are given for $\alpha/E = 0$, and can easily be adjusted for non-zero values of this variable by realizing that its effect is to shift the curve upwards to complete recovery by a fractional amount equal to its magnitude.

The results given here for the limiting cases of freedom of motion can directly be applied to situations in which the fibers form clusters in the yarn. In that case it is merely necessary to modify the values of the parameter in terms of the number of fibers in a cluster.

The recovery behavior predicted by this analysis is generally observed for textile materials where the effects of sliding against frictional forces can be ignored[34]. Note

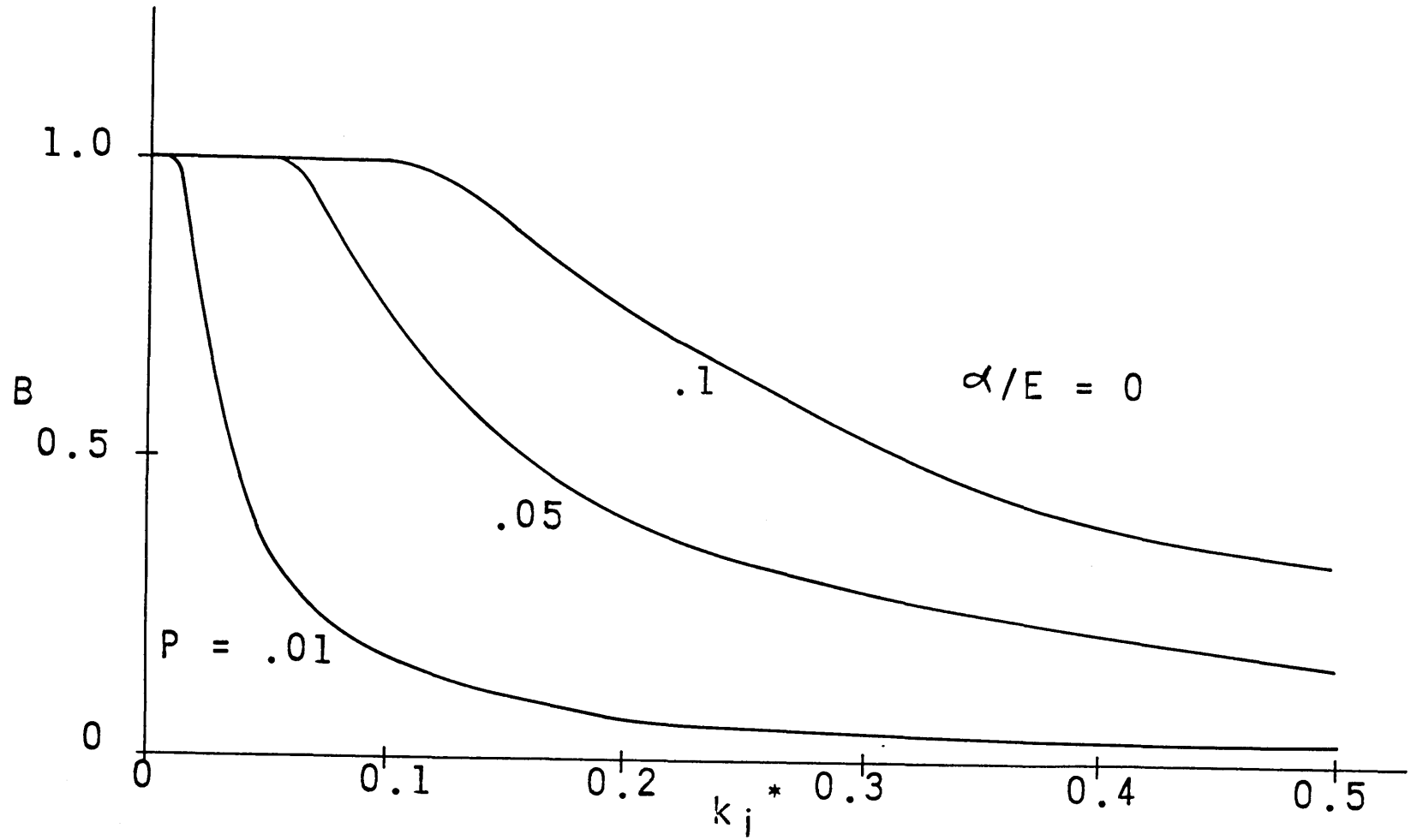

Fig.3-2 BENDING RECOVERY vs DIMENSIONLESS CURVATURE FOR PLASTIC-ELASTIC EFFECT

that the recovery is not strongly affected by the magnitude of imposed curvature for values of dimensionless curvature approximately equal to 0.5. Since the standard bending test generally operates at this level, the results can be used for constant thickness slabs even though the imposed curvature may be different for samples of different thicknesses.

EFFECT OF FRICTION ON RECOVERY

In Chapters I and II it has been shown that the effect of friction on bending of textiles or multi-layer beams is either to impose restraints on relative fiber motion or else to prevent the complete propagation of slip. Both of these effects will affect the bending recovery.

In the first case, recovery will be affected since the fibers will not reslip to the same extent that they did during bending. This type of non-recoverability due to friction was discussed analytically and experimentally in Chapter I for multi-layer beams and analytically in Chapter II for the one-dimensional case of slip and strain. Since this type of non-recoverability arises from a structural effect rather than from permanent fiber deformation, it will be referred to as the "friction-elastic" type of non-recoverability.

In the second effect, friction will prevent relative fiber motion in parts of the structure and cause larger strains to develop. This will clearly reduce the recovery.

Friction-Elastic Effect. In Chapter I, an analysis was presented to determine the recoverability of a multi-layer beam under constant pressure that is bent to a fixed curvature. The residual curvature due to the balance between the elastic and frictional forces in the system are given by equation 80. When this result is applied to a textile structure and

rewritten in terms of bending recovery, the result is,

$$B = \begin{cases} \frac{1}{4}\frac{k_i^*}{F} & 0 < k_i^* < 2F \\ 1 - \frac{F}{k_i^*} & 2F < k_i^* \end{cases} \qquad (3\text{-}7)$$

$$F = \frac{M_f\ t_f}{R2}$$

Where,

B = bending recovery

M_f = friction moment

R = elastic rigidity

t_f = fabric thickness.

This equation relates bending recovery to imposed curvature for various values of a dimensionless parameter which expresses the friction relative to the elasticity of the system. Bending recovery for this effect is plotted on Fig. 3-3. It is interesting to note the difference between the recovery resulting from this effect to that from purely plastic deformation shown on Fig. 3-2. In this case the recovery increases with imposed curvature while in the other it decreases with curvature.

Effect of Frictionally Induced Strains on Recovery (Plastic-Elastic Effect). When frictional forces prevent complete slip propagation the effect on recovery can be estimated by assuming that part of the structure bends with no freedom of motion and part with complete against a frictional restraint. This is the same assumption made and discussed in the case of frictional effects in bending in Chapter II. Again, the length of propagation of slip will be assumed to depend linearly on the frictional force as given by equation 88. If

Fig.3-3 BENDING RECOVERY vs DIMENSIONLESS IMPOSED CURVATURE FOR FRICTION-ELASTIC EFFECT

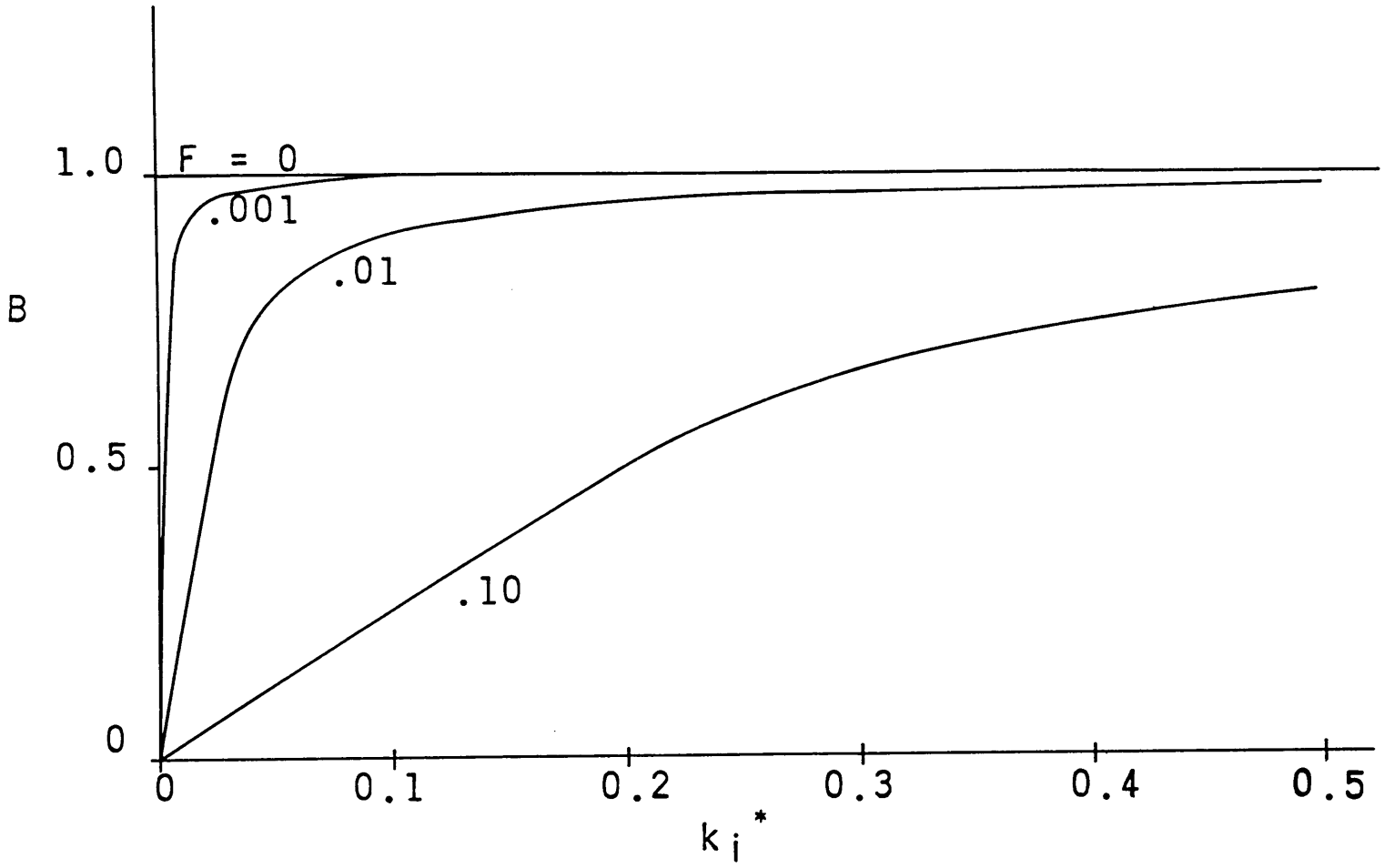

each element of yarn changes its curvature by the same amount and this change is equal to the curvature of the fabric centerline, the frictional effect can be determined from the recovery equations for complete and no freedom of motion given by equations 4, 5, and 6. The length of yarn through which slip has propagated will have the residual curvature corresponding to the complete freedom of motion case and the remainder will have a residual curvature corresponding to no freedom of motion. The fractional amount of each case is given by equation 88. This permits calculation of the average residual curvature of the fabric and this can be used to determine the bending recovery in terms of the limiting values.

$$B = (1 - \frac{f}{g})\, B_{CFM} + (\frac{f}{g})\, B_{NFM} \qquad (3\text{-}9)$$

The result indicates that on the basis of the stated assumptions, the recovery for this effect of friction will be the weighted average of the recovery curves for the limiting cases of freedom of motion. The weighting factor is dependent on the friction of the system as indicated.

It is interesting to note that the two frictional effects on recovery discussed in this section are quite different in the way they act. The first produces a non-recoverability by not allowing the fibers to return to their original relative positions. The fibers need not be permanently deformed for this mechanism to act. The non-recoverability is purely structural and arises from a balance of the friction forces with the elastic restoring forces. A good example of this type of deformation is found in fiberglass fabrics. In this type of material the recovery is often extremely poor, even though the fibers are not at all permanently deformed. This

is especially pronounced at low curvature bends when the recovery predicted by this effect is lowest.

The second effect of friction is not purely structural. It acts to reduce recovery by increasing the effect of the permanent fiber deformations by preventing relative fiber motion in parts of the fabric. In this way the recovery goes from the complete freedom of motion case to that of no freedom of motion as friction increases. This effect is greatest in large curvature bends.

Combined Effect of Friction and Permanent Fiber Deformation. The results of the previous sections can be utilized to obtain a prediction for the combined effects of friction and permanent fiber deformation on bending recovery. This combined effect will give the recovery behavior for the levels of frictional interaction between the limiting cases.

When a material is bent to a certain level of curvature and released, it will maintain some amount of residual curvature. This residual curvature was shown to arise from two different effects; permanent fiber deformations, and frictionally held deformations. In the first of these effects, referred to as the plastic-elastic case, it has been shown that the residual curvature varies with the imposed curvature in a manner that depends on the fiber properties, the structural geometry, and the interfiber frictional interaction. The frictional interaction in this case determines the level of residual curvature relative to the limiting cases of freedom of fiber motion as illustrated on Fig. 3-4. Here, it can be seen that the residual curvature due to this effect is small for low imposed curvature and increases to considerable levels at high imposed curvatures.

The second effect which produces a residual curvature results from frictionally held deformation. This friction-elastic effect arises from an inability of the fibers to reverse the relative motions which they experienced during bending. The relation between residual and imposed curvature for this effect was computed in Chapter I and is plotted on Fig. 3-4. On this graph it can be seen that this residual curvature is approximately constant for all levels of imposed curvature.

A comparison of the residual curvature relations resulting from the two effects shows that the friction-elastic effect predominates at low curvatures, while the plastic-elastic effect predominates at high curvatures. This means that the way in which interfiber friction affects bending recovery depends on the level of imposed curvature. For low curvatures, friction is important since it prevents fibers from retracing the motions which they experienced during bending. Then, at high curvatures, friction prevents the complete propagation of slip during bending and thereby increases the level of fiber strain and of the corresponding permanent deformation.

In order to evaluate quantitatively the combined effects of the two types of residual curvature, it will be assumed that the net residual curvature equals the sum of the residual curvatures due to fiber deformation and frictionally held deformation. This is shown on Fig. 3-4. The justification for this assumption is obtained from a consideration of the equilibrium configuration of the fibers. For fibers that do not undergo permanent deformations, the residual curvature corresponds to that of the friction-elastic case. This residual curvature represents a point of balance between the frictional forces, which tend to hold the material bent, and the elastic

restoring forces, which tend to return the material to the original equilibrium configuration. When the fibers do undergo permanent deformations, the elastic restoring forces will tend to return the material to the state that corresponds to the altered fiber equilibrium configurations. Since the residual curvature due to the friction-elastic effect acts to produce a fixed change in curvature from whatever equilibrium configuration exists, the assumption made appears reasonably justified. There is one difficulty however that does arise when making this assumption. The recovery behavior of the individual fibers, and therefore the plastic-elastic parameters, depends to some extent on the state of fiber strain[15] When this effect is significant, a coupling term must be introduced between the residual curvatures and the simple superposition assumption will not hold. This effect was neglected for the purposes of this investigation.

Let:

k^*_r = dimensionless residual curvature

k^*_i = dimensionless imposed curvature

$$F = \frac{M_f \, t_f}{R2}$$

$$G = Fg/f = \frac{(N_f \, D_f \, Lg/4) \, t_f/2}{N_f \, EI_f}$$

f = friction force per length between fibers

g = friction force per length between fibers required for prevention of all slip

subscripts:

p refers to plastic-elastic effect

f refers to friction-elastic effect

nfm refers to no freedom of motion

cfm refers to complete freedom of motion.

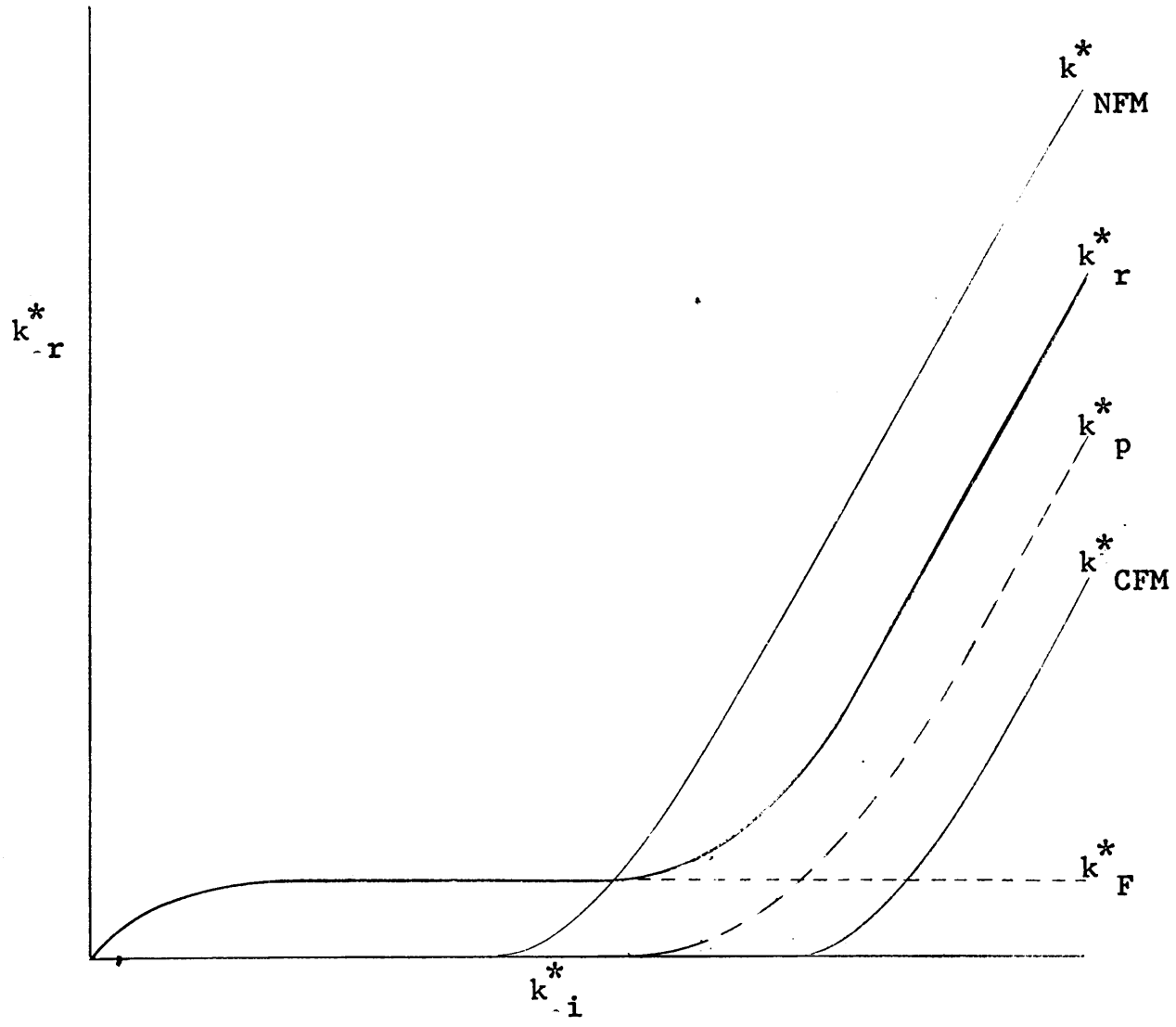

Fig. 3-4 RESIDUAL vs IMPOSED CURVATURE FOR COMBINED PLASTIC-ELASTIC AND FRICTION-ELASTIC EFFECTS

The residual curvature due to the plastic-elastic effect depends on the amount of interfiber friction and the recovery of the limiting cases as in equation 9.

$$k^*_{r,p} = \frac{f}{g} k^*_{r,nfm} + (1 - \frac{f}{g}) k^*_{r,cfm} \tag{3-10}$$

The residual curvature due to the friction-elastic effect can be obtained from equation 7. It can be rewritten in terms of the relative amount of friction by applying the results of equations

$$k^*_{r,f} = \begin{cases} \left[1 - \frac{1}{4} \frac{k^*_i}{(f/g)(1 - f/g)^2 G}\right] k^*_i & 0 < k^*_i < 2(f/g)(1-f/g)^2 G \\ G(f/g)(1 - f/g)^2 & k^*_i > 2(f/g)(1-f/g)^2 G \end{cases} \tag{3-11}$$

From the indicated assumption,

$$k^*_r = k^*_{r,p} + k^*_{r,f} \tag{3-12}$$

These equations can be combined and written in terms of bending recovery rather than residual curvature,

$$B = \frac{f}{g} B_{Nfm} + (1 - \frac{f}{g}) B_{cfm} - \frac{k^*_{r,f}}{k^*_i} \tag{3-13}$$

The individual terms of this equation can be evaluated from equations 4, 5, 6, and 11. Then, the bending recovery can be seen to depend on five parameters,

$$B = B(P_{cfm}, N_f, \alpha/E, G, f/g) \tag{3-14}$$

This bending recovery relation has been plotted on Figs. 3-5 and 6 for several values of the parameters. The most striking result that can be seen is the reduction of recovery at low levels of imposed curvature and a recovery curve that goes through a maximum. This type of behavior has

been previously observed by Daniels[15] and was also observed in this investigation. Note that the recovery curves for the combined effects reflect a combination of the recovery curves for the plastic-elastic and friction-elastic effects shown on Figs. 3-2 and 3.

On Fig. 3-5 the recovery relation is plotted for $P_{cfm} = 0.1$, $\alpha/E = 0$, and for the case of complete slip propagation ($f/g = 1$). The amount of friction acting in the system is given by the dimensionless parameter F. As this value increases, the recovery gets progressively worse at the lower levels of imposed curvature. At the higher levels, the effect of friction is less and the recovery curves are asymptotic to the zero friction case. This occurs because these recovery curves are restricted to the case of complete slip propagation.

On Fig. 3-6 the recovery curves are shown for a material in which the effect of propagation of slip is included. The curves are plotted for $P_{cfm} = 0.1$, $N_f = 100$, $\alpha/E = 0.5$, $G = 0.1$, and for various values of f/g. The limiting cases of recovery occur at f/g equal to 0 and 1. For the intermediate cases the friction-elastic effect increases and then decreases with f/g, while the plastic-elastic effect continuously shifts the recovery curve closer to the no freedom of motion limit.

The important conclusion to be drawn here is that the recovery behavior for the intermediate cases of friction differs qualitatively from that found for the limiting cases. This was also shown to be the case for the bending behavior as described by the moment-curvature relation. For the high imposed curvatures, friction acts to give a recovery which is between that of the limiting cases. At these curvatures, the recovery performance relates to the ability of a fabric to recover from imposed wrinkles or creases. At low curvatures,

Fig.3-5 BENDING RECOVERY vs DIMENSIONLESS IMPOSED CURVATURE

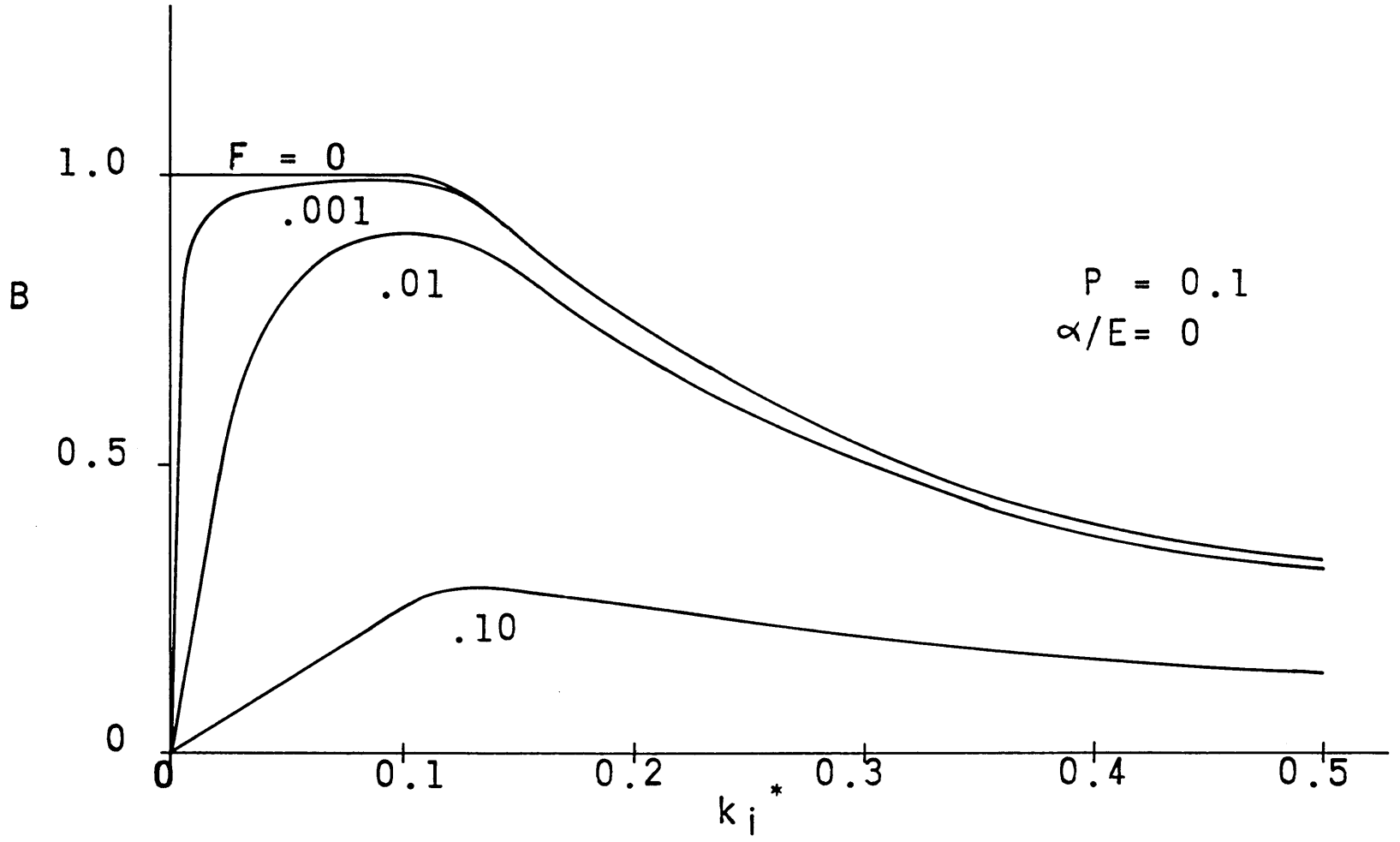

Fig.3-6 BENDING RECOVERY vs DIMENSIONLESS IMPOSED CURVATURE

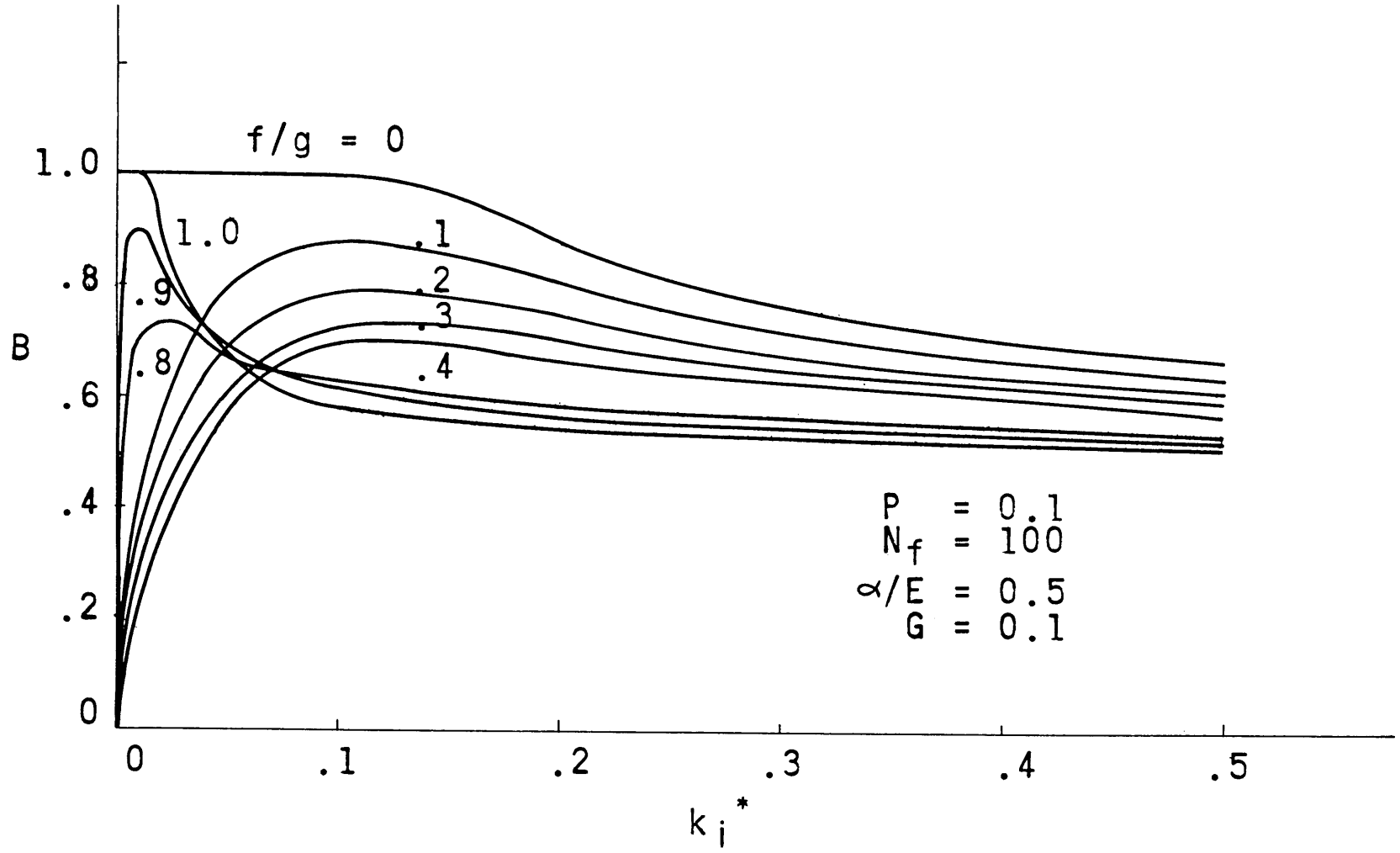

friction reduces the recovery below that of both limiting cases. At these curvatures the recovery gives only a small indication of how a fabric will recover from imposed wrinkles, but it does give a strong indication of the "hand" of the material. Fabrics with low recovery from low curvature bends differ noticeably in their aesthetic appeal from fabrics with high recovery.

A number of experiments were conducted to establish the validity of the proposed theory of frictional effect on bending recovery. The procedure used is described in Chapter IV. To illustrate the qualitative nature of the frictional effect, a cotton canvas fabric having a rather strong inter-fiber frictional interaction was first evaluated. The results of this experiment are plotted on Fig. 3-7. The recovery of this material very definitely follows the predicted trend and has very poor recovery at low imposed curvatures followed by a maximum in the curve and then a gradual decrease.

Two additional series of experiments were conducted to determine the effect of friction on the recovery behavior of a nylon and a cotton fabric. These samples were treated with varying concentrations of a softening agent and with varying concentrations of a frictionizer. The detailed sample descriptions are given in Appendix E and the results of the recovery measurements are given on Figs. 3-8 to 3-10, and on Table I in Appendix F.

The recovery of the nylon samples shown on Fig. 3-8 represents the results of a treatment with a softening agent, a frictionizer, and a control sample. The amount of frictional interaction of each of these samples is specified in terms of the fiber pull-out force, which was measured by the procedure described in Chapter IV. A similar plot for three of the cotton samples is given on Fig. 3-9. In this case the amount

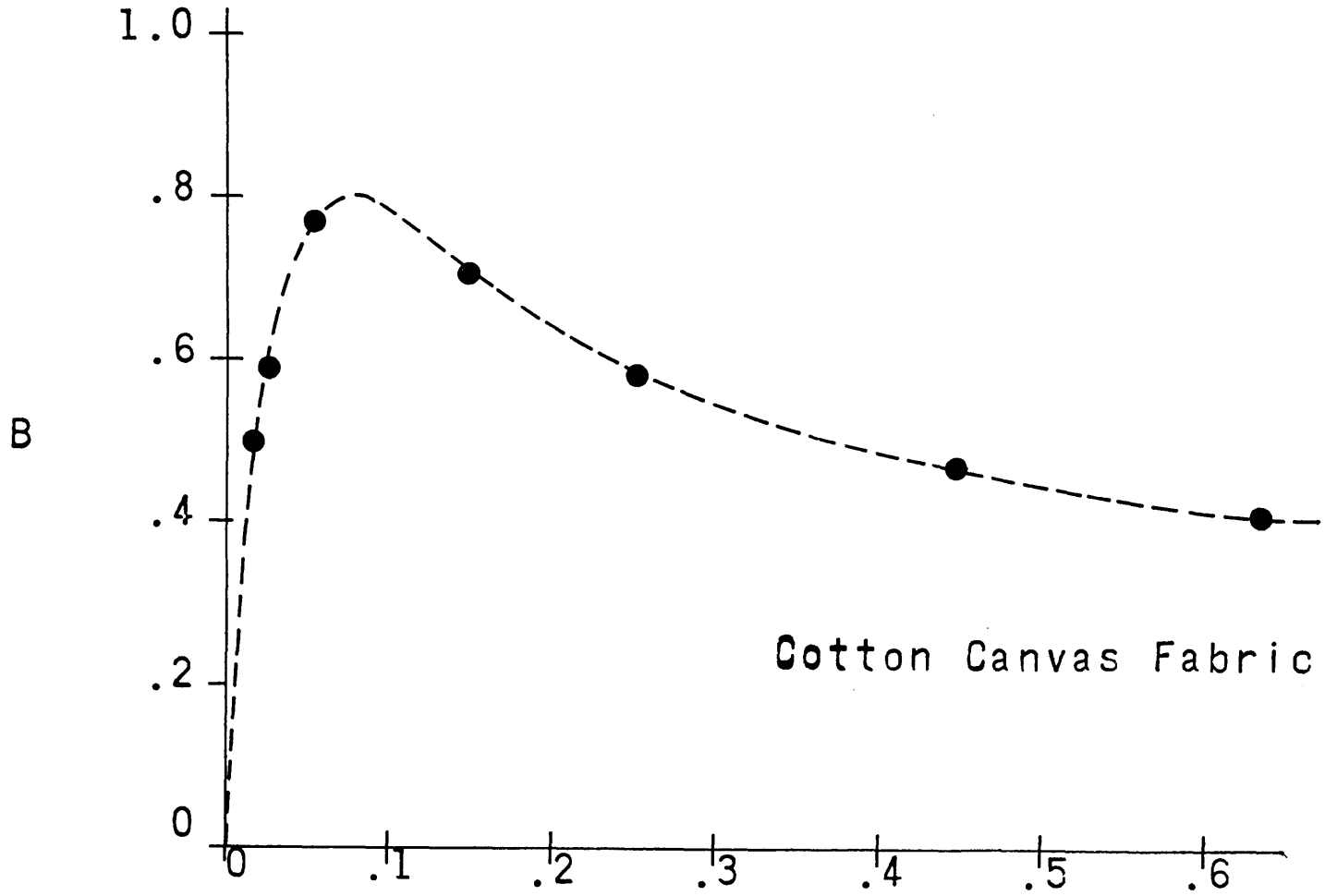

Fig.3-7 BENDING RECOVERY vs DIMENSIONLESS IMPOSED CURVATURE

Fig.3-8 BENDING RECOVERY vs DIMENSIONLESS IMPOSED CURVATURE

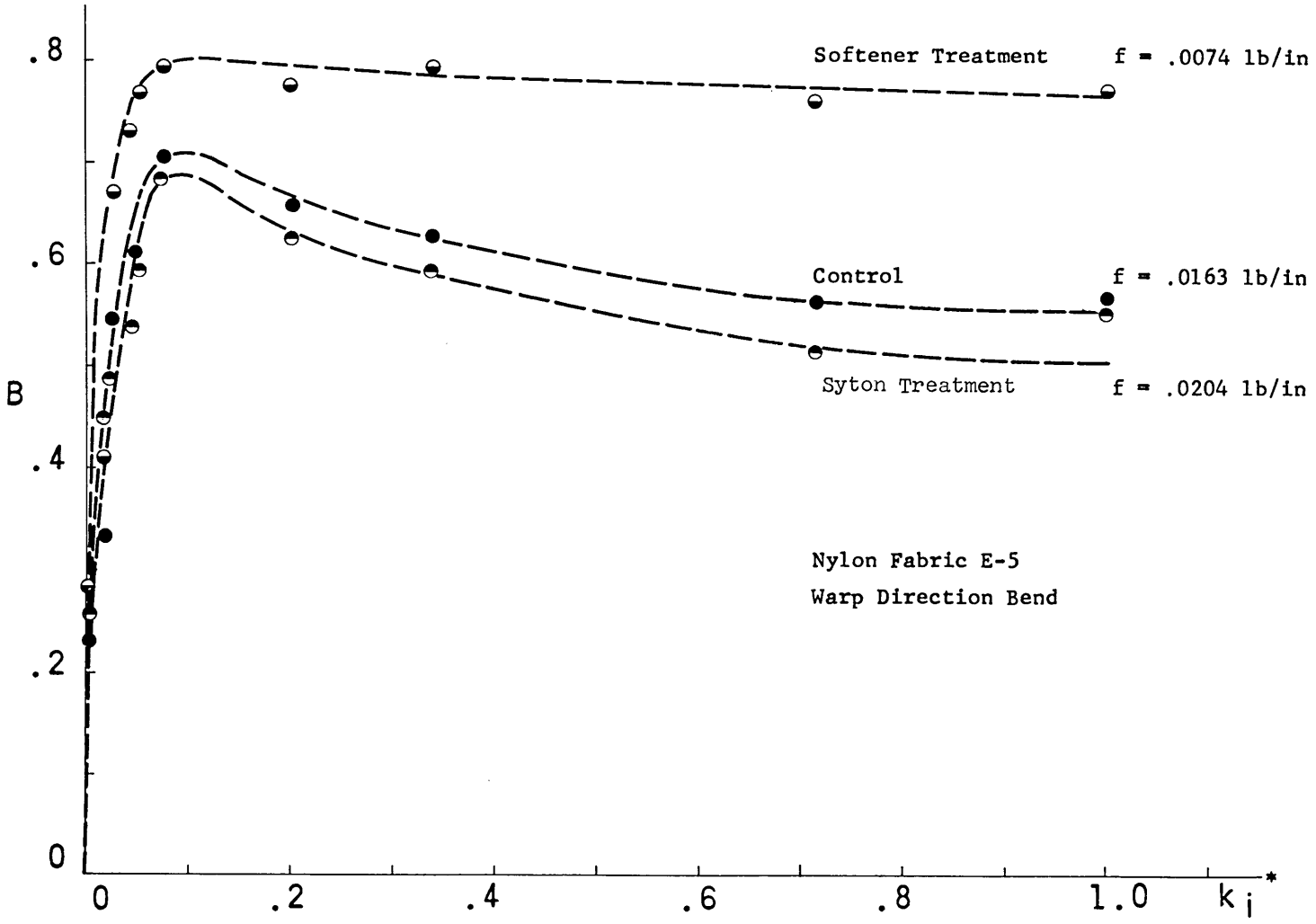

Fig.3-9 BENDING RECOVERY vs DIMENSIONLESS IMPOSED CURVATURE

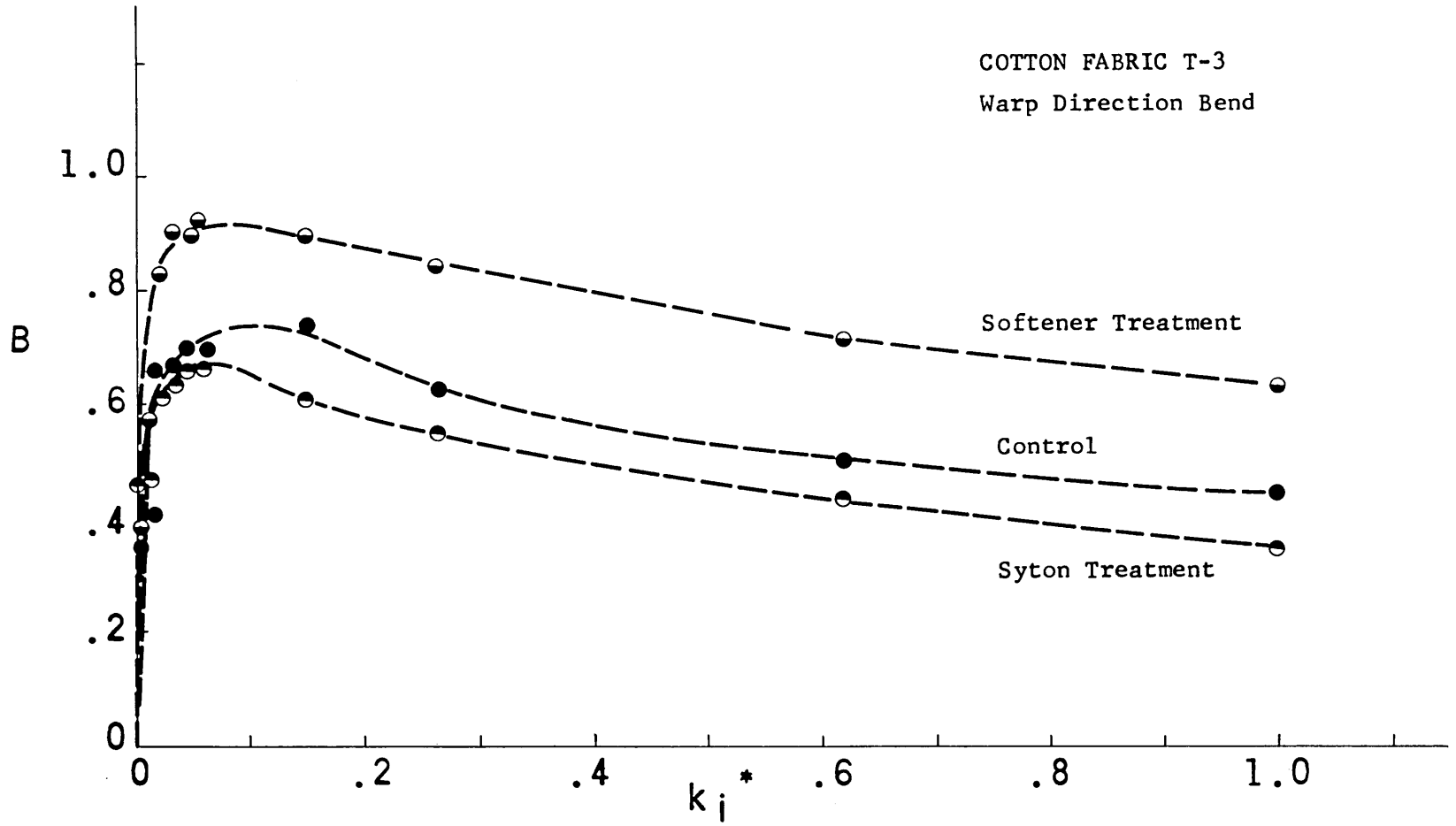

Fig.3-10 BENDING RECOVERY vs ELASTIC RIGIDITY

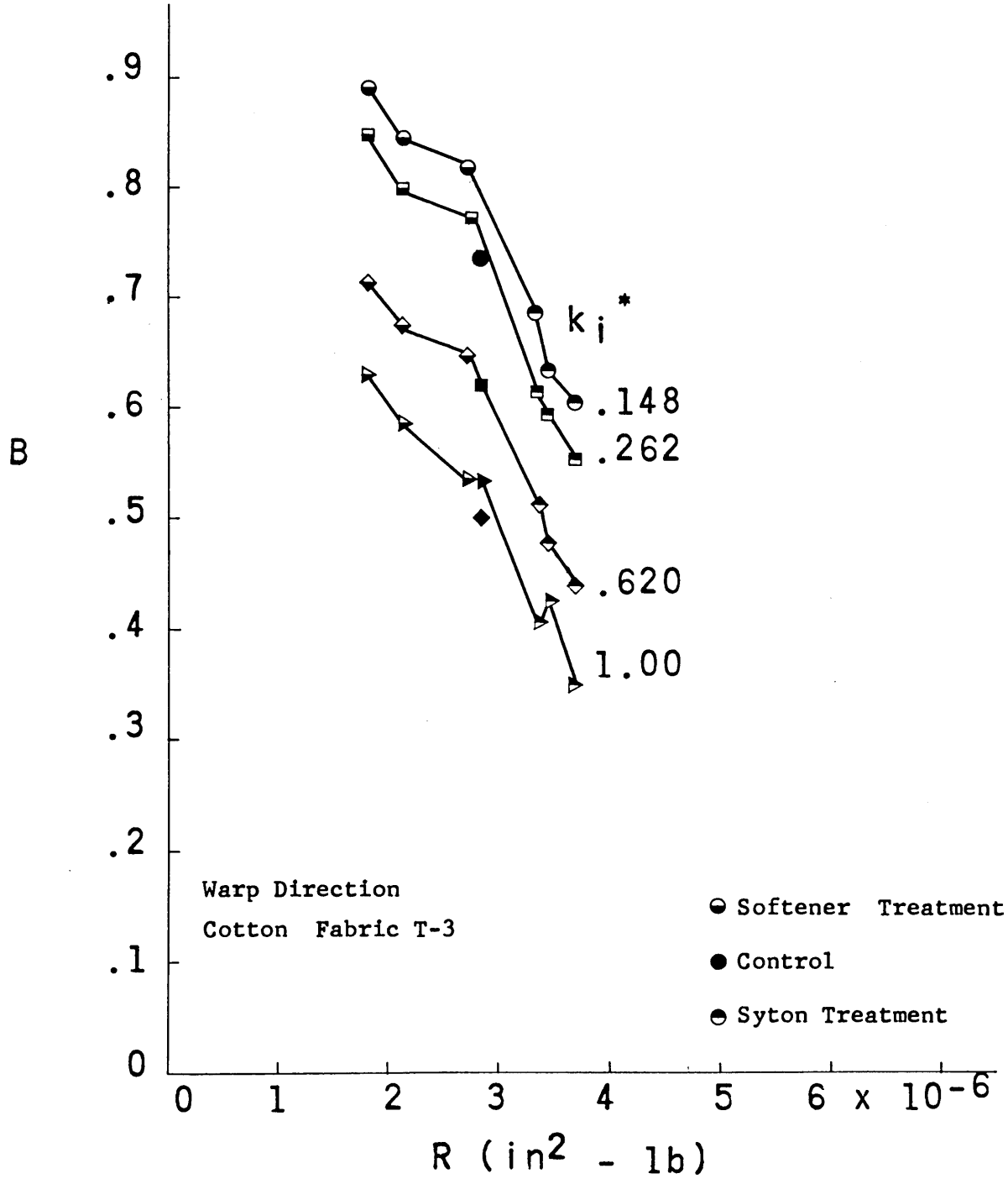

of interfiber friction is given in terms of the elastic rigidity of the sample. This quantity was shown to be a monotonically increasing function of friction in Chapter II.

The results show that friction affects the shape of the recovery curve as predicted. At both the low and high imposed curvatures the samples with the higher friction levels showed poorer recovery. In the low curvature region this was due to increased resistance to relative fiber motion, and in the high curvature region it results from a reduction in the extent of slip propagation.

For an additional representation of the recovery results, the bending recovery is plotted as a function of friction, measured in terms of elastic rigidity, for various levels of imposed curvature on Fig. 3-10. This curve illustrates the strong effect that friction has on bending. By changing the frictional interaction between the fibers it was possible to obtain changes in recovery amounting to almost a factor of two.

EVALUATION OF CROSS-SECTIONS OF BENT FABRICS

In order to obtain a better understanding of the structural geometry that develops during fabric bending, a number of fabric samples were bent, embedded, cross-sectioned, and examined microscopically. The technique employed is described in detail in Chapter IV. Several of these samples were photographed and are shown in Figs. 2-18, 3-11, and 3-12. These photographs include three series of samples which illustrate the effects of frictional changes, structural changes, and curvature changes. The following observations can be made from these cross-sections:

1.. There are two fundamental modes in which a fabric

can bend at high curvatures[36]. The first is a "square" mode and it is characterized by a yarn path which is asymmetric to the plane of bending. Cross-sections taken of adjacent yarns in this mode are mirror images of each other. The second mode is a "round" mode and it is characterized by a symmetrical yarn path. In this case, sections taken at adjacent yarns are different since the bent yarns will alternatingly pass over and under the cross yarn at the center of the bend. Both of these modes occur in each of the fabric series photographed. Because of the similarity of adjacent yarn sections in the square mode, only one cross-section is required to describe this geometry, whereas two are required for the round mode. It is interesting to note that the frequency of occurrence of the square mode is considerably greater than that of the round mode. This was not only found to be the case in the sections shown, but also in a number of additional samples which were sectioned.

2. During bending the yarns experience only small curvature changes in the regions where they form outside crowns. This observation corresponds to the assumption made in the analysis for predicting the effect of cross yarn restriction on elastic rigidity. This effect is most pronounced in fabrics having round cross yarns, since only a small amount of yarn compaction takes place in these materials.

3. In order to satisfy the continuity requirements of bending, the fibers at the inside crowns buckle towards the inside of the bend. The extent of this buckling is small but it can be seen by careful examination of the cross-sections on Fig. 3-11. Another form of buckling can also be seen in the loosely woven fabrics in this figure. This buckling involves a lateral movement of the yarns out of their original plane.

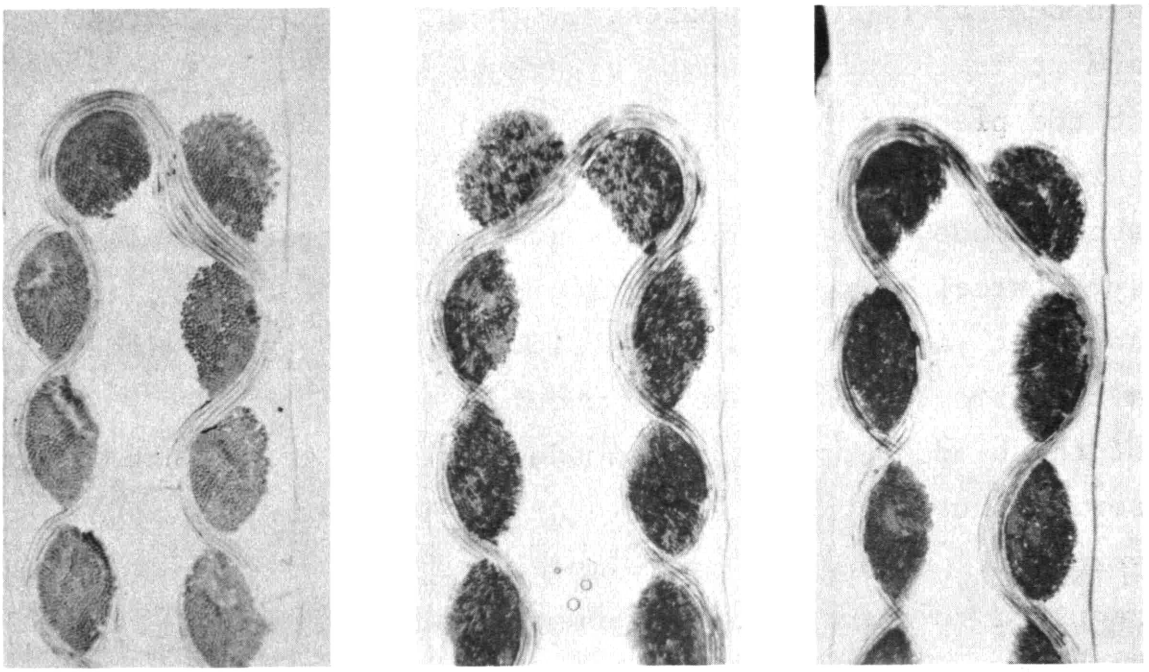

a b c

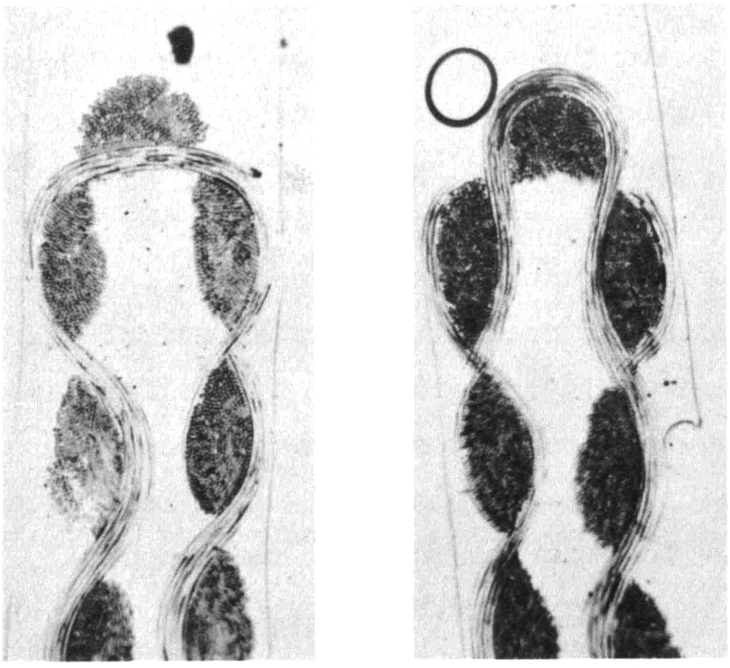

d e

Fig 3-11a CROSS SECTIONS OF BENT FABRICS (NYLON SERIES N)

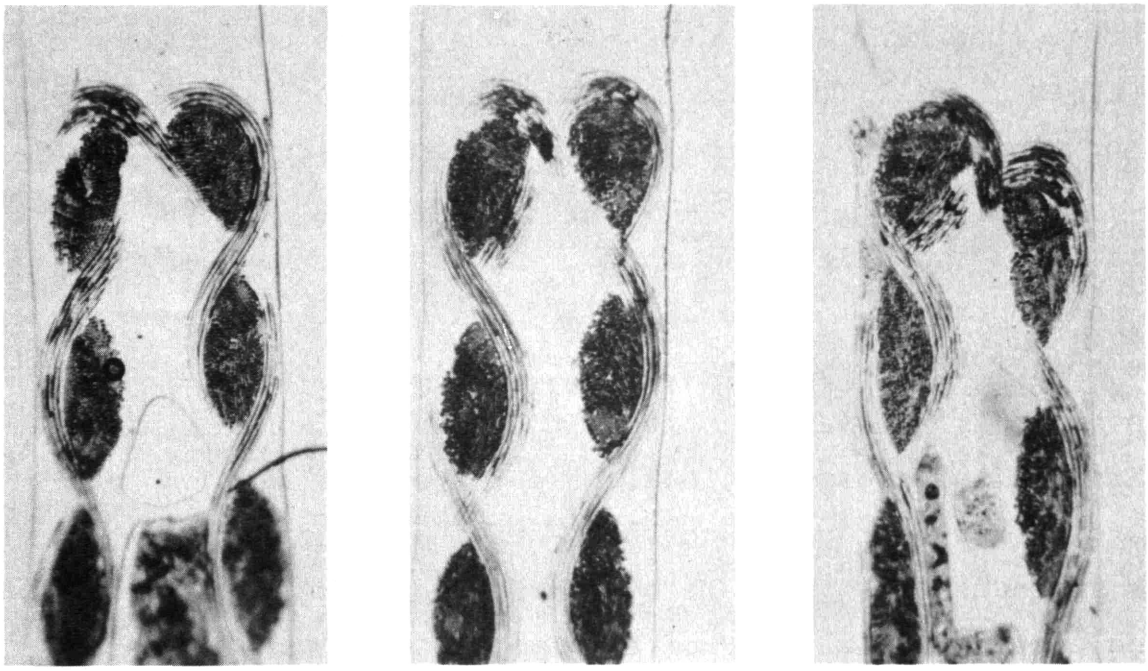

f g h

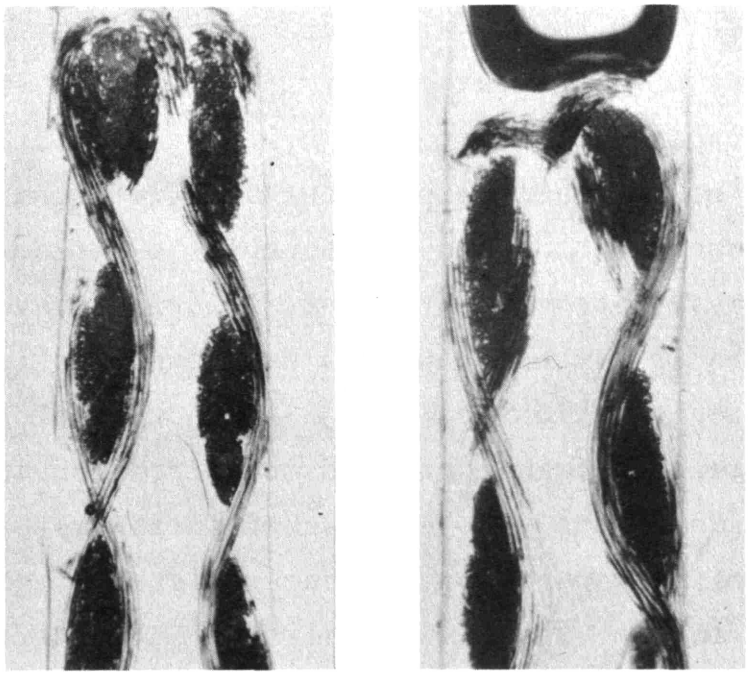

i j

Fig 3-11b CROSS SECTIONS OF BENT FABRICS (NYLON SERIES N)

4. Perhaps the most pronounced effect that can be observed from the fabric cross-sections is the compaction of the cross yarns. The effect of this compaction is to change the original cross-sectional shape of these yarns to a circular form. This effect is, of course, less noticeable when the cross yarns are originally round. Since the extent of compaction can be considerable in some fabrics, it appears that this factor may have some influence on their bending recovery. If the yarns are able to recover elastically to their original cross-sectional shape, they will assist in returning the bent yarns to their original configuration. This suggests that it would be advantageous to design yarns which compact readily during bending and then rapidly spring back to their original shape during recovery.

5. The fabric series shown on Fig. 3-12 is composed of seven samples each having a different interfiber frictional interaction, but an identical geometric structure. These samples were prepared by treating a nylon fabric with various concentrations of both softening agent and frictionizer (Syton). The bending and recovery behavior of these samples, reported previously, demonstrates that friction played a significant role in establishing the fabric properties. However, the cross-sections on Fig. 3-12 show that there is no apparent difference between the bent geometries of the samples. This indicates that although friction may effect the extent of slip propagation and the resistance against relative fiber motion, it does not significantly affect the geometry of bending at high levels of curvature.

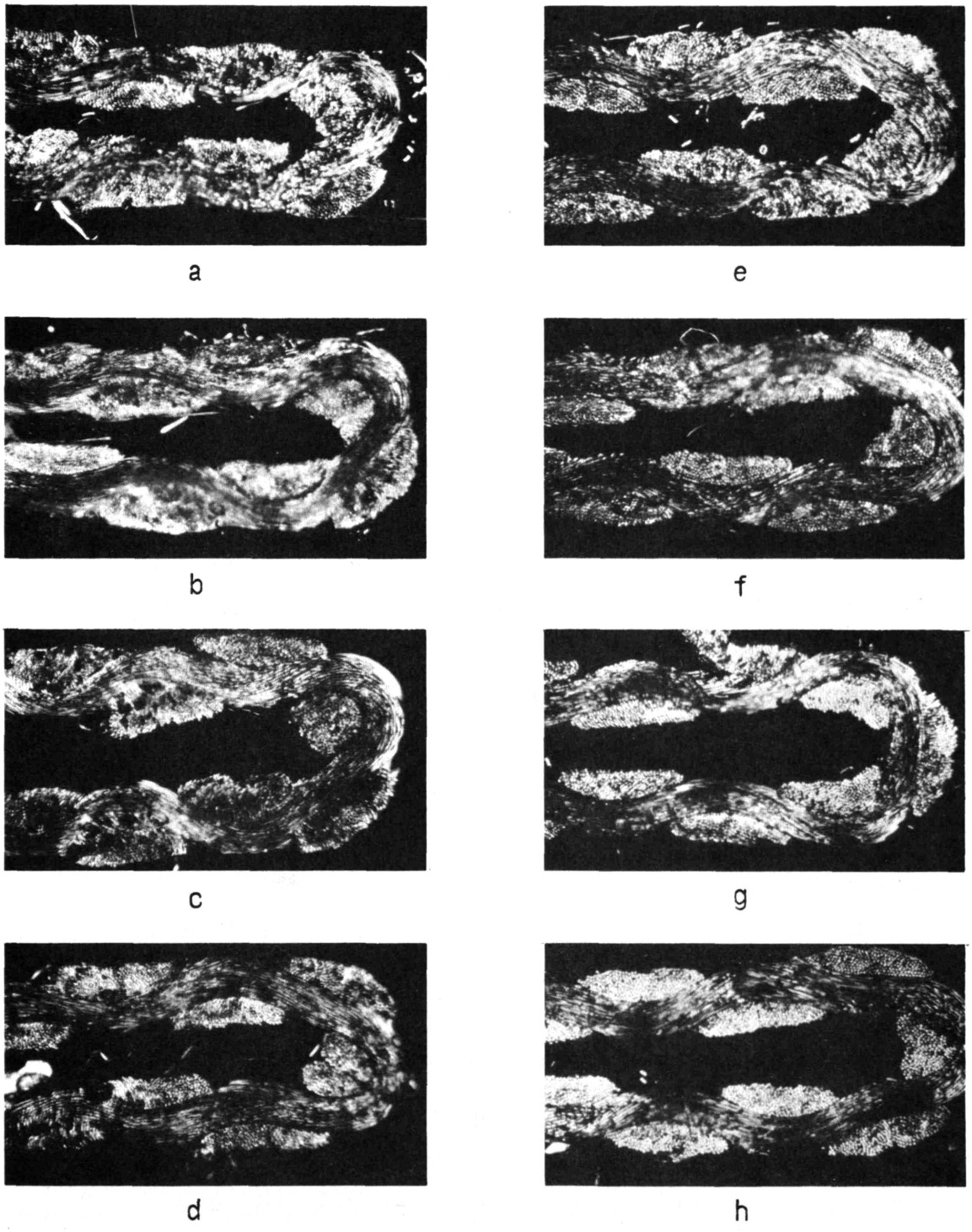

Fig 3-12 CROSS SECTIONS OF BENT FABRIC WITH VARYING FRICTION TREATMENTS

CHAPTER IV. EXPERIMENTAL TECHNIQUES

INSTRUMENT FOR MEASURING MOMENT-CURVATURE RELATION

The fundamental characterization of the bending behavior of a material is given by the moment-curvature relation. This curve can be used to determine such quantities as stiffness, non-linearity of bending, energy loss in bending,and non-recoverability in bending. An instrument for making this measurement was designed and constructed. This instrument imposes a constantly increasing or decreasing curvature while measuring bending moment continuously.

In an ideal, linearly elastic material there is no need for any elaborate equipment for measuring the moment-curvature relation. In that case this relation will be linear and can be described by only one number. There will be no rate dependence and the behavior will be independent on the direction of loading. Because of this, very simple evaluation techniques can be used to measure the bending behavior of ideal materials. For relatively rigid materials a beam or strip can be loaded as a simply supported beam or a cantilever and the loads required to produce a certain deflection can be used to compute bending rigidity. This type of test[37] is used for many applications, such as the evaluation of reinforced plastics and stiff fabrics.

For relatively flexible materials that can be considered as ideal, it is possible to measure the rigidity by a number of gravity loading techniques. A sample is placed in a configuration in which gravity forces will cause deflections. The extent of deflection or the amount of material length necessary to produce a certain deflection can then be used to determine the rigidity relative to the weight per length of the test strip. The most commonly used of these techniques for textiles are the cantilever and heartloop tests[38]. In both of these tests the relation between gravity deflected geometry and rigidity has been determined by rather sophisticated mathematical techniques. However,

since the assumption of ideal bending behavior was made in the mathematics, the rigidity calculations are not valid for non-ideal materials. This means that accurate quantitative measurements of many textile materials are not possible by these methods. And, it has been shown that sometimes even qualitative measurements are not possible. This was shown by Shwartz[39] in an experiment in which fabrics were evaluated by a number of techniques and the relative rankings of rigidity were not found to be fully consistent.

Because of the general non-ideal bending behavior of textile materials, it is not always possible to use an experimental technique which can only properly be used for ideal materials. To do so would be equivalent to measuring tensile modulus of a material by merely applying a constant weight and measuring deflection. This may be satisfactory for certain cases, but it is not so for research investigations in which fundamental mechanisms of deformation are under consideration.

A number of attempts have been made in the past to measure the complete moment-curvature relation rather than just measure a single number to describe bending. Eeg-Olofsson[12,21], Isshi[11], and Livesey and Owens[7] have constructed instruments for this purpose. Although each of these instruments operates on a different principle, the general procedure involves subjecting a fabric or yarn sample to progressively increasing curvatures and then measuring the applied bending moment.

In Eeg-Olofsson's instrument the curvature is imposed by the rotation of one end of the sample while the other end is fixed. A clamp connected to the rotating end floats on a pool of mercury so that the ends of the sample can come together during bending. The bending moment is measured from the current flow in a coil which transmits torque to the rotating end. This method seems to have been used with reasonable success. However, there appear to be several difficulties in sample mounting and maintenance of the pool of mercury.

Isshi's device imposes a progressively increasing curvature to the sample by moving and rotating one end of the sample in a

prescribed manner. This involves a complicated arrangement of gears, cams, slots and sliders. The other end of the sample is fixed to a shaft which is mounted on jewel bearings and which is prevented from rotating by a torsion spring. As the sample is bent, the fixed end will cause a slight rotation of the torsion spring. This rotation is reversed by another spring until the original rotation is nullified. The deflection of the second spring for nulling can be related directly to the bending moment on the sample. The major disadvantage of this method is that the test is performed in a series of steps and during each such step the load is changed slightly by the measurement procedure.

The method of Livesey and Owens is an approximation to a pure moment-curvature measurement. A sample is mounted on a clamp which can be rotated about a horizontal axis. A small tab with a protruding pointer is connected to the free end of the sample. The gravity acting on the pointer will produce a moment and a force on the sample. But, according to Owens, the force will be negligible under certain conditions. The curvature can be increased by rotating the clamped end of the sample and the bending moment can be obtained by measuring the angle of the pointer. The difficulty with this procedure lies in the fact that the readings are taken stepwise, tabs must be cemented to the ends of the samples, and the loading is not accomplished by a pure bending moment. Nonetheless, this method of measurement is relatively simple and has already been used by Owens to obtain interesting results.

There are several other methods of obtaining the moment-curvature curve that operate on an indirect principle. These involve measurement of two parameters which from other considerations have been shown to be capable of describing bending--the friction moment and the elastic rigidity. The methods use either modified cantilever or buckling tests[13]. The difficulty in these methods lies in the fact that they do not actually measure a moment-curvature relation, but just fit parameters to an assumed

form. Furthermore, imposed curvatures vary along the lengths of the samples and they are not imposed at constant rates.

During the course of this investigation a moment-curvature measuring instrument was developed. Although certainly not without faults, it has eliminated many of the disadvantages of the previous designs. The instrument, shown on figure 4-1 and 4-2, operates by imposing a constantly increasing curvature to one end of a sample. The other end is instrumented with a cantilever spring, a differential capacitor, and suitable circuitry to give a continuous output signal which is proportional to the applied bending moment. This signal is fed to a recorder to give the final moment-curvature plot.

The design has been made for maximum versatility. Provisions are included for changing the rate of change of imposed curvature, the sensitivity, the sample length, and the sample grips. In addition, the imposed curvature change can be reversed or stopped to measure load-unload, cyclical, or relaxation behavior. The following sections will include detailed descriptions of the component parts of the instrument.

Drive mechanism. Since one end of the sample is held fixed, the moving end must execute a translation and rotation so that the sample is always in a circular arc of constant length. The curvature of this arc must increase linearly with time.

The moving end of the sample is mounted on a carriage, and in order to meet the stated requirements this carriage must move in a certain way. The equations of motion can readily be derived using the method of Isshi[11]. Referring to figure 4-3, let

r, θ = polar coordinates of point on carriage relative to fixed end of sample and original straight line of fabric.

G = gage length of sample.

θ_c = rotation angle of carriage.

k = sample curvature.

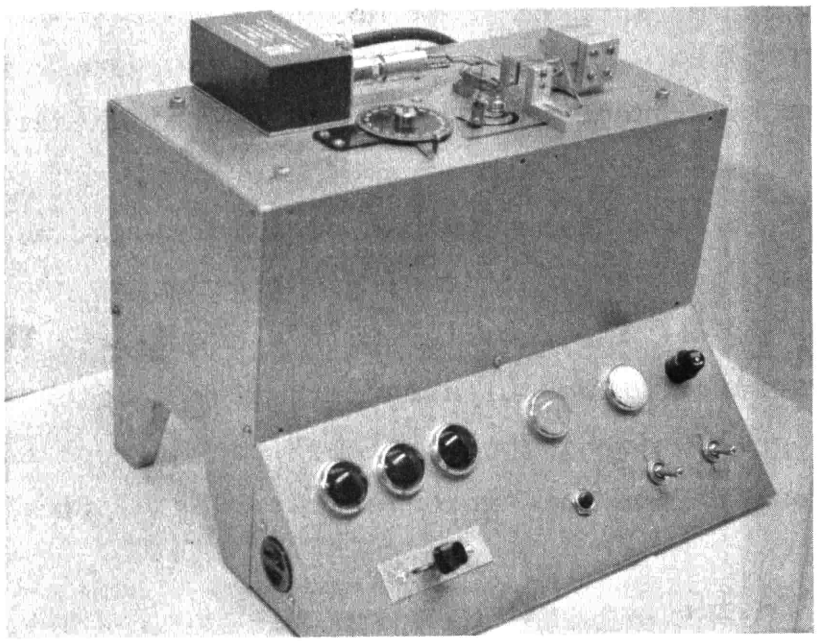

Fig.4-1 MOMENT-CURVATURE INSTRUMENT

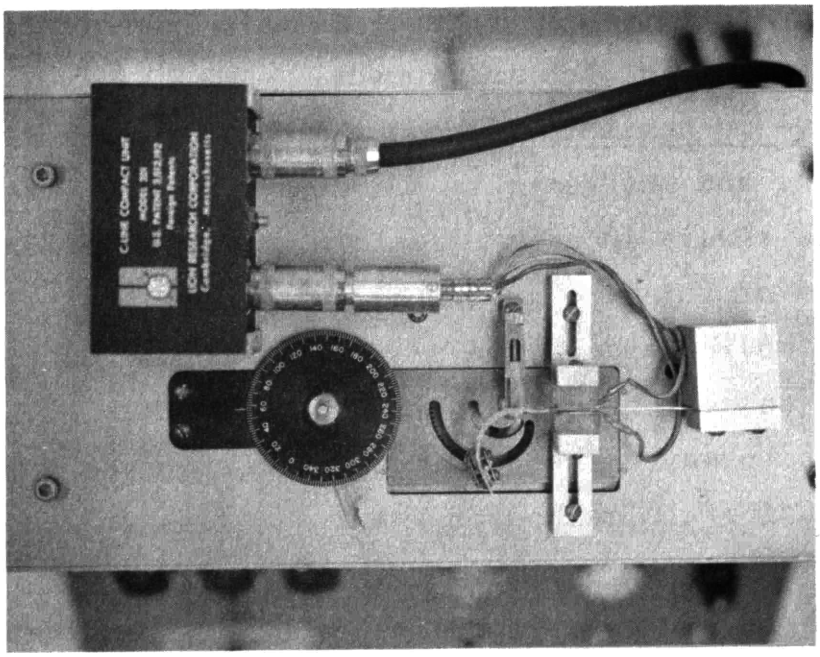

Fig.4-2 TOP VIEW OF MOMENT-CURVATURE INSTRUMENT

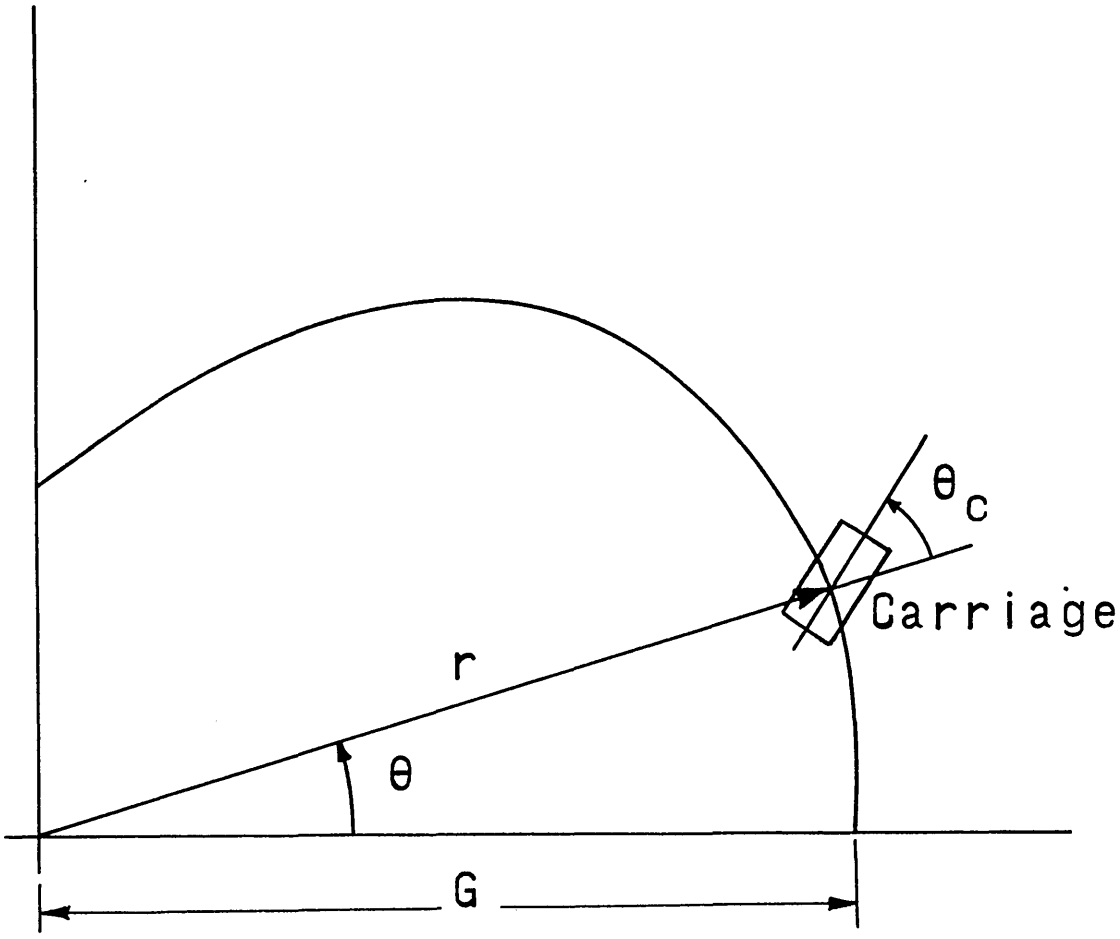

Fig. 4-3 Required Carriage Motion on Bending Instrument

To maintain a constant length of circular arc of the sample, the required translation of the carriage can be shown to be,

$$r = \frac{G}{\theta} \sin \theta \qquad (4\text{-}1)$$

To insure that the tangent angle of the bent sample ends corresponds to that of a circular arc of appropriate radius, the required rotation of the carriage can be shown to be,

$$\theta_c = 2\theta \qquad (4\text{-}2)$$

The curvature of the sample at any position of the carriage is,

$$k = \frac{2\theta}{G} \qquad (4\text{-}3)$$

This means that if the angular position of the carriage is increased linearly with time, the curvature will increase linearly with time, and the boundary conditions of position and slope will correspond to that of a circular arc.

The mechanisms employed to generate the required motions of equations 1, 2, and 3 follow a modification of that developed by Isshi[11]. Referring to Fig. 4-4, the power comes into the system at shaft S_1 from a synchronous motor. The rotation is transmitted to S_2 through gears and a slip clutch. This clutch is used as a safety device and as a means for providing a break in the gear train so that the carriage may be rotated by hand. The next shaft, S_3, is rotated by gears M and N which may be changed to vary the rate of imposed curvature. The motion then rotates shaft S_4 and gear A. This is the input point of motion to the carriage drive unit.

Figure 4-5 shows the carriage drive unit in greater detail. Rotation of gear A causes a circular motion of the bearing of shaft S_5. In addition, this causes a rotation of S_5 because gear B rolls around stationary gear segment H. This rotation is transmitted through gears C, D, E, F, and G to shaft S_9 which carries the carriage. Linkages L_1 and L_2 hold the shafts parallel, and the slot in gear A holds S_5, S_4, and S_9 in one plane. As a result of this, and the fact that gears H, B, C, E, and G have the same number of teeth, the rotation of shaft S_9 is twice the rotation of

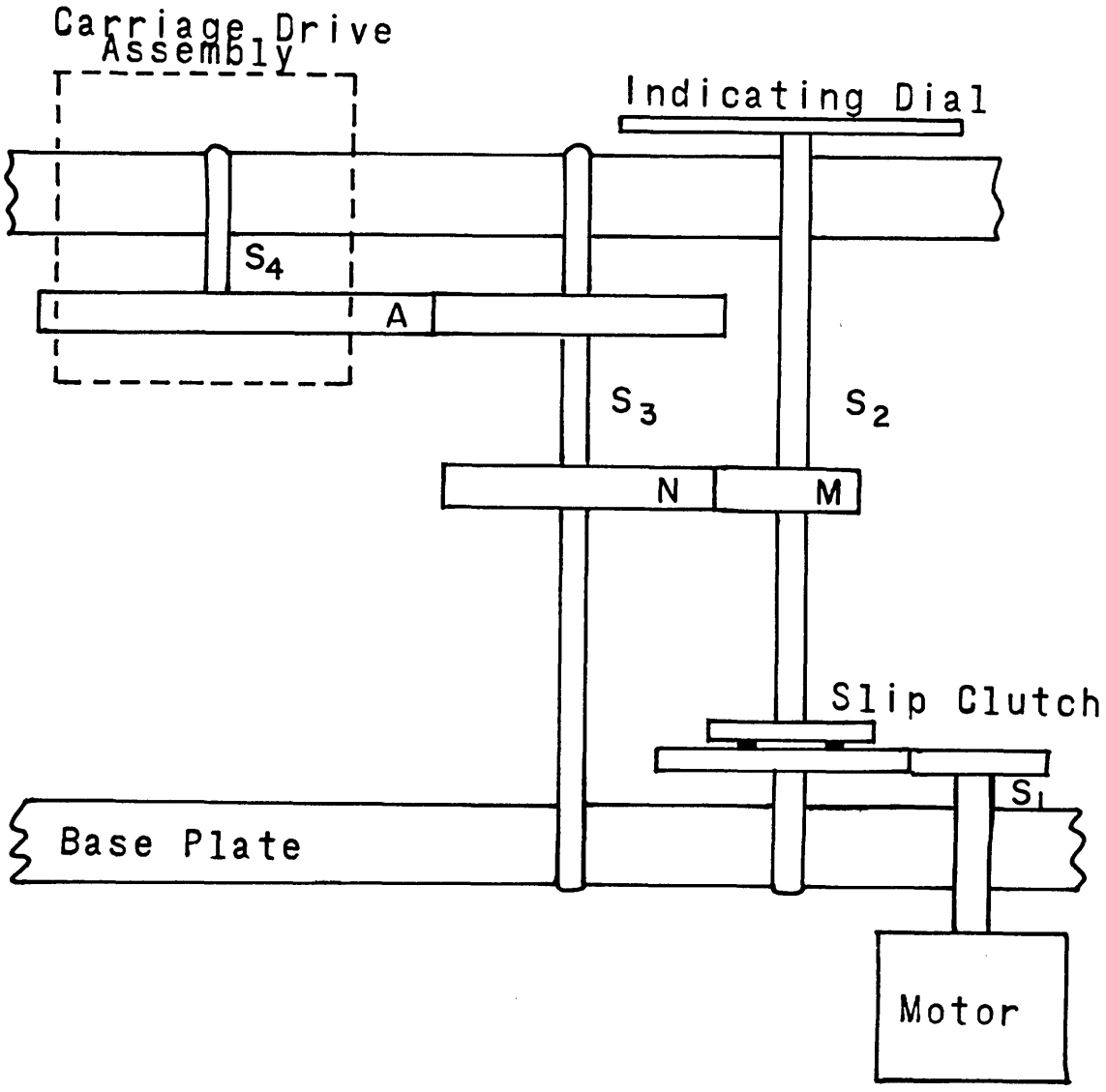

Fig. 4-4 Drive Mechanism for Moment-Curvature Instrument

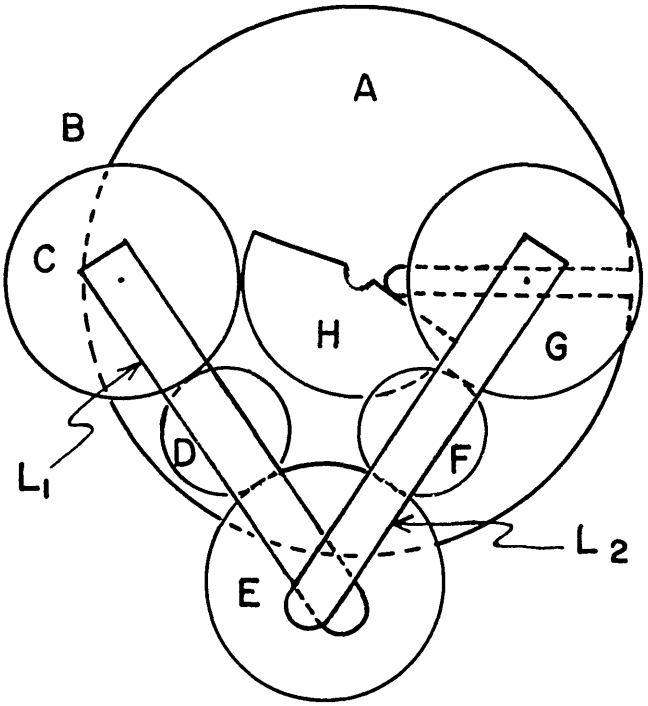

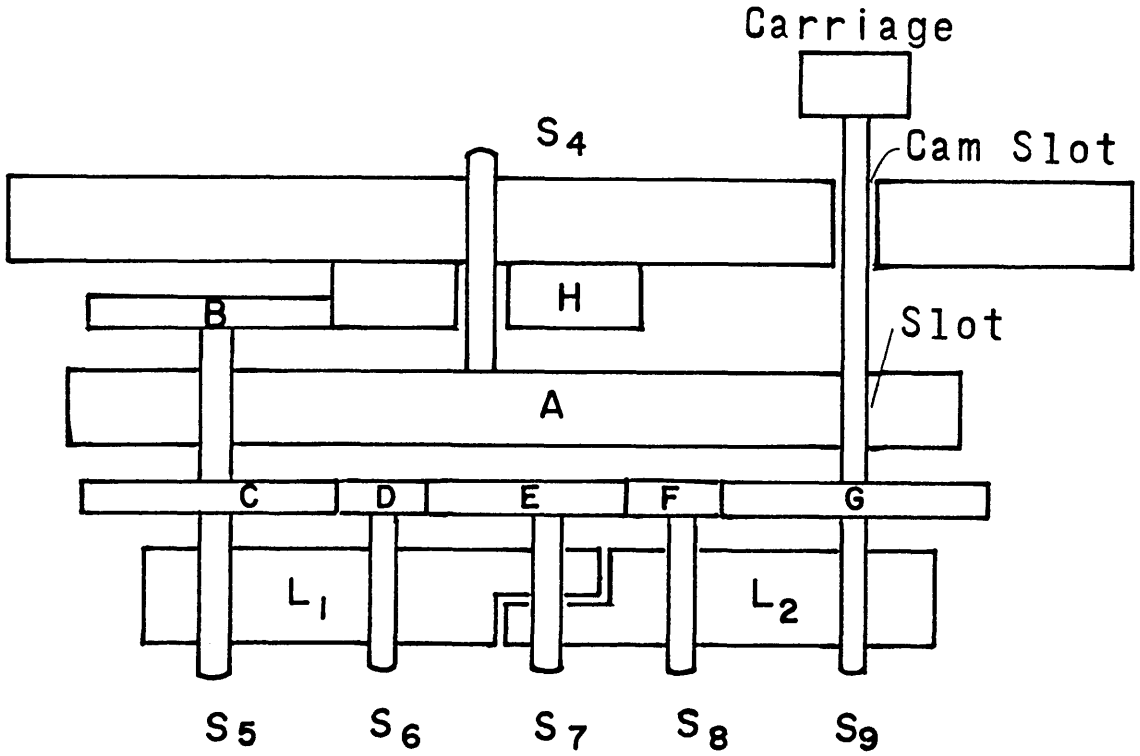

Fig. 4-5 Carriage Drive Assembly

S_4 independent of the distance between the two shafts. This then satisfies the required carriage rotation given by equation 2. The proof that S_o rotates twice as fast as S_4 can be obtained by applying the theory of epicyclic gears.

Having satisfied the rotational requirement of the carriage, it only remains to produce the translational motion dictated by equation 1. This was done by using a slot cam which was machined to meet this requirement. Shaft S_9 rides in this cam; and, since the rotational motion of this shaft is independent of its distance from S_4, the final required motion is obtained.

Two cam slots were cut, each corresponding to equation 1 with different values of "G". This permits the testing of samples of different gage lengths.

In an attempt to minimize backlash of the system, a number of springs were installed to insure that S_9 remains on the same side of both the slot in gear A and the cam.

Method of Gripping Sample. Preliminary tests on this instrument have shown that the method of gripping the sample requires careful control. The best method found was to use a four-point loading system whereby the sample is fixed between two sets of pins (actually fine drill bits) and bent by the couple set up by each such set. The pins in each set may be separated by either 1/8" or 1/4" and they can be individually adjusted to permit testing of samples of different thickness. As the pins are vertical, some provision must be made to keep samples from sliding down in the initial portions of the test. This is accomplished by the use of small beads of modelling clay.

One pair of pins is mounted on the moving carriage with a screw thread arrangement for adjusting the individual positions. The other pins are supported individually. One is fixed to the instrument frame through an adjusting screw and the other is mounted on a stiff cantilever spring. The deflection of this spring is measured by the transducer to determine the moment exerted on the sample.

Measurement of Bending Moment. The bending moment is measured by determining the force on one of the pins holding the fixed end of the sample. This is done by mounting the pin on a cantilever spring, and measuring the small deflections of this rather stiff member. One section of the cantilever forms the central plate of a differential capacitor which is used to measure the deflections.

The differential capacitor is used in conjunction with suitable circuitry (a non-linear twin-T circuit[40]) to obtain an output signal which is proportional to the displacement of the central plate. The input to this circuit is a 40 volt, 2 megacycle signal, and the output is a D. C. voltage which can be fed directly into a recording unit. The required oscillator and capacitance circuit used was a commercially available unit sold by Lion's Research Corporation[41].

Since the voltage output is proportional to the displacement of the cantilever, and this displacement is proportional to the bending moment, the output is a direct measure of the bending moment.

The balancing of the capacitor circuit is accomplished in two ways. A coarse adjustment can be made by varying the positions of the fixed plates of the differential capacitor relative to the central plate. Then a fine adjustment is made by setting a potentiometer included in the capacitor circuit.

Calibration. Both the curvature and bending moments must be calibrated to set the scales of the output curve. The rate of change of curvature is determined by determining the speed of the instrument relative to the chart and applying equation 3. The moment calibration requires more care. This was done by preparing a sensitive calibrated spring capable of applying a known horizontal force on the pin of the cantilever. The relation between force and output voltage was recorded. From this relation and the spacing between the pins of each pair, the moment-voltage relation was computed. This relation was found to be linear in

the operating range.

To check on the validity of the calibration, a strip of rubber having a rigidity close to that of the fabrics to be measured was tested on the instrument using the calibration performed by the spring. Then the rigidity of the rubber was measured by two other means: a tensile test; and a cantilever bending test. These measured rigidities were then compared to the linear moment-curvature plot which was obtained on the instrument and excellent agreement was achieved.

MEASUREMENT OF BENDING RECOVERY

In Chapter III the variables of importance in describing the recovery behavior of a material were defined. It was found that this behavior could be characterized by the relation between dimensionless imposed curvature and bending recovery (or dimensionless residual curvature). This relation could be obtained by two series of measurements covering both the low and high range of imposed curvature. This was done by using a standard technique for the high curvature range and a specially devised technique for the low range.

Previous measurements of bending recovery were made by a number of investigators[15,21]. They used a number of techniques ranging from floating bent samples on pools of mercury to using specially designed equipment for the purpose. Some of these experiments may have been more sophisticated than those used in this investigation; however, the methods used were simple and found to give consistent, useful results.

Measurement of Low Curvature Recovery. The method used for measuring low curvature bending recovery was merely to bend samples around mandrels of varying curvatures and optically measure the residual curvature. Although this measurement could also be made on the moment-curvature instrument, it was found to be more convenient to use this direct method.

In order to hold time effects constant in all of the bending tests, the length of time for bending and recovery were each held constant at two minutes.

The effects of gravity were minimized in this measurement by using samples of sufficiently short length. This made deflections due to gravity much less than those due to residual curvature from bending. This was checked by bending around mandrels having a vertical axis. The optical measurement of residual curvature was made with a telescope mounted in a specially prepared rotating stand as shown on figure 4-7. The angle between the tangents at the ends of a sample were measured. This measurement in radians divided by the length of the sample gave a direct measure of residual curvature. This could be converted to bending recovery by dividing the recovered curvature by that imposed.

Measurement of High Curvature Recovery. For the purpose of this measurement a standard Monsanto Recovery Tester[32] was used with some modification. This test involved bending a sample to a 180° bend over a slab of predetermined thickness. The recovery is made in an apparatus designed to minimize the effects of gravity. And, as in the previous case, the times of bending and recovery were both held fixed at two minutes each.

The geometry of this test is shown in figure 4-6. From the assumption that only a fixed length of the sample bends and recovers, the bending recovery can easily be computed as follows:

Let,

R = bending recovery

k_i = imposed curvature (in^{-1})

k_r = residual curvature (in^{-1})

t_s = thickness of the spacer slab (in.)

t_f = thickness of the fabric (in.)

$|\theta|$ = recovery angle (°)

k_i^* = dimensionless imposed curvature.

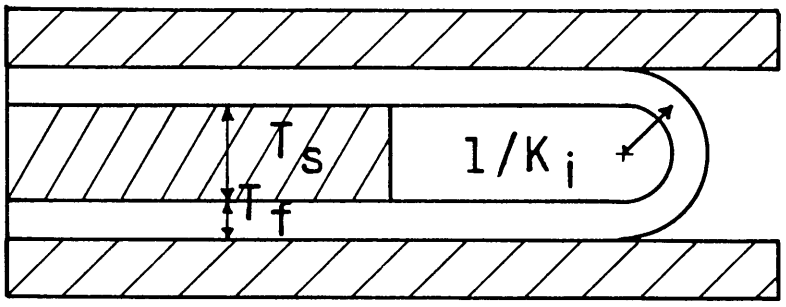

a.

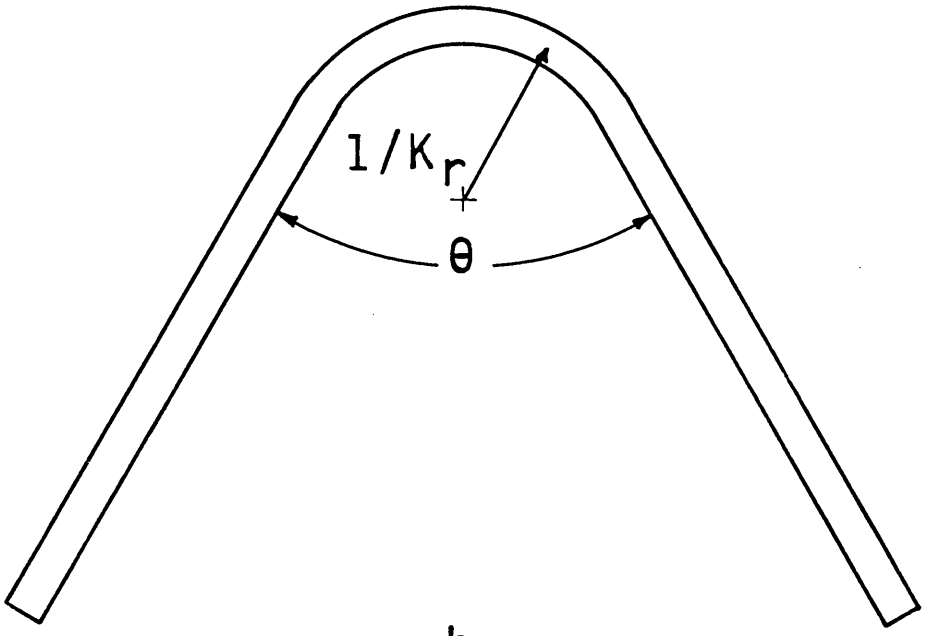

b.

Fig. 4-6 Geometry of Bending Recovery Test

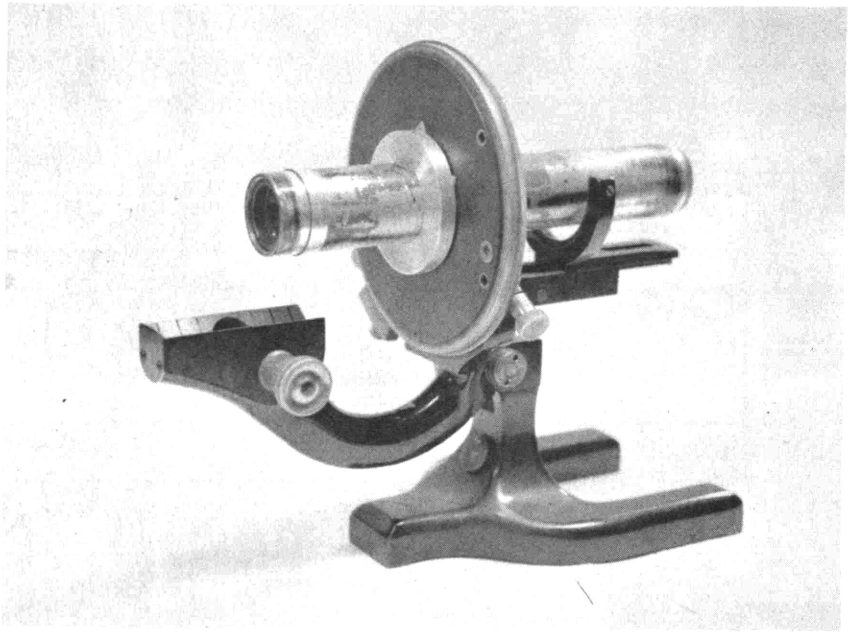

Fig.4-7 ROTATING TELESCOPE USED FOR MEASURING LOW CURVATURE RECOVERY

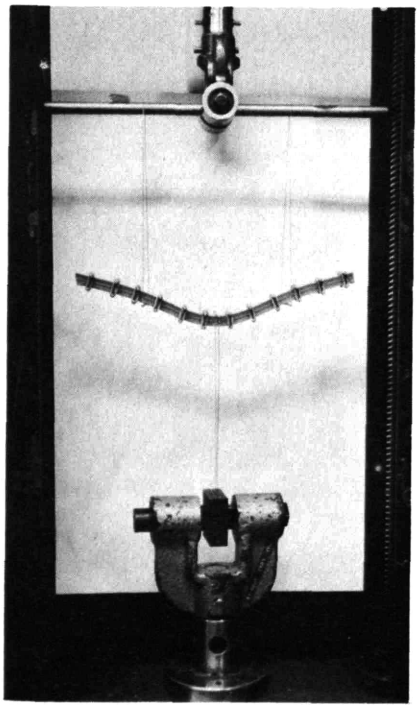

Fig.4-8 METHOD OF MEASURING BENDING BEHAVIOR OF MULTI-LAYER BEAMS

$$k_i^* = \frac{k_i t_f}{2} = \frac{1}{1 + \frac{t_s}{t_f}} \qquad (4\text{-}4)$$

$$R = 1 - \frac{k_r}{k_i} = \frac{\theta}{180^\circ} \qquad (4\text{-}5)$$

Varying curvatures were imposed by changing the thickness of the spacer slab. The lowest curvature used in this measurement overlapped the highest curvature tests of the preceding method and the measured bending recoveries were found to produce continuous curves.

MEASUREMENT OF FRICTIONAL FORCE

In both the textile materials and the multi-layer beams tested, the frictional force between the elements was measured by a pull-out test. The frictional force determined by this technique is a combined measure of normal pressure and coefficient of friction. Since this quantity is the variable of interest, additional measurements were not generally made to isolate the pressure and the coefficient of friction.

The principle of this measurement is based on the well-known stick-slip phenomenon. When a system consisting of a mass with dry frictional constraint and a spring in series is subjected to a constant rate of displacement, the force will follow a saw-tooth shaped curve. The upper peaks of this curve will correspond to the static friction force and the average between the upper and lower peaks will correspond to the sliding friction force. This can be demonstrated by either force or energy considerations.

Friction Force Measurements in Multi-Layer Beams. The friction force between the layers of a multi-layer beam was measured on an Instron Tensile Testing Machine. One layer was partially withdrawn a known amount from the interior of the beam. Then the force-time curve required to move this layer through the beam at a constant rate was recorded. A stick-slip behavior was found, but in contrast to the case of the mass-spring-friction system

described above, the level of force fell as the layer was withdrawn. This resulted from a reduction of layer length subjected to the friction force.

The static force was found from the upper peaks of the force-time curve and the sliding force was found from the mid-point between the upper and lower peaks. This friction force was divided by the length of layer in the beam and this value was halved to determine the friction force per length of each side of a layer.

Friction Force Measurements in a Woven Fabric. Fibers were withdrawn from fabrics made of continuous filament materials to determine the friction force at their interfaces[5]. The procedure was very similar to that used in multi-layer beams.

A fabric strip approximately 1" x 2" was used. One yarn was cut a known distance from one of the edges; and then a single fiber from this yarn was partially extracted to enable gripping it for withdrawal. The fabric was gripped by one clamp of an Instron Tensile Tester and the single protruding fiber was gripped by the other. The fiber was then withdrawn at a constant rate and the force-time behavior was measured.

The original length of fiber in the fabric was recorded and used to compute the friction force per length. As in the case of multi-layer beams, the total friction force per length was halved to give the force on each side of the fiber. This in effect assumed that the friction force developed from the pressure of the fibers in adjacent layers only. It was further assumed for this measurement that fiber rigidity effects are negligible. That is, it was assumed that the friction forces resisting fiber withdrawal were independent on the fiber rigidity.

As in the previous case, the static and kinetic friction forces were determined from the peaks of the pull-out force trace. The results were found to be relatively insensitive to the original fiber length and the rate of testing.

MEASUREMENT OF BENDING BEHAVIOR OF MULTI-LAYER BEAMS

The results presented in Chapter I were those taken from bending tests of simply supported multi-layer beams. The procedure used required a three-point loading of one of these beams with measurements of force vs. deflection taken at one of the loads. This was done on an Instron Tensile Testing Machine.

As illustrated in figure 4-8, a 1/2" rod was fastened to the upper jaw of the machine. From this were suspended two "trapezes" made of strain-hardened copper wire and steel rods. These rods were used to suspend the sample and to apply point loads at the required locations. Another "trapeze" was inverted and used to apply the central point load. This unit was connected to the lower jaw of the testing machine. During a test, the lower jaw moved down at a constant rate while loads on the upper jaw were measured continuously.

The deflected multi-layer beams were photographed with a Polaroid camera to determine the deflected shape for various conditions of loading, geometry and pressure.

The rigidity of each layer of the beam was determined by a separate bending test on the Instron Machine. Specimens were supported as cantilevers and force displacement measurements were taken to determine rigidity.

The sliding friction force between the layers was measured by a pull-out test similar to that described in Section IV of this chapter.

TECHNIQUE FOR EMBEDDING BENT FABRIC SAMPLES

In order to obtain a better understanding of the nature of bending deformation in fabric samples, a technique was developed by which fabrics could be bent to various curvatures, embedded, sectioned, and then observed microscopically. Previous work of this sort was done by investigators such as Coplan[44] and Eeg-Olofsson[21]. However, in their work there was no provision made for imposing controlled amounts of curvature. Otherwise,

the technique used in this work follows similar lines of approach.

Prior to embedding the samples, the following items were prepared:

1. Strips of steel approximately 0.15 x 0.5 x 1.7 inches covered by aluminum foil.

2. Strips of aluminum .006 x 1/2 x 1 inch to be used as spacer slabs.

3. A box made of heavy aluminum foil 1.5 x 5 x 2 inches to contain the embedding medium.

4. Butyl methacrylate monomer (Rohm and Haas) with a catalyst of benzoyl peroxide.

5. A mixture of parafin wax and polymer (for example, Fisher Scientific, Paraplast, M. P. 56-57°C).

6. Gelatin capsules about 1/2 in. diameter x 1-1/2 in. long, with the ends cut off.

7. Microtome specimen holders.

The procedure involved the following steps:

1. A fabric sample (1/2 x 2-1/2 inches) is bent around a fixed number of spacer slabs and sandwiched between the steel strips. The geometry is similar to that shown on figure 4-7a. The imposed curvature is controlled by the number of spacer slabs used and the fabric thickness.

2. The steel strips are clamped using conventional "bulldog" type fasteners.

3. About five samples are inserted in an embedding box and supported from the top by the clamps. Butyl methacrylate is added.

4. The embedding box is heated gradually on a hot plate for about several hours and then permitted to cool. If the polymer has not hardened to a sufficient extent, the box is reheated in an oven.

5. The polymer block is removed from the box and the individual specimens are cut and trimmed by hand with a razor blade.

6. The clamps and steel strips are removed carefully.

Then the embedded bent section of the fabric is cut from the polymer containing the spacer slabs.

7. The small piece of polymer containing the bent fabric section is placed in a microtome holder and oriented as desired.

8. A gelatin capsule is placed over this holder and is filled with melted parafin. This forms a cylinder of parafin around the small block of polymer containing the bent fabric.

9. Thin sections are cut with a microtome and the parafin is removed. These sections are then mounted on glass slides. A drop of solvent is placed on each section to insure adhesion to the slide and to clear the cutting marks made by the microtome blade.

Fabric sections prepared by this technique were studied microscopically under conditions of both normal and polarized light. Photomicrographs were made using a Polaroid back camera.

It should be noted that it was not possible to determine directly whether the geometry of the bent fabrics was substantially affected by the embedding process. However, since there was relatively little opportunity for fiber rearrangement in this embedding technique and since the bent geometries observed corresponded to those of large scale models, distortions due to embedding were neglected.

CONCLUSIONS

1. Friction has two effects on the bending behavior of textile materials. It provides a resistance against the relative motions of the fibers and it prevents the complete propagation of slip throughout the structure. This results in a moment-curvature plot as shown in Fig. 1-16. The first effect causes an energy loss and requires that a friction moment be applied during bending. The second effect causes the material to have an elastic rigidity that is greater than it would have if no interfiber friction existed.

As friction increases from zero to the level required for the complete prevention of slip, the friction moment increases from zero to a maximum and then falls to zero. At both limiting cases of frictional interaction the friction moment is zero. At the lower limit of friction it is zero because no force opposes the relative fiber motion; and at the upper limit it is zero because no relative fiber motion takes place. The elastic rigidity increases monotonically with friction from the value corresponding to the complete freedom of motion case to that corresponding to no freedom of motion.

2. Bending recovery is also affected by the two frictional effects. The frictional restraint that acts against the relative fiber motions prevents the fibers from completely reversing the relative motions that occurred during bending. This results in a structurally held deformation that acts even if the fibers are not permanently deformed. The second effect of friction acts to prevent the complete propagation of slip and in so doing increases the level of fiber strain and permanent fiber deformation.

The resulting relation between recovery and imposed curvature is shown on Fig. 3-6 for both the limiting and

intermediate cases of frictional interaction. For the intermediate cases the recovery curves differ qualitatively from those obtained for either of the limiting cases. The recovery is very low at low imposed curvatures, goes through a maximum, and then follows the trend of the limiting cases. At all levels of imposed curvature, friction reduces the amount of recovery. At low imposed curvatures the reduction in recovery is large and is caused by frictional forces preventing the fibers from reslipping after bending. At high imposed curvatures the reduction in recovery results from the incomplete slip propagation caused by friction.

3. The mechanical behavior of multi-layer beams with friction between the layers differs considerably from that of conventional beams. The proposed theory which describes this behavior appears to be in reasonable agreement with experimental observations. As predicted, interlayer friction results in an increased resistance to deformation, energy loss during bending, and non-recoverability from imposed deformations. It also causes the multi-layer beams to have an unusual mechanical behavior that differs qualitatively from the behavior of beams with either zero or infinite friction. One example of this behavior is the "reverse curvature" that develops as a direct result of friction. This effect involves beam deflections in which the curvature is in a direction opposite to that which would develop if no friction were present. (See Fig. 1-8.)

During the first stage of loading, multi-layer beams act as solid beams. Then, as the load is increased, slip begins to propagate throughout the structure. It was found that this propagation could proceed either across the section of the beam or along its length.

4. The geometric arrangement of twisted yarns provides the fibers with a convenient path along which slippage can occur. In a zero twisted arrangement of fibers there is no such path, and in order for the structure to bend, it is necessary for the individual fibers to strain or buckle. This is a consequence of the fact that the required amount of slip between fibers in this case is proportional to the length of the yarn. In the twisted yarn, the amount of slip required is proportional to the length of one turn of twist, and is independent on the sample length. For this reason, the magnitude of the slip required in twisted yarn can be much less than that required in an untwisted yarn.

Two types of relative fiber motion occur during the bending of a twisted yarn. The fibers in adjacent layers slide relative to each other with a sinusoidal distribution of slip. This slip is zero at the outside and inside of the bend and reaches a maximum value at the sides. The second type of slip occurs between fibers of the same layer. This slip is a result of local changes of the fiber helix angle. It is also distributed sinusoidally with the same amplitude, but is maximum at the inside and outside of the bend and zero at the sides. Since these relative motions may occur against a frictional restraint, energy will be lost in the process of bending and a frictional moment will develop. The magnitude of this moment will depend on the pressure distribution within the yarn.

5. During bending, a woven fabric loses energy due to relative fiber motions and thereby develops a friction moment. The magnitude of this moment depends on the slip distribution and the local pressure distribution between the fibers. To a first approximation this moment is given by equation 2-76 which is a relation between fiber properties, structural

geometry and friction moment. The structural variable in this equation is a factor involving the crimp of the bent yarns and the spacing of the cross yarns.

In addition to losing energy due to relative fiber motions, it is possible for certain types of fabrics to lose energy due to relative motions of adjacent yarns. The amount of energy lost by this effect depends on the structural geometry and interyarn forces as given by equation 2-80.

6. The elastic rigidity of a woven fabric is greater than that of the component yarns before weaving. This is due to the restrictions to curvature changes imposed by the cross yarns of the fabric. As a result, the rigidity of a fabric remains approximately constant, and equal to the sum of the yarn rigidities, for large cross yarn spacings. Then, as this spacing gets small, the rigidity increases sharply.

Yarn crimp has two effects on elastic rigidity. It reduces yarn rigidity by providing excess length and it increases fabric rigidity by increasing the effect of cross yarn rigidity. It was shown that the latter effect predominates and crimp increases fabric rigidity.

SUGGESTIONS FOR CONTINUING RESEARCH

The following suggestions for continuing research are based on the various research problems encountered in this investigation. In most cases, the experimental results or mathematical analyses presented here would form a starting point for this continuing research.

1. Experimental Investigations of Multi-Layer Beams. Since the theoretical work presented on this type of structure is of a rather general nature, there are many more areas to which it can be applied and evaluated experimentally than were investigated in this study. It would also be of importance to investigate the strain distributions that develop in this type of structure and this could probably be done by suitable photoelastic techniques. On the basis of this extension of experimental work, it may be possible to improve or extend the proposed theory.

2. Experimental Investigation of Twisted and Ply Yarns. A useful extension of the work presented in this area would be the evaluation of this type of structure for varying twists and frictional effects. This would enable the determination of such things as friction moment, elastic rigidity, and extent of slip propagation. The moment-curvature instrument developed in this research could be used for these measurements.

3. Evaluation of the Degree of Slip Propagation. Since the degree of slip propagation plays an important role in establishing the friction moment, the elastic

rigidity, and the recovery, it would be important to extend the work done on this factor. This could be done by direct experimental observations on large scale models or by careful examinations of photomicrographs of actual samples that are marked along their length.

4. Time Dependence of Bending Behavior. Using the moment-curvature instrument developed it is possible to study the effects of loading rate on bending behavior. This effect would be particularly pronounced for samples treated with "wet" type lubricants. Another important time dependent effect that can easily be evaluated is the relaxation of bending moment when a sample is held at a constant curvature bend. The relaxation behavior of bending can then be compared to that of tension to obtain a measure of the degree of strain which the individual fibers experience. One investigation of this sort conducted by Suzuki[45] showed that the distribution of relaxation times for the two types of loading differ considerably.

5. Effect of Temperature and Humidity on Bending Behavior. Since textiles are used under a wide variety of conditions of temperature and humidity, it is important to characterize their bending performance in terms of these variables. As temperature and humidity change, the fibers will experience a change in modulus and tensile recovery. These changes will affect the fabric properties since they involve alterations of both fiber properties and fiber to fiber interactions. To measure these affects on bending it is proposed

that the moment-curvature instrument be outfitted with a variable temperature and humidity chamber. The recovery experiments can also be run in such a chamber.

6. Effect of Fiber Blends on Bending Behavior. As blends of fibers involve both changes of fiber properties and their interactions, experiments involving this variable would be of both practical and fundamental importance in this field. This type of investigation has, of course, been done in the past in connection with bending recovery. However, the emphasis has usually been placed on the effect of fiber properties. When fibers of high recovery are added to fibers of low recovery, the bending recovery generally improves. The question still remaining is the determination of how much improvement can be attained by adjusting the interactions between fibers or the geometry of the structure. For example, would a significant improvement in properties be attained by adding fibers of extremely low friction to a blend? Or, would it be possible to make a good fabric by blending a large number of very fine fibers (for good recovery) with a small number of stiff, recoverable fibers (for adequate fabric stiffness).

7. Instrumentation for Measuring Recovery Behavior. Since the relation between bending recovery and imposed curvature was found to be of fundamental importance, it would be desirable to have an instrument for making this determination automatically. This could be done by constructing a device which automatically bends

yarns or fabrics to varying curvatures and measures recovery or residual curvature by an optical or electrical system. Such an instrument should have the capability of varying such factors as pressure, time of bend and recovery, temperature, and humidity.

8. Fundamental Studies on the Geometric Structure of Bent Fabrics. Using the technique developed for embedding fabric specimens at varying curvatures, it is possible to analyze the geometric structure in the bent state in detail. For example, the geometry of a yarn in a bent fabric can be compared to that in the flat form by measuring the local curvature as a function of position for both situations. This would make it possible to determine the local changes of curvature that occur; and this can be used in conjunction with the continuity equation which was developed to determine the relation between fiber slippage, straining, and buckling. In addition, a number of important factors can be studied from this type of test: relative yarn motions at sharp bends; effects of yarn compaction during bending; and possible variations of fabric geometry during bending. The last item involves the probability that the fabric will form a square, round, or intermediate type bend.

9. Effect of Distribution of Imposed Fiber Curvatures. In the analyses presented, it was generally assumed that the fibers of a yarn all bend to the same curvature. This approximation may not be valid in certain situations, particularly if one set of yarns has a smaller diameter than the other, or if certain fibers have the opportunity to buckle laterally. The

recovery of the structure will then be based on a balance of the restoring forces of fibers which have been deformed different amounts. The analysis of this situation would be quite involved, but may yield useful results.

10. Effect of Lateral Fiber Motion During Bending. During bending, the fibers of both the bent yarn system and the cross yarn system may move laterally relative to one another. This effect is particularly apparent in the cross sections of bent fabrics where large motions occur between the fibers of the cross yarns. This motion will cause an energy loss during bending and a non-recoverability due to entanglement. These effects would probably be most pronounced in materials having highly disordered arrangements of fibers.

11. Frictional Effects of Fabrics Bent on the Bias. The work presented here for woven fabrics is restricted to bends directly across one set of yarns. In other investigations it has been shown that fabric properties can vary considerably when bends are imposed at intermediate angles. For this type of bend a frictional effect occurs that was not considered in this investigation--namely that of yarn rotation at the crossing points. This rotation occurs because of an angular change between warp and filling along the line of bend. This angular change may not be recoverable and cause permanent deformation. This effect was observed qualitatively for fiberglas fabrics which had relatively high interyarn pressures. Since fabrics are frequently bent on the bias in actual use, it

would be of considerable importance to study this effect in greater detail.

12. Extension of Application of Fundamental Relations. A number of fundamental relations were derived which relate to fiber motions. As mentioned previously, some of these relations may be applied to problems in textile technology that are not restricted to bending mechanics. For example, the one-dimensional slip-stretch theory could be applied to stretch garment extensions and sliding relative to the skin or to the mechanics of fiber drafting. The continuity equation which was derived could be used for characterizing torsional or tensile behavior.

13. Geometric Restrictions to Fiber Motion. In Chapter II it was shown that under certain circumstances there is a restriction to relative fiber motion even if there is no friction. This occurs when the geometry of the structure fails to provide a path along which the fibers can slide. This effect is particularly important in tightly twisted yarns with fiber migration or in ply or cabled structures. An investigation of available slip paths for these and other types of structures would probably provide useful results.

14. Determination of Friction Moment for Braid and Pressurized Structure. Using the energy approach, the friction moment can be determined for these types of textile structures. In the braid, the energy loss arises from a local change in helix angle during bending. Its magnitude can be determined in a

manner similar to that used for the twisted yarn. For pressurized structures, the mode of relative yarn motion must be established and combined with the forces resisting it to give the frictional energy loss and the friction moment. This type of computation is particularly important for such applications as full pressure suits where a non-recoverability from bending due to friction is actually desirable.

15. Relation Between Frictional Effects and Fabric Hand. Fabrics having a high friction moment relative to the elasticity of the structure have a noticeably poor "hand". Correlation experiments between these measurable quantities and hand would be useful in providing further insight into how the aesthetic properties can be evaluated in a quantitative manner.

APPENDIX A

The shear stress distribution in a rectangular slab subjected to a sinusoidal pressure on two opposite sides as in Fig. A-1 can be obtained by the use of stress functions. This is done by Goodier[43] with the result,

$$\tau_{xy} = -\frac{(A+B)\alpha c \cosh\alpha c \sinh\alpha y - \alpha y \cosh\alpha y \sinh\alpha c}{\sinh 2\alpha c - 2\alpha c}\cos\alpha x$$

$$-\frac{(A-B)\alpha c \sinh\alpha c \cosh\alpha y - \alpha y \sinh\alpha y \cosh\alpha c}{\sinh 2\alpha c - 2\alpha c}\cos\alpha x$$

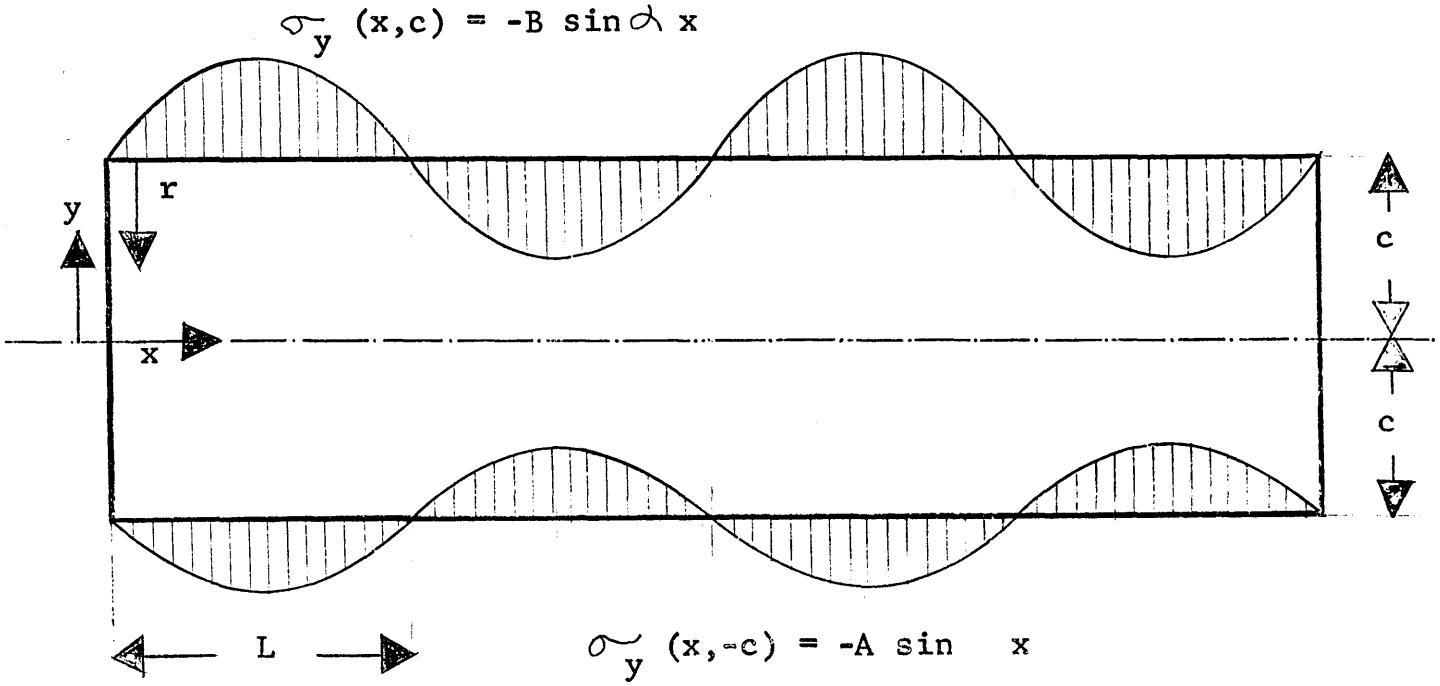

Fig. A-1 BOUNDARY CONDITIONS FOR SHEAR STRESS PROBLEM

For equal amplitude sin waves, and values of c approaching infinity, the shear stress can be written in terms of the

coordinate v.

$$\tau_{xy} = - A\alpha v \; e^{-\alpha v} \cos \alpha x$$

Using the principle of superposition, this result can be used to determine the shear stress distribution for a saw tooth surface stress. This is done by expanding the saw tooth function in a Fourier series.

$$\sigma = \frac{2\sigma_{max}}{\pi} \sum_{n=1}^{\infty} \frac{(-1)^{n+1}}{n} \sin \frac{n\pi x}{L}$$

Summing the shear stresses for the individual sin functions in this series requires the indexing of both the amplitude and frequency as follows,

$$A_n = \frac{2\sigma_{max}}{\pi} \left(\frac{1}{n}\right)(-1)^{n+1}$$

$$\alpha_n = \frac{n\pi}{L}$$

The resulting shear stress is,

$$\tau_{xy} = \sum_{n=1}^{\infty} -A_n \alpha_n v e^{-\alpha v} \cos \alpha_n x$$

$$= \sum_{n=1}^{\infty} - \frac{2\sigma_{max}}{\pi} \frac{(-1)^{n+1}}{n} \left(\cos \frac{n\pi x}{L}\right) \frac{n\pi v}{L} e^{\frac{-n\pi v}{L}}$$

At the point of discontinuity of the saw tooth function (x - L), the shear stress distribution can be shown to be,

$$\tau(L, v) = \frac{2\sigma_{max}}{\pi} \left(\frac{v\pi}{L}\right) \left(\frac{e^{\frac{-v\pi}{L}}}{1 - e^{\frac{-v\pi}{L}}} \right)$$

This equation is rewritten in equation 38 in terms of the variables used in Chapter I.

APPENDIX B

From reference 18 equations 32 and 44 (authors' equations)

Complete Freedom of Motion

$$(EI)_{cell} = \frac{3}{8} N_c EI_i \left(1 + \frac{1}{3\ (1+\mu)}\right) \qquad [32]$$

N_c = number fibers in unit cell

μ = Poissons ratio

N_f = number fibers passing through square cross-section = $N_c t$

t = fabric thickness

D_f = fiber diameter

A_f = fiber area

γ_B = packing factor

Taking a cell having a width equal to the fabric thickness gives,

$$\left(\frac{M}{k}\right)_{CFM,t} = t(EI)_{cell} = \frac{3}{8} N_f EI_i \delta \qquad (2\text{-}10)$$

No Freedom of Motion

$$(EI)_{cell} = \frac{1}{32} N_f E_f A_f t^2 \qquad [44]$$

$$A_f = \frac{\pi D^2}{4}$$

$$I_f = \frac{1}{4\pi} A_f^2$$

$$NA_f = t^2 \gamma_B$$

Substituting in equation 44 gives the result

$$\left(\frac{M}{k}\right)_{NFM,t} = N_f^2 EI_i \frac{\pi}{8\gamma_B} \qquad (2\text{-}11)$$

APPENDIX C

From reference 17 equation 33, using the author's notation,

$$\tan \alpha_B = \frac{a_B \lambda_B}{r_B - a_B \cos \varphi_B}$$

Converting this notation to the form used in Chapter II gives,

$$\alpha_B = Q$$

$$r_B = \frac{1}{k}$$

$$a_B = r$$

$$\theta_B = s\ k$$

$$\varphi_B = \theta$$

$$\lambda = \frac{\varphi_B}{\theta_B} = \frac{2\pi}{L_t\ k}$$

Substituting gives,

$$\cot Q = (1 - r\ k \cos \theta) \frac{L_t}{2\pi r}$$

APPENDIX D

Using variables defined in the text,

$$p_A(r) = 2\pi F T^2 \left(1 - \frac{r^2}{R^2}\right)$$

$$u_r = \frac{D_f k}{2\pi T} \sin\theta$$

$$u_\theta = \frac{D_f k}{2\pi T} \cos\theta$$

$$f_i = \mu p_A D_f \frac{\pi}{4}$$

$$w_i = 2T f_i \frac{L_t}{2} u_{avg}$$

$$u_{avg} = \frac{2}{\pi} \left(\frac{D_f k}{2\pi T}\right)$$

Combining these equations gives,

$$w_i = \mu D_f^2 k F T^2 \left(r \frac{r^2}{R^2}\right) \frac{L_t}{2}$$

From geometry,

$$L_t \approx \frac{1}{T} (1 + 2\pi^2 r^2 T^2)$$

To find the total energy loss requires a summation over all the interfaces. To do this requires a correction for the fact that there are different numbers of fibers in each layer. Let,

N_ℓ = number of fibers in layer at r

N_i = number of interfaces for fibers at r contributing to energy loss

ℓ = number of layers

From the geometry of an idealized yarn,

$$N_\ell = \frac{8r\gamma_y}{D_f}$$

$$N_i = 2\,N_\ell$$

Summing over all layers each subscripted by i gives,

$$w_T = \sum_{i=1}^{\ell} N_i\, w_i$$

$$= \mu\, D_f k\, FT\, 8\gamma_y\, R \sum_{i=1}^{\ell} \left(\frac{r}{R}\right)_i \left(1-\left(\frac{r}{R}\right)_i^2\right)\left(1+\left(\frac{r}{R}\right)_i^2 (2\pi RT)^2\right)$$

This equation can be solved by approximating the summation by an integral. The result is then differentiated to obtain the friction moment,

$$M_f = 4\,R^2\,\gamma_y\,\mu FT \qquad (2\text{-}63)$$

APPENDIX E

SAMPLE DESCRIPTIONS

Cotton Series Ca and Cc

Sample No.	Ends/Inch	Picks/Inch	% Warp Crimp	% Filling Crimp
Ca 1	45.1	46.1	4.20	11.13
Ca 2	45.4	40.5	3.99	9.28
Ca 3	44.3	36.0	5.32	7.70
Ca 3A	43.2	33.9	5.85	6.88
Ca 4	43.1	31.2	5.05	6.78
Ca 4A	42.9	27.0	5.49	5.51
Ca 5	42.6	25.0	5.50	3.67
Ca 6	41.5	20.0	4.90	3.61
Cc 1	41.8	20.0	3.20	2.69
Cc 2	42.1	27.7	2.96	5.69
Cc 3	43.2	33.6	4.33	5.67

All samples are unfinished

Warp Yarn: Ca Series 2/22's
Cc Series 2/22's

Filling Yarn: Ca Series 2/22's
Cc Series 2/40's

Nylon Series N-1	Picks/Inch	% Warp Crimp	Position on Fig.3-11
N-S 1	34	16	
N-S 2	32.5	14	a
N-S 3	29	12	b
N-S 4	27	11	c
N-S 5	25	9	d, e
N-S 6	22	7	f
N-S 7	20	6	g
N-S 8	18	4	h
N-S 9	15.5	3.5	i
N-S 10	13	3	j

Nylon Series N-1 (continued)

Sample No.	Picks/Inch	% Warp Crimp
N-H 1	33	16
N-H 2	31	
N-H 3	28.5	13
N-H 4	27	
N-H 5	25	
N-H 6	22	10
N-H 7	20.5	
N-H 8	18	5.5
N-H 9	15.5	
N-H 10	13	4.5

Sley: 44 epi

Warp Yarns: T-100 Nylon 400/68/.75 Z

Filling Yarns: T-100 Nylon 400/136/4 Z 3 plied at 4S

All fabrics scoured after weaving and the "H" numbered samples were also heat set.

Cotton Fabric T-3

Yarns: Warp: 2/20's, Filling 2/20's

Fabric: 53 ends/inch, 38 picks/inch, plain weave
warp crimp 8.5%, filling crimp 12.5%, fabric weight 6.7 oz/yd^2. Commercially finished material.

Nylon Fabric E-5

Yarns: Warp 933 de, Filling 924 de.

Fabric: 48 ends/inch, 48 picks/inch
weave 2 x 2 basket
warp crimp 4%, filling crimp 10%
fabric weight 12.2 oz/yd^2.

Friction Treatments Applied to T-3 and E-5

All samples were scoured before treatment in a warm solution of

soap and caustic soda, and then rinsed several times and dried. Then the samples were treated with various concentrations of softener or Syton and subsequently rinsed, dried, and conditioned for testing.

Concentration of Treatments (by volume)

Softener (commercially available type) 2½%, 5%, 10%

Syton 2½%, 5%, 10%

Control 0%

Position on Fig.3-12	Interfiber Friction Force (lb/in)	Treatment
a	.0066	5% Softener
b	.0060	10% Softener
c	.0122	2½% Softener
d	.0353	Control
e	.0303	2½% Syton
f	.0424	10% Syton
g	.0347	5% Syton
h	.0347	5% Syton

APPENDIX F

Bending Recovery vs. Imposed Curvature for Cotton Fabric T-3 Treated with Various Concentrations of Softener and Frictionizer

Warp Direction Bend

k_i^*	1.81 5	2.15 6	2.75 7	2.84 4	3.36 2	3.46 1	3.68 3	R T
.00483	.386	.477	.309	.370	.353	.509	.462	
.0133	.570	.688	.626	.397	.514	.526	.470	
.0237	.828	.770	.732	.660	.651	.705	.615	
.0329	.902	.820	.775	.658	.665	.690	.644	
.0343	.900	.834	.734	.690	.695	.660	.662	
.0543	.917	.862	.800	.683	.695	.682	.671	
.148	.889	.845	.817	.734	.684	.632	.606	
.262	.844	.800	.770	.623	.612	.592	.550	
.620	.712	.672	.645	.500	.512	.478	.439	
1.00	.628	.584	.538	.434	.406	.428	.350	

Filling Direction Bend

k_i^*	1.85	2.28	2.29	2.79	3.58	4.32	3.14	R
	5	6	7	4	2	1	3	T
.00483	.432	.462	.417	.358	.370	.356	.461	
.0133	.597	.683	.638	.500	.537	.521	.470	
.0237	.848	.813	.750	.678	.722	.687	.571	
.0329	.845	.853	.787	.730	.729	.626	.676	
.0343	.878	.882	.799	.784	.750	.683	.695	
.0543	.889	.900	.776	.810	.755	.673	.746	
.148	.862	.872	.755	.778	.734	.656	.661	
.262	.822	.855	.788	.705	.672	.584	.605	
.620	.684	.695	.621	.584	.533	.505	.466	
1.00	.622	.589	.544	.444	.444	.417	.392	

k_i^* = Dimensionless imposed curvature

R = Elastic rigidity per yarn (in^2 - lb x 10^{-6})

T = Treatment number.

BIBLIOGRAPHY

1. Timoshenko, S., "Strength of Materials", McGraw-Hill, New York, 1955.

2. Sonntag, G., "Die in Schichten gleich Dicke rebungsfrei geschichtete Halbebene mit periodisch verteilter Randbelastung", Forsch. Ing.-Wes. 23, 1957, p.S3.

3. Bufter, H., "State of Stress in a Laminated Slab", ZAMM 41, 1961, p. 158 (in German).

4. Goodman, L. E., Klumpp, J. H., "Analysis of Slip Damping with Reference to Turbine-Blade Vibration", J. Applied Mechanics 78, 1956, p.421.

5. Platt, M. M., Klein, W. G., Hamburger, W. J., "Factors Affecting the Translation of Certain Mechanical Properties of Cordage Fibers into Cordage Yarns", TRJ 22, 1952, p. 641.

6. Sloan, A., Mechanics of Materials, Macmillan, New York, 1952, p.141.

7. Livesey, R. G., Owen, J. D., "Cloth Stiffness and Hysteresis in Bending", JTI 55, 1964, p. T516.

8. Platt, M. M., Klein, W. G., Hamburger, W. J., "Some Aspects of Bending Rigidity of Singles Yarns", TRJ 29, 1959, p.611.

9. Abbott, N. J., Coplan, M. J., Platt, M. M., "Theoretical Considerations of Bending and Creasing in a Fabric", JTI 51, 1960, p. T1384.

10. Zorowski, C. F., Chen, C. S., "Cantilever Bending Behavior of Continuous Filament Cords", TRJ 35, 1965, P. 529.

11. Isshi, T., "Bending Tester for Fiber, Yarns, and Fabrics," Textile Machinery Society of Japan Journal 1, 1957.

12. Eeg-Olofsson, T., "Some Mechanical Properties of Viscose Rayon Fabrics:, JTI 50, 1959, p. T112.

13. Grosberg, P., Private Communication.

14. Bostwick, C., Behre, B., Karrholm, M., "Some Fundamental Theoretical and Experimental Aspects of Fabric Creasing", JTI 53, 1962, p. P116.

15. Daniels, W. W., "Relationship Between Fiber Properties and Wrinkle Recovery", TRJ 30, 1960, p.656.

16. Matsuo, T., "Crease and Elastic Recovery of Fabrics", Textile Machinery Society of Japan Journal 16, 1963, P. 354 (Japanese Edition); 10, 1964, P. 37 (English Edition).

17. Backer, S., "The Mechanics of Bent Yarns", TRJ 22, 1952, p. 668.

18. Freeston, W. D., Platt, M. M., "Bending Rigidity of Nonwoven Fabrics," TRJ 35, 1965, p. 48.

19. Platt, M. M., "Yarn Bending Rigidity", letter to the Editor, JTI 56, 1965, p. T509.

20. Backer, S., Petterson, D. R., "Some Principles of Non-Woven Fabrics," TRJ 30, 1960, p. 704.

21. Eeg-Olofsson, T., "A Contribution to the Experimental Study of the Bending Properties of Fabrics", Doctoral Thesis, C. T. H., Gotherburg, 1957.

22. Czitary, E., "On the Bending Strains of Wire Cables", Osterreichische Ingenieur-Archiv 1, 1947, p. 342.

23. Machida, K., "Mechanics of Rupture in Blended Yarns", Masters Thesis, M.I.T., 1963.

24. Pierce, F. T., "Geometry of Cloth Structure", JTI 28, 1937, p. T45.

25. Chadwick, G. E., Pollitt, J., Taylor, H. M., "Relations Between Cloth, Yarn, and Fibre Properties with Particular Reference to Blended Cloths", JTI 54, 1963, P. P126.

26. Matsuo, T., "Bending Rigidity of Fabrics", Journal of the Textile Machinery Society of Japan 11, 1965, P. 58.

27. Popper, P., "The Design of Materials for Use in Full Pressure Suits", Masters Thesis, M.I.T., 1959.

28. Tovey, H., "Wrinkle Resistance and Recovery from Deformation", TRJ 31, 1961, P. 185.

29. Marsh, J. T., "Crease Resisting Fabrics", Rheingold, New York, 1962.

30. Beste, L. F., Hoffman, R. M., "A Quantitative Study of Resilience", TRU 20, 1950, P. 441.

31. Steele, R., "Some Fabric Properties and Their Relation to Crease-Proofing Effects", JTI 53, 1962, P. P7.

32. ASTM D1295-60T

33. Bostwick, C. O., "Comparison of Some Methods for Testing Wrinkle Recovery", American Dyestuff Reporter 51, 1962, p. 21.

34. Freeston, W. D., Platt, M. M., "Filament Bending Recovery", TRJ 34, 1964, P. 308.

35. Skelton, J., "The Measurement of the Bending Elastic Recovery of Filaments", JTI 56, 1965, P. T454.

36. Hamburger, W. J., Platt, M. M., Morgan, H. M., "Some Aspects of Elastic Behavior at Low Strains", TRJ 22, 1952, p. 695.

37. Hynek, W. J., Winston, G., "A Comparative Study of the Tinius Olsen and Peirce Stiffness Testers", TRJ 23, 1953, P. 743.

38. ASTM D1388-55T

39. Winn, L. J., Schwarz, E. R., "Technical Evaluation of Textile Finishing Treatments: III Flexibility and Drape as Measurable Properties of a Fabric", TRJ 10, 1939, p. 5.

40. Lion, K., "Nonlinear Twin-T Network for Capacitive Transducers", Review of Scientific Instruments 35, 1964, P. 353.

41. Lion Research Corporation, Cambridge, Massachusetts, Bulletin #0100, "C-Line Transducer System".

42. Backer, S., "An Analysis of Deformation Mechanisms of Textile Structures under Varying Conditions of Stress", Doctoral Thesis, M.I.T., 1953.

43. Timoshenko, S., Goodier, J. N., "Theory of Elasticity", 2nd Edition, McGraw-Hill, New York, 1951, P. 46.

44. Coplan, M. J., Golub, S. J., "Some Observations on Distortions at a Wrinkle", TRJ 29, 1959, p. 500.

45. Suzuki, M., "Mechanics of the Crease of Fabrics: The Relaxation of Bending Moment of Bent Yarn", Hogh Polymer Chemistry, 17, 1960, p. 289 (in Japanese).